IVW - Schriftenreihe Band 94
Institut für Verbundwerkstoffe GmbH - Kaiserslautern

Muhammad Amir Khan

Experimental and Simulative Description of the Thermoplastic Tape Placement Process with Online Consolidation

Bibliografische Information Der Deutschen Bibliothek

Die Deutsche Bibliothek verzeichnet diese Publikation in der Deutschen Nationalbibliografie; detaillierte bibliografische Daten sind im Internet über <http://dnb.ddb.de> abrufbar.

Bibliographic information published by Die Deutsche Bibliothek

Die Deutsche Bibliothek lists this publication in the Deutsche Nationalbibliografie; detailed bibliographic data is available in the Internet at <http://dnb.ddb.de>.

Herausgeber: Institut für Verbundwerkstoffe GmbH
Prof. Dr.-Ing. Ulf Breuer
Erwin-Schrödinger-Straße
TU Kaiserslautern, Gebäude 58
67663 Kaiserslautern
http://www.ivw.uni-kl.de

Verlag: Institut für Verbundwerkstoffe GmbH

Druck: Technische Universität Kaiserslautern
ZBT – Abteilung Foto-Repro-Druck

D 386

Als Manuskript gedruckt. Printed in Germany.
ISSN 1615-021X
ISBN 978-3-934930-90-2

Experimental and Simulative Description of the Thermoplastic Tape Placement Process with Online Consolidation

Beim Fachbereich für Maschinenbau und Verfahrenstechnik

der Technischen Universität Kaiserslautern

genehmigte Dissertation

zur Erlangung des akademischen Grades

Doktor-Ingenieur (Dr.-Ing.)

vorgelegt von

MSc. Muhammad Amir Khan

aus Karachi, Pakistan

Tag der mündlichen Prüfung:	30.08.2010
Prüfungsvorsitzender:	Prof. Dr.-Ing. Paul L. Geiß
1. Berichterstatter:	Prof. Dr.-Ing. Peter Mitschang
2. Berichterstatter:	Prof. Dr.-Ing. Martin Maier

D 386

Preface

I would like to express my sincere gratitude to Prof. Dr.-Ing. Peter Mitschang, whose unparalleled compassion, kindness and generosity allowed me to cruise through the demands of this research during the period from 2006 to 2010. One thing among many which I learned from him is how to stay positive in every problem you face.

I would also like to profoundly thank my advisor Dr.-Ing. Ralf Schledjewski. His guidance, continuous encouragement and support right from the start to the end enabled me to successfully complete this work. He was always there to listen and to give advice. His constructive comments and remarks during the meetings helped me in understanding the problem and the relevant concepts. Furthermore I would like to thank Prof. Dr.-Ing. Paul L. Geiß for chairmanship in the examination board and Prof. Dr.-Ing. Martin Maier for examining my thesis.

I greatly acknowledge the financial support from Higher Education Commission (HEC) and Institute of Space Technology, Pakistan for the pursuit of this research work. Also I want to say thanks to DAAD (German Academic Exchange Service) whose cooperation with HEC accommodated a number of students in Germany.

Let me also give thank to my colleagues (past and present) with whom I had a wonderful time and had very helpful discussions. I am obliged to thanks Jens Lichtner and Angelos Miaris for their very friendly and always ready-to-help attitude. Special thanks to Rene Holschuh and André Meichsner for proof-reading the manuscript. I also want to thank Steven Brogdon, for all wonderful conversations we did from technical issues to horse riding.

There are no words to thank my parents who supported me over the years and brought me up to what I am today. I am greatly indebted to my wife Maryam Naz, for her love, support and patience.

Kaiserslautern, September 2010

For Ammi Jan and all family members

Contents

Abbreviations

Short form	*Description*
1D, 2D, 3D	*One Dimensional, Two Dimensional, Three Dimensional*
ASTM	*American Society for Testing Material*
CCD	*Charge Coupled Device*
CFD	*Computational Fluid Dynamics*
CF-PEEK	*Carbon Fiber reinforced Polyetheretherketone*
DCB	*Double Cantilever Beam*
DIN	*Deutsches Institut für Normung*
DMA	*Dynamic Mechanical Analysis*
DSC	*Differential Scanning Calorimeter*
DTGA	*Differential TGA*
FFT	*Fast Fourier Transformation*
ILSS	*Inter Laminar Shear Strength*
IVW	*Institut für Verbundwerkstoffe*
MPP	*Material Process Product*
ProSimFRT	*Process Simulation for Fiber Reinforce Thermoplastic*
TGA	*Thermo Gravimetric Analyser*
VARTM	*Vacuum Assisted Resin Transfer Moulding*
nl/min	*Norm liter per minute*
rad/sec	*Radian per seconds*
m/min	*meter/minute*

Symbols

Symbol	Unit	Description
A		Pre exponential component in Arrhenius relation
A_1, B_1, C_1		Extensional, coupling, bending matrices
B	K	Component in Arrhenius relation
C	$J/Kg.K$	Volumetric specific heat
c	%	Volume fraction crystallinity
c_r	%	Relative crystallinity
c_α	%	Equilibrium volume fraction crystallinity
D_b	%	Bonding degree
D_h	%	Degree of healing
D_{ic}	%	Degree of intimate contact
E	Pa	Elastic modulus
E_a	J/mol	Activation energy
f		Scaling ratio for cantor set
F_c	N	Compaction force
FD		Fractal dimension
h	m	Thickness
$\dot{h}$	m/s	Thickness compaction rate
h_f	m	Final thickness
h_i	m	Initial thickness
h_m	$W/m^2\ °K$	Convective heat transfer coefficient
h_r	m	Recess depth of 1st generation in cantor set
J'	m^2/MN	Storage flexure modulus
J''	m^2/MN	Loss flexure modulus
k	$W/m\ °K$	Thermal conductivity
K_1,k_2		Kinetic parameters for crystallization model
K	$Pa\text{-}s/m$	Friction factor
K_m		Pre exponential Arrhenius relation in melt kinetics
L	m	Length
L_c	m	Roller contact length
L_r	m	Total length of cantor set
m		No. of asperities generation
$M^{CT}_{x,y,z}$	$N\text{-}m$	Thermally induced moments
$N^{CT}_{x,y,z}$	N	Thermally induced forces
P	Pa	Pressure
P_g	Pa	Void pressure
P_R	N	Failure load in ILSS test

$\dot{q}$	*J/sec*	*Heat flow rate*
R	*m*	*Void radius*
R_c	*J/K.mol*	*General gas constant*
R_r	*mol/g*	*Crosslinking rate*
R_z	*µm*	*Average maximum height of the surface profile*
S	*m*	*Radius of continuum surrounding the void*
t	*s*	*Time*
T	*°C or °K*	*Temperature*
T_g	*°C*	*Glass transition temperature*
T_m	*°C*	*Melt temperature*
t_w	*s*	*Weld time*
V	*m/s*	*Lay up velocity*
V_v	m^3	*Volume*
w	*m*	*Tape width*
w_1, w_2		*Weight factor*
x	*m*	*Spatial coordinate in width direction*
X_f	*%*	*Degree of melting*
y	*m*	*Spatial coordinate in length direction*
z	*m*	*Spatial coordinate in thickness direction*
α	*%*	*Fractional decomposition*
β	*°C/min*	*Heating rate*
$\varepsilon^{CT}_{x,y,z}$	*%*	*Thermally induced strains*
v_x	*m/s*	*Continuum velocity*
ξ		*Dummy variable for integration*
ψ_1, ψ_2		*Kinetic parameters for crystallization model*
ρ	Kg/m^3	*Density*
σ	*Pa*	*Interlaminar shear strength*
η	*Pa·s*	*Viscosity*
η'	*Pa·s*	*Dynamic viscosity*
η_T	*Pa·s*	*Transverse viscosity*
η^*	*Pa·s*	*Complex viscosity*
τ	*mN/m*	*Surface tension*

Kurzfassung

Das Ziel der vorliegenden Arbeit ist es die auftretenden Phänomene der Konsolidierung beim thermoplastischen Tapelegen zu beschreiben. Ein genaues Verständnis der auftretenden Zusammenhänge ist unabdingbar um hochqualitative Bauteile zu fertigen und den Prozess für industrielle Anwendungen im Automobil, Luft- und Raumfahrtsektor konkurrenzfähig zu machen. Die größte Herausforderung bei dieser Technik ist die prozessbedingt sehr kurze Verweildauer des Materials unter der Konsolidierungsrolle, in der eine vollständige Polymerdiffusion in der Fügezone erreicht werden soll. Infolgedessen wurden ausführliche Untersuchungen hinsichtlich der optimalen Prozessparameter durch Halbzeug-, Prozess- und Bauteiltests, sowie durch Prozesssimulation durchgeführt.

Die Temperaturverteilung unter der Heißgasdüse wurde untersucht. Die anfängliche Annahme eines größeren Wärmeeintrages bei höherem Gasvolumenstrom konnte als teilweise richtig bewiesen werden. Durch den sinus-, beziehungsweise wellenförmigen Verlauf bei der konvektiven Wärmeübertragung wird eine geringere Wärmeabgabe bei höheren Gasvolumenströmen induziert. Folglich wirkt sich dieser Effekt auf die interlaminare Festigkeit aus. Untersuchungen haben gezeigt, dass das Heißgas Temperaturen von über 1700°C erreichen kann. Eine derartig hohe Temperatur kann zu einer thermischen Alterung, sowie Degradation des abgelegten Materials führen.

Der Verbindungsprozess zwischen den einzelnen Lagen kann als die Kombination der Effekte Grenzflächenkontakt D_{ic} und der dort ablaufenden Polymerdiffusion D_h angesehen werden. Die Polymerkettendiffusion startet nur in den Materialzonen, in denen ein direkter Kontakt zwischen den Materialzonen hergestellt wurde. Unebenheiten auf der Halbzeugoberfläche behindern eine gleichmäßige Ausbildung des Grenzflächenkontakts. Die Abplattung der Oberflächenrauhigkeit kann als stufenweise Funktion angenommen werden, somit wird beim Ablegen mit jedem sukzessiven Überfahren der Verbundzone der Grenzflächenkontakt verbessert. Folglich verbessert das fortlaufende Ablegen (Dickenaufbau des Laminats) den Konsolidierungsgrad in den bereits abgelegten Lagen. Dieses Phänomen wirkt sich jedoch nur auf wenige aufeinanderfolgende Lagen (1-6 Lagen), in denen die Temperatur über den Schmelzpunkt steigt, aus.

Auf der Kombination der Prozessgeschwindigkeit und des Heißgasdüsenvolumenstroms basierende drei Energieeintragslevel konnten identifiziert werden. Bei Wahl einer Kombination der beiden Parameter mit insgesamt niedrigem Eintragsniveau ist der Energieeintrag sowohl in das abzulegende Tape als auch in das bereits abgelegte Substrat begrenzt und ein daraus resultierender unvollständiger Grenzflächenkontakt verhindert den Verbund. Obgleich ein hoher Energieeintrag den Grad des Verbundes D_b bis hinzu 97% anhebend kann, tritt hierbei das Phänomen der thermischen Degradation auf. Die Polymerdiffusion und die Polymervernetzung folgen der Arrhenius-Gleichung mit Aktivierungsenergien von 43 KJ/mol und 276 KJ/mol. Die Polymervernetzung bei hohem Temperatureintrag erschwert die Polymerdiffusion und resultiert somit in einer verringerten Verbundstärke. Somit ermöglicht die Wahl optimierter den Energieeintrag betreffenden Prozessparametern eine kontinuierliche über den gesamten Legeprozess fortschreitende Verbesserung des interlaminaren Verbundes.

Eine Multi-Parameter-Studie hat gezeigt, dass eine verlängerte Konsolidationsphase, einerseits erreichbar durch Erhöhungen der Anzahl der Überfahrvorgänge, andererseits durch Verlängerung der Konsolidierungstrecke, oder durch Einsatz von mehreren Konsolidierungsrollen, in einer Aufweitung des Profilverlaufs des Verbundgrades D_b resultiert. Auf diese Weise sind hohe Ablegegeschwindigkeiten (bis zu 7 m/min) realisierbar und machen den Prozess für industrielle Anwendungen geeignet. Mit der am IVW vorhandenen Tapelegeeinheit mit einer Kompaktierungsrolle ist eine Laminatherstellung möglich, welche autoklav-ähnliche Güte besitzt (bezogen auf ILSS und Porengehalt), wenn das bändchenförmige vorimprägnierte Halbzeug einen Porengehalt kleiner 1% aufweist.

Als auf die Zugfestigkeit 90° primärer beeinflussender Parameter konnte die Deformationen der Tapekante identifiziert werden. Laminate, welche mit einer leichten Überlappung der Tapes erstellt wurden, weisen eine ca. 10% Steigerung bezüglich der Querzugkraft verglichen zu Laminaten mit reiner Stoß-an-Stoß Ablage.

Ein hohes Energieeintragsniveau wirkt sich im Ablegeprozess jedoch negativ auf die Güte des Querverbundes der Laminate aus, da sich hierbei Lufteinschlüsse bilden. Nachträgliche Konsolidierungsschritte wie beispielsweise zusätzliche Überfahrvorgänge mit geringem Gasvolumenstrom haben sich als positiv erwiesen um die eingeschlossenen Poren zu eliminieren und die Gesamtqualität des Laminats zu ver-

bessern.

Letztlich kann die in dieser Arbeit entwickelte Simulation dazu verwendet werden um bestehende limitierende Parameterkonstellationen zu identifizieren um somit durch optimierte Prozessfenster eine vollständige Konsolidation zu erreichen. Die ausgeführte Parameterstudie hat gezeigt, dass mit der aktuell am Markt angeboten Halbzeuggüte (ursprünglicher Porengehalt 3,1%) Laminate mit einem Verbundgrad D_b > 97%, bei jedoch gleichzeitig erhöhtem intralaminaren Porengehalt, erstellt werden können. Obgleich es sich in dieser Arbeit durch experimentelle Untersuchungen gezeigt hat, dass sich das Vorhandensein von intralaminaren Poren nicht negativ auf ILSS-Werte auswirkt, gibt es Anwendungsfälle (Luft- und Raumfahrt oder Medizintechnik) in denen ein Porengehalt < 1% gefordert ist. Die Werkzeugtemperatur konnte neben der Heißgastemperatur und der Prozessgeschwindigkeit als dritter Parameter mit starken Auswirkungen auf die Laminatgüte identifiziert werden. Ein hochtemperiertes Werkzeug (260-290 °C) begünstigt einerseits den Verbund innerhalb des Laminates, andererseits jedoch wird hierdurch eine Porenexpansion gefördert. Simulationsergebnisse zeigen, dass eine Porenexpansion durch eine kalte Werkzeugoberfläche verhindert werden kann. Jedoch die zur Ausbildung der Adhäsion zwischen Erstlage und Werkzeug notwendige erhöhte Temperatur steht dem entgegen.

Abstract

The aim of this study is to describe the consolidation in thermoplastic tape placement process to obtain high quality structure, making the process viable for automotive and aerospace industrial applications. The major barrier in this technique is very short residence time of material under the consolidation roller to accomplished complete polymer diffusion in the bonded region. Hence investigation is performed to find out the optimize manufacturing parameters by extensive material, process, product testing and through process simulation.

Temperature distribution and convective heat transfer under the hot gas torch is experimentally mapped out. Bonding process inside the laminate is the combine effect of layers (tapes) intimate contact D_{ic} development and resulting polymer diffusion D_h at these contacted sections. Three energy levels are identified based on the process velocity and hot gas flow combinations. For the low energy parameter combinations, the energy input to the incoming tape and substrate material is limited and result in incomplete intimate contact which restricts the bonding process. On other hand high energy input although could increase the bonding degree D_b even up to the 97%, but also activate the thermal degradation phenomena. It is found out that the rate of polymer healing (diffusion) and polymer crosslinking follows the Arrhenius laws with the activation energies of 43 KJ/mol and 276 KJ/mol. The polymer crosslinking at high temperature exposure hinder the polymer diffusion process and reduces the strength development. So the parameters combination at intermediate energy level provides the opportunity of continuous interlaminar strength improvement through out the layup process.

Deformation of tape edges is identified as the dictating factor for the laminate's transverse strength. Tape placement with slight overlap reinforced the transverse joint by more 10 % as compared to pure matrix joint. Finally the simulation tool developed in this research work is used for identifying the existing limitation to achieve full consolidation. A parameter study shows that extended consolidation either by mean of additional pass or by increasing consolidation length widens the high strength (over 90%) bonding degree D_b contour. Thus high lay-up velocity (up to 7 m/min) is viable for industrial production rate.

1 Introduction

The high demand for light weight structure has given a way for the technological progress in the field of composite material. The fiber reinforced composite materials are preferably used by the sport, automobile and aerospace industries for their high strength, cost effectiveness and excellent resistance against thermal / chemical environment. On the basis of adhesive matrix system, fiber reinforced composites are broadly classified as thermoset and thermoplastic material [1]. Processing of the thermoset composite involves steps such as impregnation, lamination and curing. Thermoplastic materials on other hand are commercially available in fully polymerized form, and the manufacturing process is based only on lamination and curing.

Thermoplastic materials offer some unique processing opportunities like hot laminate can be reshaped or formed to produce three dimensional parts. Thermal welding can be done with similar thermoplastic material as well as with metal to produce assemblies. Material can be reconsolidated to eliminate defects and recycled for new application. These features lead to various manufacturing processes, such as hand lay-up, autoclaved molding, fusion bonding, press molding, diaphragm forming, filament winding and automated tape placement process.

Among them the automated tape placement process has some additional interest due to high processing rate and potential cost saving in manufacturing because no secondary processing is needed to complete the consolidation process. Thermoplastic tape placement with online consolidation is a discontinuous process in which a thermoplastic prepreg material is laid up on the tool or mandrel and consolidated immediately with the application of heat and pressure. Compared to the filament winding, it provides several additional flexibilities such as the possibility to manufacture non rotational structures even with concave curves and free fiber orientation.

Online or insitu consolidation is a processing step in which heat and pressure are applied simultaneously to the thermoplastic material to eliminate spatial gaps and force out any entrapped air, thereby initiating the interface bonding through polymer chain diffusion process. Improper consolidation can lead to voids, residual stresses, warpage and in some cases premature mechanical failure of the composite part [2]. This study explains and addresses the several critical issues of the thermoplastic

tape placement process with online consolidation that must be overcome to obtain a composite laminate with optimum properties.

1.1 Objectives

According to the experimental testing conducted on the tape placement setup at IVW [3-4] the selection of manufacturing conditions highly influences the quality of the final parts. Hence the optimized process parameter should be identified to produce a unidirectional laminate with bonding strength comparable to other established manufacturing process like autoclave. The objectives of this research work are three folds and Figure 1.1 shows the process improvement cycle based on these three steps:

1. Scientific investigation of the thermoplastic tape placement process with the understanding of the occurring physical phenomena. This will allow better process modeling to determine if the consolidation quality is acceptable to industrial scale.

2. Experimental characterization of the material, process and product (MPP) using carbon fiber with polyetheretherketone (CF-PEEK) thermoplastic material.

3. Parameter study, addressed to the existing technological limitation and insight into future improvements.

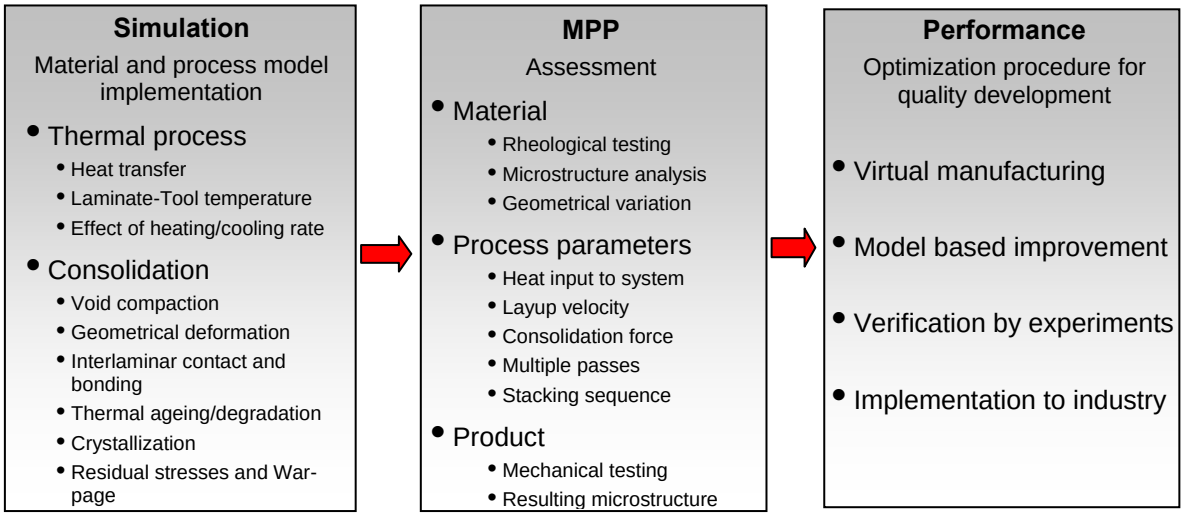

Figure 1.1: Process improvement cycle.

1.2 Approach

The chapter two discusses the basic principal and introduces the basic terminologies of the thermoplastic tape placement process. The tape placement head involving different mechanism of heating and consolidation conceived within the last few decades are also discussed. On theoretical side, state of the art models explaining the thermo-kinetic mechanism for strength development are presented.

Chapter three is focused on the experimental techniques to characterize material, process and product. The anisotropic nature influences the material response during the process. Hence the methods are explained for the detail geometrics, rheometric, mechanical and as well as micro structural examination. The setup parameters are also monitored using a variety of sensors. The interlaminar bond strength is examined to develop the quality criteria for the final part. Peel testing and interlaminar shear strength (ILSS) test are selected for investigating the laminate quality with the variation of processing parameters. Relative comparison is performed with the referenced autoclaved plate to see the maximum achievable consolidation level.

With sufficient theoretical and experimental explanation of the process parameters, chapter four drives the research work into the simulation stage. The chapter is divided into two sections. In the first section the results are compared with experimental measurement to confirm and fine tune the simulation tool. The comparison of void content, peel strength and ILSS values shows high conformation and accuracy of the implemented models. In second section results are generated for parameters study to identify the process window.

Chapter five provide the answers to several design and development related issues. The thermal degradation, weight loss, details of process parameter selection, effect of material and technological improvement are all discussed and explained with the aid of simulation and experimental results.

Chapter six lists the main achievement of this study and present the outlook for the automatic tape placement process with online consolidation.

2 State of the art

The thermoplastic tape placement process is developing towards industrial application. An overview about the technological and theoretical advancements to exploit the rapid processing potential of the process in order to achieve the desired cost-effectiveness, flexibility and quality is presented. Therefore this chapter will first describe the major setup / components, processing steps, and technical terminologies. In later section several models will be discussed to explain the incurring phenomenon in lay-up process.

2.1 Thermoplastic tape placement setup

Manufacturer often come across with complex structure which requires specific amounts of fibers orientation in particular direction or sections with different thicknesses to achieve optimum performance with minimum weights. Also the high cost of material motivates the manufacturer to reduce the material waste. The idea of automatic thermoset lay-up process developed in 60's resolved this problem [1]. With the flexibility and sticky characteristics of thermoset material, it can be placed in nearly net shape structure through an automatic tape placement head (see Figure 2.1 a).

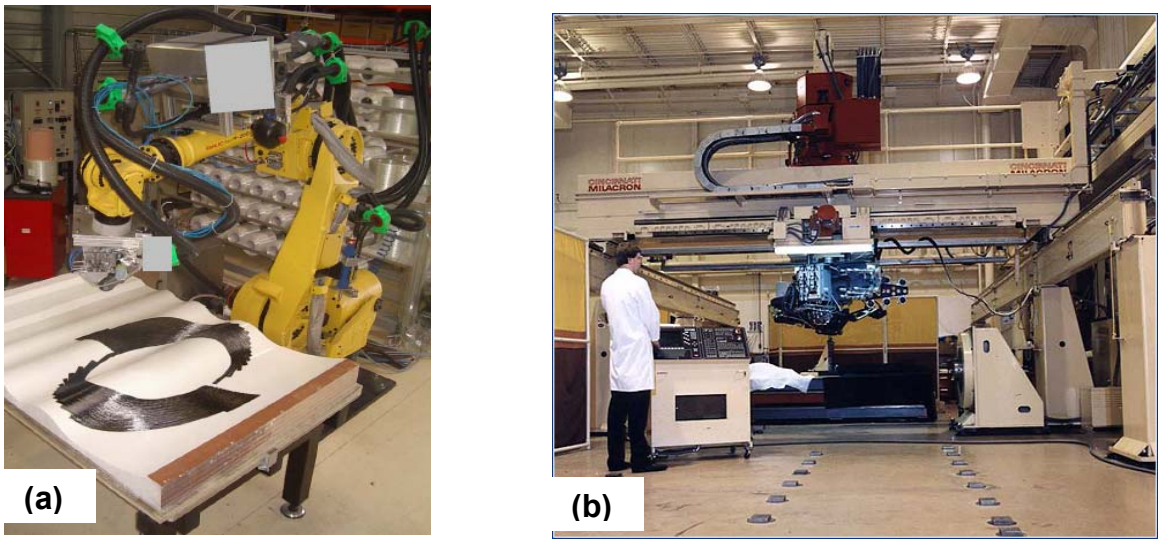

Figure 2.1: Automatic tape placement head attached to robot arm / gantry (a) for thermoset material [5] (b) thermoplastic material [6].

Since most of the thermoset materials have curing cycle above the room temperature, a post consolidation step is inevitable for the complete strength development. Beside this, the tacky state of the material creates several handling and safety hazards in production environment. The introduction of the preimpregnated thermoplastic material offered new synergy in the lay-up process. The thermoplastic plies offer ease of handling and can be completely consolidated during the placement without long time curing.

The lay-up manufacturing setup consists of the placement head attached to the robotic arm or gantry, the motion controller with positioning software, the tooling for stacking the laminate and the tape spool. The tape placement head itself consists of following major components as shown in Figure 2.2.

- Compaction force assembly (roller / pads with pressure application device)
- Heat source(s) and cooling system(s)
- Tape feed and guiding system

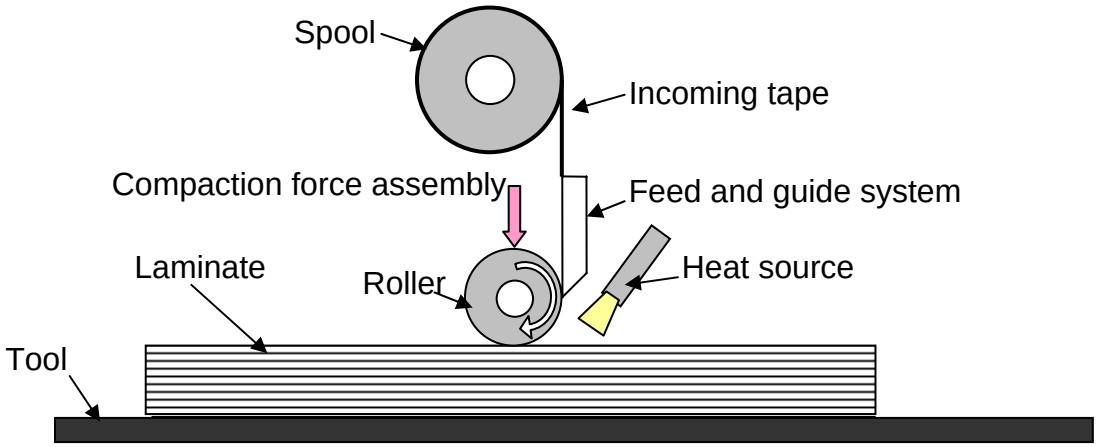

Figure 2.2: Sketch of an automated tape placement setup.

The laminate manufacturing process involves three main stages; the sub steps involved in these stages are described in Figure 2.3.

Stage 1: Preparation stage marks the idealization of the lay-up configuration and setting up of the work cell for lay-up. This includes mounting of the spool and manually

feeding the tape to the feed / guide assembly, tool heating and positioning of the placement head to the start position.

Stage 2: A brief description of the tape placement process with online consolidation (i.e. second stage) is as follows: the incoming thermoplastic tape after passing through the guided assembly heats up with the help of a hot gas torch / laser and is placed on the hot tool with the aid of a temperature controlled consolidation roller. The basic principal of the process is to create the bonding between the incoming tapes and already laid up substrate through sufficient heating and pressure. The bonded state is then frozen under the temperature controlled roller. Several tapes can be placed side by side and the laminate can be manufactured by placing the additional layers over the previously laid up layers.

Stage 3: When the stacked laminate reaches the desired thickness and dimensions, this state marks the termination of the further lay-up process. The laminate is then allowed to cool down by switching off the tool heating. Placement head is then position back to its initial position. Generally the laminate detaches automatically from the tool once temperature drops below the glass transition temperature T_g.

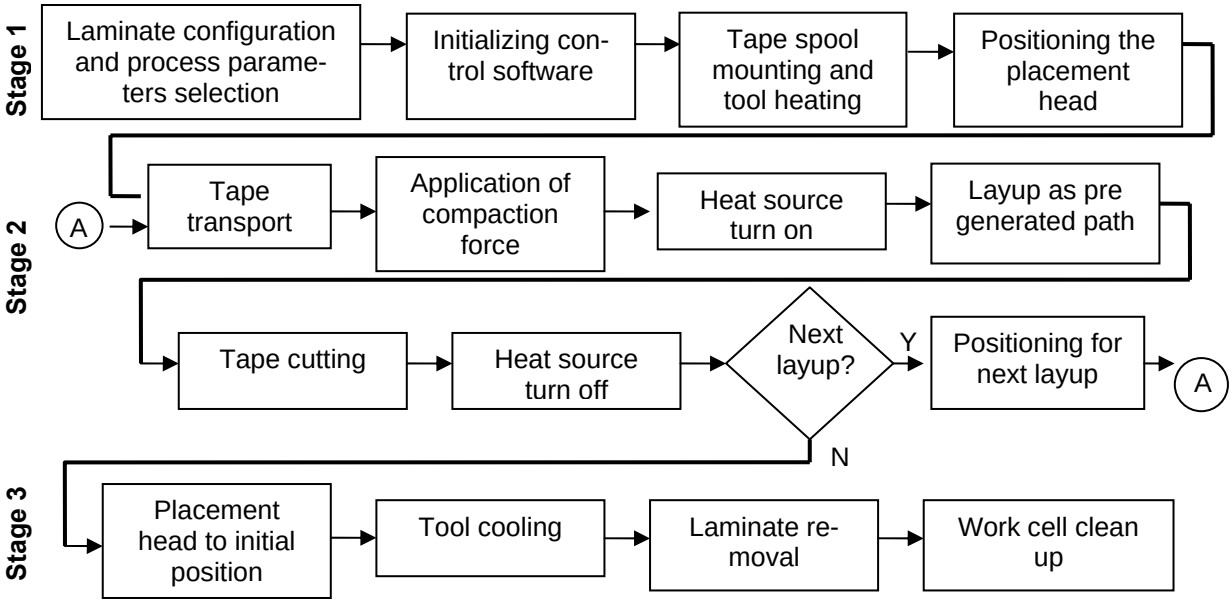

Figure 2.3: Process plan for the laminate manufacturing in a lay-up work cell.

2.2 Classification of thermoplastic tape placement head

Several placement head configurations have been realized and practically implemented. The research programs have addressed several requirements for the automatic tape placement setup such as precise control of head position, material placement rates, heat delivery to the lay down zone, cut / add and start / stop capability.

Classification on broad scale can be performed on the basis of compacting and heating mechanism. The placement head configuration with single roller (Figure 2.4) resulted in a compact placement assembly and has been preferably selected by several manufacturers like AFPT, Coriolis, Automated Dynamics, etc. For this configuration, the roller, torch / laser, material guidance and force mechanism are all available in compact lightweight fiber placement head assembly. Lay-up on the geometrical complex structure can be easily resolved with this configuration by placing the tape on difficult curvature utilizing the flexibility of the robotic arm or gantry and different roller sizes.

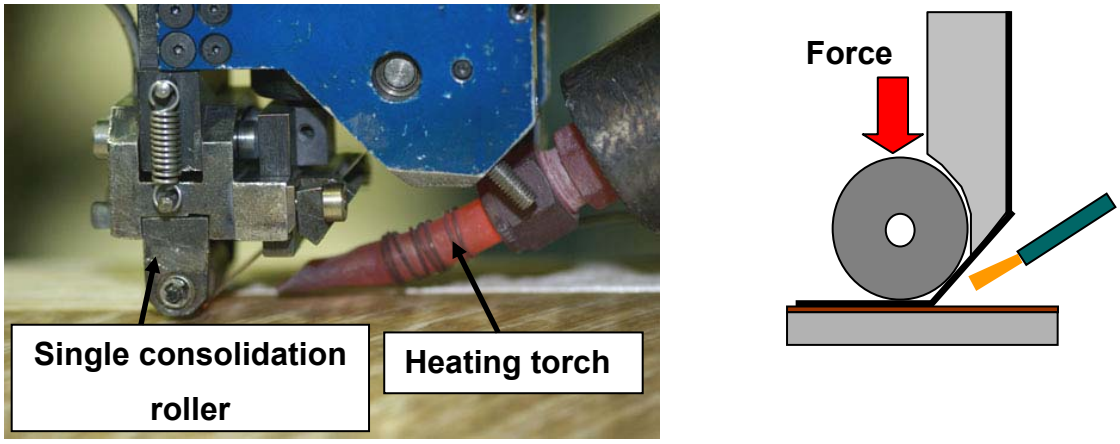

Figure 2.4: Single roller configuration - placement head by ADC [7].

Identifying the need of additional consolidation, tape placement head with multiple heating sources and rollers have also been realized (Figure 2.5). The first source either heats the substrate material or the interface between the incoming tape and the substrate for initiating the bonding process. Consolidation starts under the first roller with the application of force. The laid down tape and partially consolidated laminate is then reheated and reconsolidated by the second torch and roller to improve the bonding process.

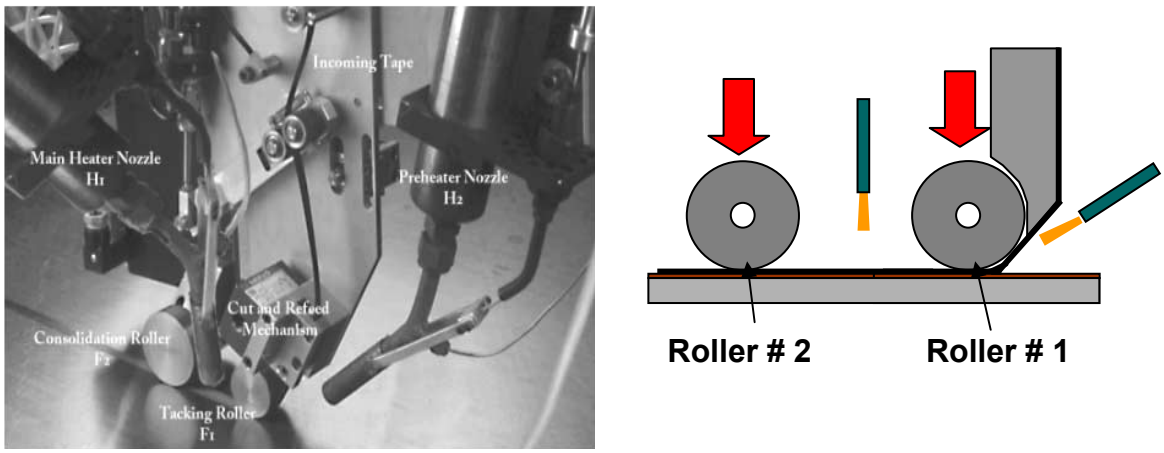

Figure 2.5: Multiple rollers and heating configuration [8].

With the theoretical understanding of the online consolidation phenomena, efforts have also been directed in producing laminates with not only higher mechanical strength but with superior structural quality. Void elimination from the tape and its re-consolidation immediately after the roller, is identified as one of the influencing factor. The concept of consolidation under the roller is then combined with the temperature control pads to foster the bonding process and to prevent void growth by maintaining extended pressure and temperature cycles. Figure 2.6 integrates the equipment developed with the process concept detailed above.

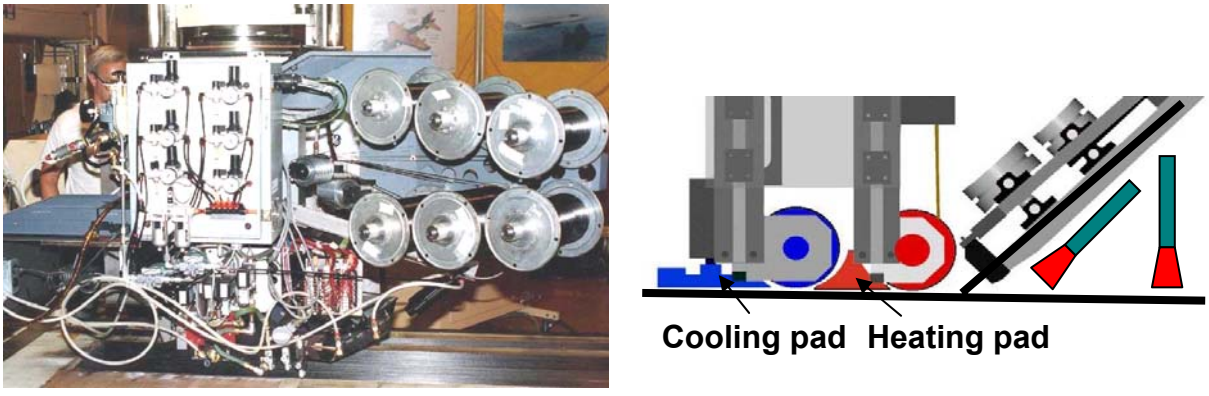

Figure 2.6: Multiple rollers with pads configuration [6].

The first torch heats the bare tool or previously laid up composite, while the second heats the substrate and the incoming material. Two rollers alternately heat and cool the composite. The first roller establishes the initial intimate contact between the lower surface of the incoming composite and the upper surface of the substrate, and

initiates healing in those locations where intimate contact has been achieved. A heated shoe / pad maintains the temperature long enough to foster further intimate contact and to complete healing of the longest polymer chains in order to develop interlaminar strength. The second roller consolidates and cools the material, re-freezing it in place and compressing the voids. A chilled shoe extends the freezing process by maintaining consolidation pressure to avoid the void deconsolidation [6].

To deal with the lay-up difficulties on geometrically complex tools such as S-curves or the surfaces which are not flat, the concepts of adaptive consolidation roller [9] and conformable line / area compactor [10] have been developed. Figure 2.7 shows the tape placement head with line and area compactor, the compacting assembly comprises of multiple vertically movable metal segments that conform themselves as per lay-up contour. The overall head system design consists of a frame with vertically articulating segment drawers, and a shim drive apparatus to manipulate the segments extension to conform to the tool or part, thereby achieving the process motions. Hot / cold area compactor maintains the high pressure over the tape for extended duration ensuring condition for sufficient interlaminar bonding development within the laminate.

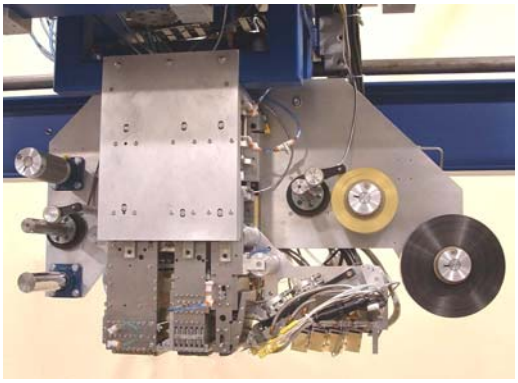

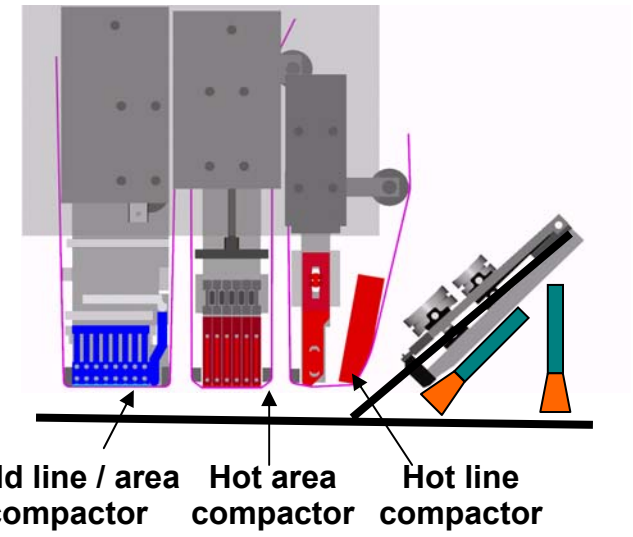

Figure 2.7: Contour conformable placement head [11].

2.3 Tape placement setup at IVW

Decade of research work at IVW has resulted in the robust, efficient and high performance thermoplastic tape placement head EVOI which encompasses the state of the art technologies (Figure 2.8). Based on the single roller configuration, high quality laminate can be laid down up to the process velocity of 8 m/min. The mechanical performance of such laminates is comparable to any other composite manufacturing process. Some prominent features are as follows

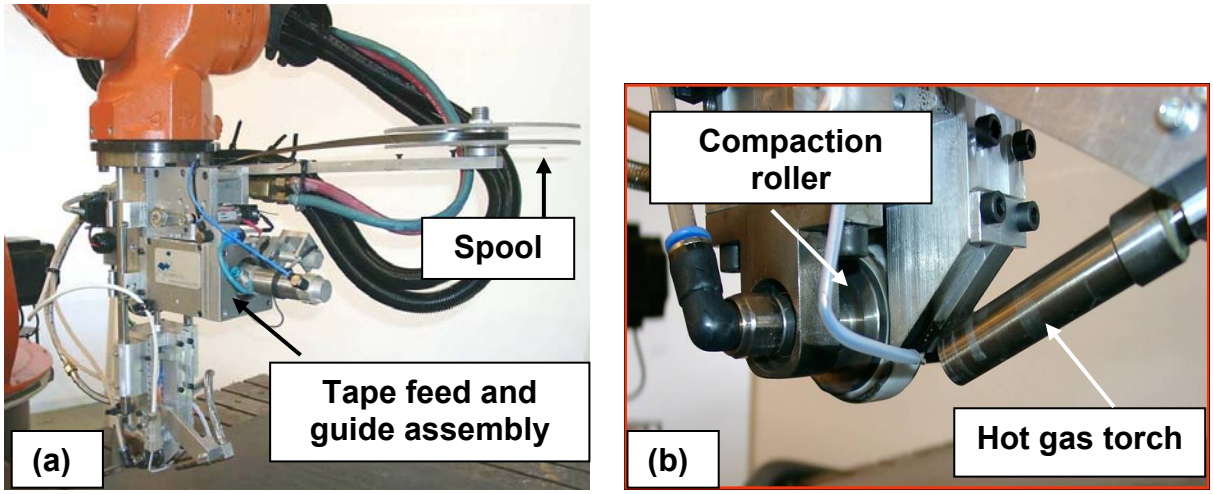

Figure 2.8: (a) Tape placement head EVOl (b) Detail of compaction roller and hot gas torch.

Compacting mechanism: Single steel roller configuration with the possibility of using different diameters to lay-up on the wavy or non planer surfaces. An advanced surface conformable adaptive roller provides additional flexibility to deposit material even on geometrically complex structures, by maintaining the high compaction pressure ensuring perfect bonding between the layers. By using different cooling / heating mediums like water and air the roller temperature can be actively controlled to freeze or to improve the bonding state.

- Variation in roller temperature: 25 – 95 °C with water cooling.
- Compactions load: 50 - 220 N.
- Roller diameter: 25 - 75 mm.
- Process lay-up velocity: 3 - 10 m/min.

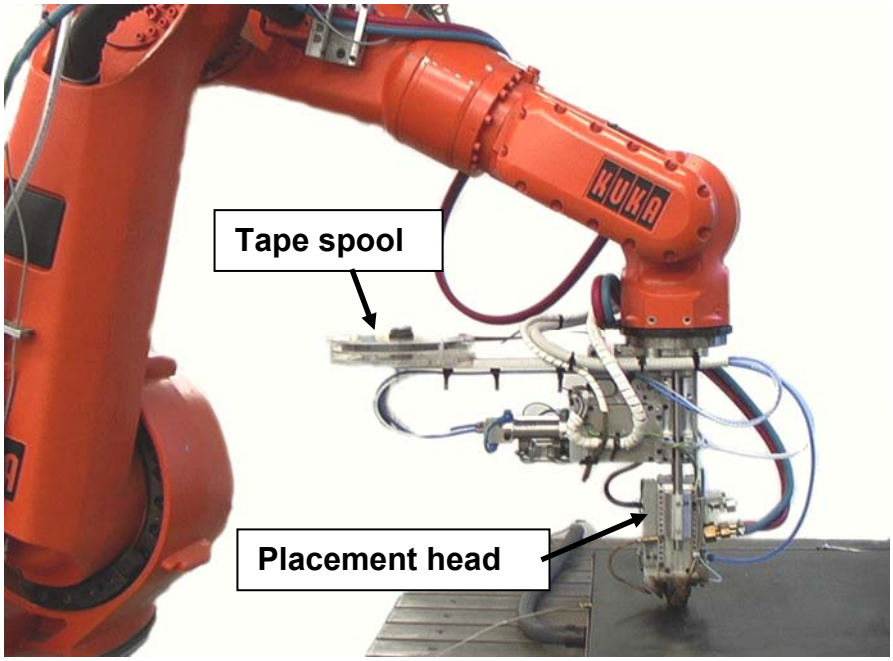

Figure 2.9: Robotic arm equipped tape placement head.

Installation: Compact assembly allows an easy integration with different manufacturing setups. Figure 2.9 shows the placement head attached to the KUKA robotic arm, with a provision of six degree of freedom and the maximum reachable range of 3500 mm. The offline path generating software pre-handles several technical issues before the start of actual lay-up process. The precise head positioning enhanced the tape laying capability and laminate stacking quality. The placement head can be kept normal to the lay-up surface even on the curvy lay-up path to ensure sufficient material compaction. Other possibility is its installation on the commercially available bridge, gantry or CNC machines, like Viper 1200 from Cincinnati machine. For laboratory scale setup, to perform rigorous testing and evaluation of the process and the product, the head with some reduced capabilities is also installed on the test rig at IVW (Figure 2.10).

Heating source: Effective heating of the material before the roller, is obtained either by using hot gas torch or by the diode laser heating. The control flow of hydrogen and oxygen (3-20 norm liter/min) in combustion section of the torch can varied the hot gas temperature on the composite surface over 1700 °C. Heat distribution on incoming tape and on substrate material can be adjusted by varying the angle of impinging jet.

The laser system is a LDL40 – 550 diode laser system manufactured by the company ‘Laserline’ has been tested for the process evaluation at laboratory scale. The laser has a wavelength of 980 nm and a maximum power of 600 W. An optic lens mounted on the laser creates a rectangle beam with a cross section of 12.00 mm x 2.08 mm. Heat flux over rectangular section can be varied by changing the power input to the system.

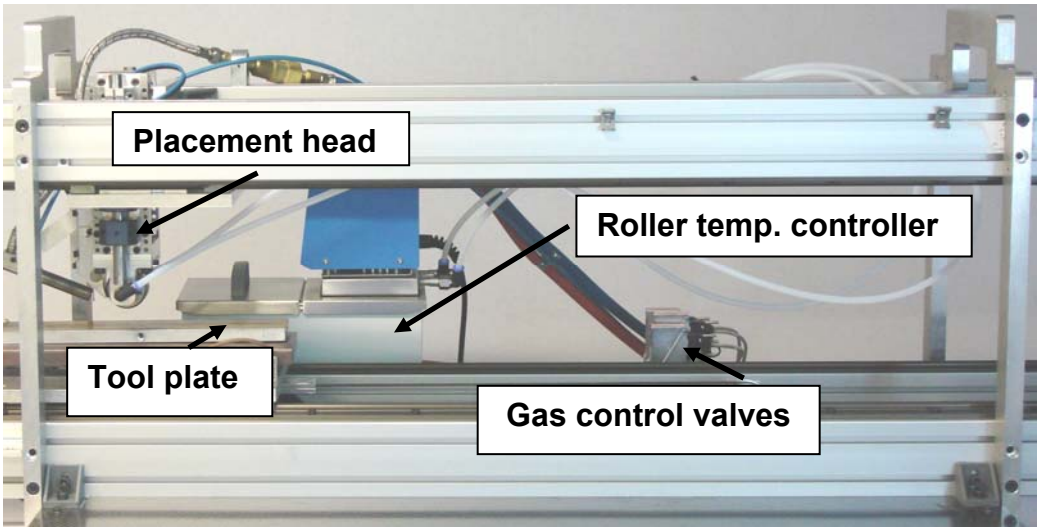

Figure 2.10: Tape placement test rig at laboratory level.

2.4 Process modeling

Special interest lies in those composite manufacturing techniques where the pre-impregnated material is laid up to produced a laminated structure. Laid up or stacked material undergoes heating, consolidation and solidification possessing steps to form a finished laminated part as shown in Figure 2.11. High temperature heating melts the thermoplastic matrix material to facilitate the polymer flow and diffusion at the layer’s interfaces. Application of high pressure (or vacuum) in consolidation step removes the spatial gaps, trapped voids and generates a matrix rich bonded region by eliminating the layers interfaces. Consolidation step is followed by the cooling of material to allow re-solidification of bonded state. As composite manufacturing like tape placement process involves several simultaneous occurring physical phenomena, knowledge of their source of generation, mechanism and effect requires unlimited number of experiments. This invokes the need of reliable simulation tool to optimize the process manufacturing.

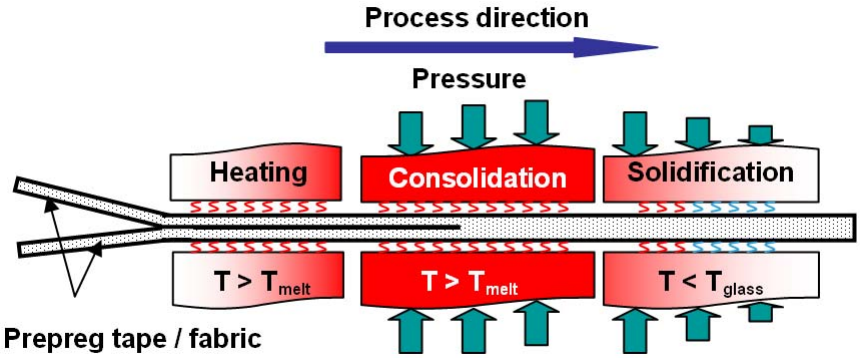

Figure 2.11: Manufacturing with thermoplastic composite material.

Reliable mathematic models although cannot replace the experiments, but in combination with physical experiment, they provide interesting information which cannot be directly measured. Therefore researchers focused their energies in developing process models for better understanding and explanation of the occurring phenomena. In the following section, a brief description is provided for the state of the art models to explain the possessing of thermoplastic composite material with focus on tape placement process.

2.4.1 Heat transfer model

In the thermoplastic tape placement process the incoming tape is first heated up and bonded to the substrate material with the application of pressure through the consolidation roller. Thermal gradient inside the laminate can be analyzed through the general energy equation (2.1),

$$\nabla \bullet k\nabla T + \rho\dot{q} = \rho C\left(\frac{\partial T}{\partial t}\right) + C\nu\nabla T \qquad 2.1$$

Here $$t = \frac{L}{V} \qquad 2.2$$

Where ρ is the density, C is the volumetric specific heat, k is the thermal conductivity T is the temperature, $\dot{q}$ is the rate of energy released during the crystallization or energy absorbed during the melting of the thermoplastic matrix, ν is the mass flow rate, t is the travel time to cover lay-up length L and V is the process velocity.

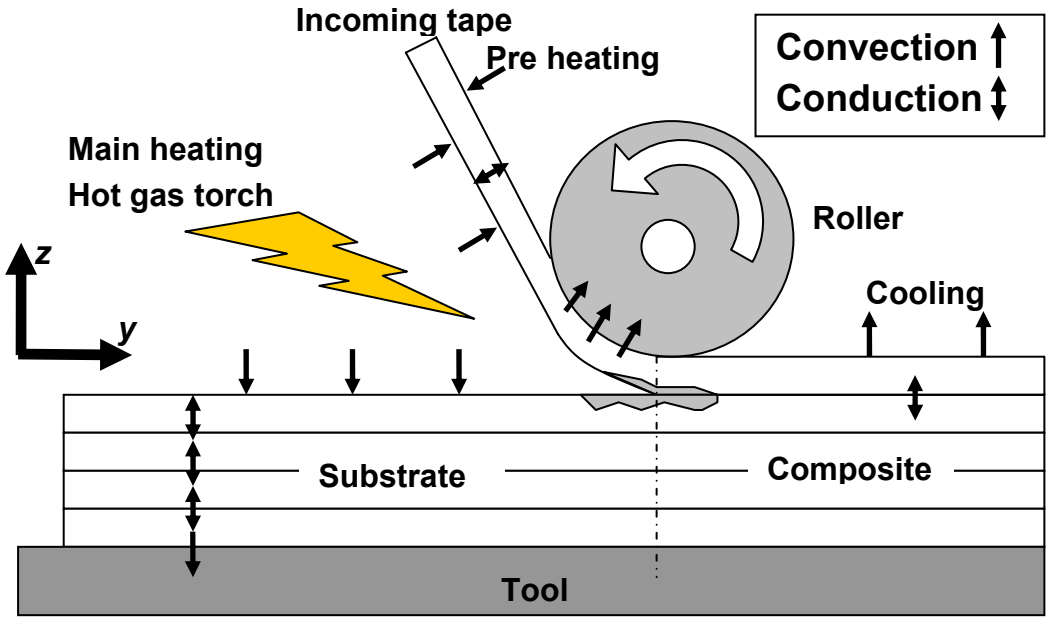

Figure 2.12: Illustration of different thermodynamic phenomena during tape placement process.

Boundary and Initial Conditions

Figure 2.12 shows the different mode of heat transfer in tape placement process. Thermal conduction within the material and heat convection to / from the surrounding is the major source of heat transfer. To solve the equation (2.1), the boundary and initial conditions must be defined. The condition at a surface can be specified by

a) Material surface temperature , $T = T_{surface}$
b) Temperature and convective coefficient of the surrounding atmosphere

$$-k\nabla T = h_m \Delta T$$

Where h_m is the convective heat transfer coefficient. Along with heat transfer between composite and its surrounding atmosphere, contact of tool and roller with composite is also modeled as convective medium [12-13]. By doing so, physical modeling of tool / roller is substituted by the source temperature and heat transfer coefficient on respective location. A number of diversity exists in literature regarding the implementation of this model for tape placement process. The techniques used can be broadly classified into two categories [14]. In the first case, quasi steady state is assumed throughout the process to simplify the problem and steady state heat transfer

problem is analyzed by moving the boundary conditions only. While in second case, the transient heat equation is solved using different numerical techniques by also incorporating material movement. Table 2.1 give an insight about the techniques used for model implementation with their considerations and resulting outputs.

Table 2.1: Overview on the implementation techniques of energy equation (2.1) for tape placement process.

Model type	Dimension	Technique	Consideration for		Output	Ref
			Tool / Roller	Heat generation / absorption		
Transient	3D	FE	X	X	T(t,x,y,z)	[14]
Transient	3D	FE	X		T(t,x,y,z)	[15]
Quasi steady state	2D	FE, FD	X	X	T(t,y,z)	[16-19]
Quasi steady state	2D	FE, FD	X		T(t,y,z)	[12, 20-21]
Quasi steady state	1D	FD	X		T(t,z)	[22-25]

2.4.2 Consolidation under roller

Heating of the incoming tape and substrate material starts prior to the application of consolidating pressure. During this brief interval, the polymer softens and thermally expands and any crystallinity that it has probably melts [26]. The polymer losses strength and releases carbon fiber stresses, dissolved volatiles and entrapped air. This results in an initiation of void growth in the tow. The subsequent application of compaction pressure serves not only to stop void creation, but to reverse it. Similarly material leaving the compacting roller is usually above the glass transition temperature, causing another void growth phenomenon. The level of consolidation is largely associated with the presence of void contents in thermoplastic material.

Two different strategies have been used in the literature to describe the consolidation in thermoplastic material during layup process. The first theory relates [22, 27] the consolidation to bulk matrix and fiber bed compression as a result of matrix flow along the fiber direction. Therefore the pressure distribution under the roller is explained on the basis of D'Arcy's law, which assumes that the matrix flow parallel to

the fibers and there is no macroscopic transverse flow. The other theory [28] based on the experimental testing [29] on unidirectional laminate (that showed prominent transverse squeeze flow but no flow in fiber direction due to high melt viscosity) contradicts this assumption. Experimental testing performs in this study also confirm the transverse flow mechanism [30]. Therefore later approach is selected preferably by researcher for modeling consolidation phenomenon during tape placement process. Table 2.2 summarizes the consolidation model for the tape placement process available in the literature.

Table 2.2: Consolidation model for tape placement process.

Model basis	Ref	Description				
		Non-iso thermal condition	Roller contact pressure	Dimension	Void dynamic	Geometrical changes
Transverse squeeze flow	[28]	X	X	1D	X	X
D'Arcy Flow	[2]		X	1D		X
Viscoelastic	[31]	X	X	2D		X
Intimate contact	[16, 32]	X		1D		

Model for continuum pressure and velocity

Ranganathan et al. [28] developed a model consisting of an integral differential equation (2.3) which determines the pressure *P* under the rotating roller as a function of change in continuum (laminate) thickness *h* (see Figure 2.13).

$$h\frac{\partial \rho^*}{\partial t}+\frac{\partial}{\partial x}\left(\rho^*\int_0^h\left[v_x(0)+\frac{dP}{dx}\int_o^z\frac{\xi}{\eta_T}d\xi+C_1(x)\int_0^z\frac{1}{\eta_T}d\xi\right]dz\right)+\rho^*\frac{dh}{dt}=0 \qquad 2.3$$

Where η_T is the temperature dependent transverse viscosity, ξ is a dummy variable of integration, ρ^* is non-dimensionalized density of the continuum. The values of $C_1(x)$ and $v_x(0)$ in equation (2.3) may be evaluated from the velocity boundary conditions. The equation for the velocity of viscous material can be written as

$$v_x(\xi) = \frac{dP}{dx}\left(F_1(\xi) - \frac{h + K_t F_1(h)}{K_b + K_t + K_b K_t F_2(h)} \left[1 + F_2(\xi) K_b\right] \right) \qquad 2.4$$

Where K_b and K_t are the friction factors at the bottom and top of the ply. F_1 and F_2 are the viscosity function. The change in tape width w can be obtained from the average velocity at the free surface (tape edge)

$$\frac{dw}{dt} = \frac{1}{h}\left[\int_0^h v_x dz \right]_{x=w} \qquad 2.5$$

The compaction force F_c under the roller can be calculated by integrating the pressure along the length L_c and width of the tow i.e.

$$F_c = 2\int_0^{L_c}\int_0^{w} P(x,y)\,dx\,dy \qquad 2.6$$

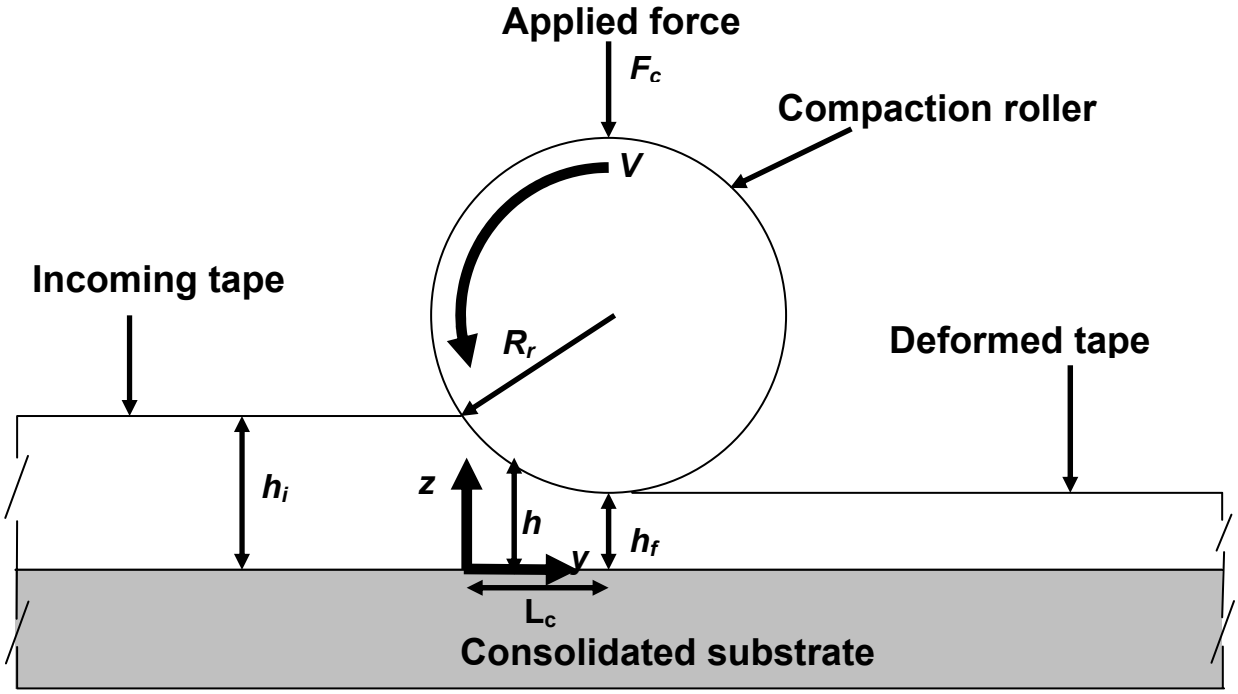

Figure 2.13: Thickness reduction for incoming tape under the roller.

Model for void dynamics

Two mechanisms: void transportation with resin and void compression / decompression has been identified as the major source of intra ply void content variation in insitu consolidation process. Consider a single void in a thermoplastic material represented by the sphere of radius *R* and surrounded by the sphere of continuum fluid with radius *S* in Figure 2.14. The ratio of *R* and *S* will determine the void fraction at this location. Void growth and collapse is governed by a balance between pressure inside and outside the void, the surrounding surface tension and the fluid viscosity. The change in the void radius [28] can be represented by equation (2.7)

$$4\left(\frac{R^{*3}}{S_o^{*3}+R^{*3}-1}-1\right)\frac{dR^*}{dt}+\left(\frac{P_{go}T}{R^{*3}T_o}-P\right)\frac{R^*}{\eta_T}-\frac{2\tau}{\eta_T R_o}=0 \qquad 2.7$$

Where R^* and S^* are non dimensionalized with initial void radius R_o, P_{go} is initial void pressure and τ is the surface tension. Further simplification of this equation; give the relation for rate of change of density as:

$$\frac{\partial\rho^*}{\partial t}=\frac{-3R^{*2}\left(S_o^{*3}-1\right)}{\left(S_o^{*3}-1+R^{*3}\right)^2}\frac{dR^*}{dt} \qquad 2.8$$

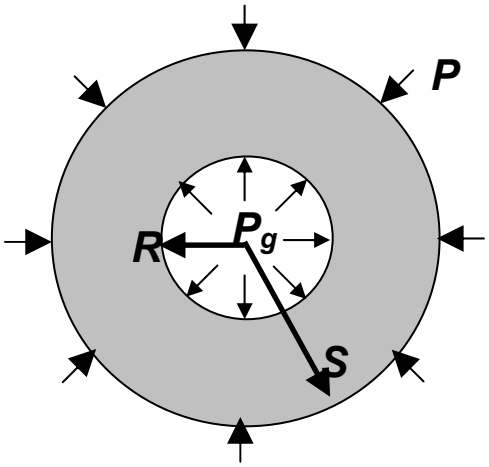

Figure 2.14: Void compression / decompression under the action of surrounding pressure.

2.4.3 Intimate contact and polymer healing

The thermoplastic tape inherits surface irregularities in forms of asperities which arise during the pre-impregnation process. To establish a bond between the layers these asperities should be flatten down as shown in Figure 2.15.

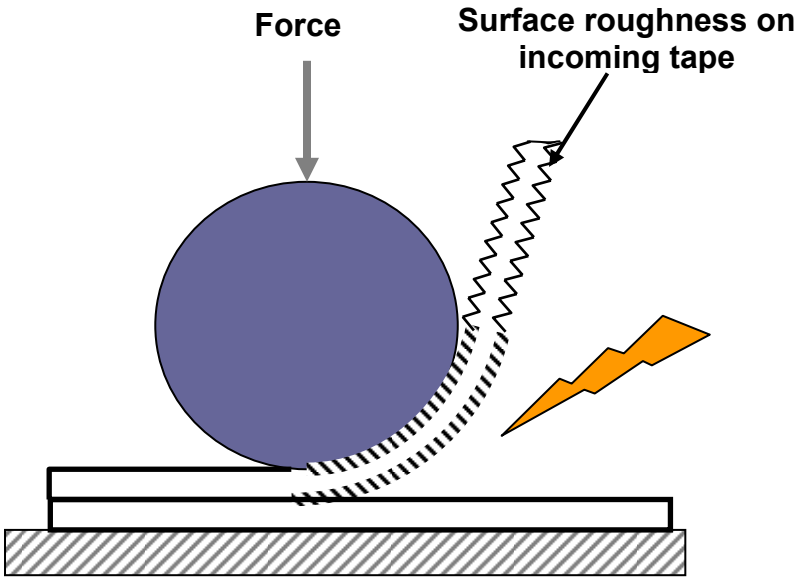

Figure 2.15: Removal of surface roughness and development of intimate contact.

Loos [32] describe the roughness as a rectangle of varying size to model intimate contact development between the layers. Lee and Springer [33] simplify the model with identical size rectangle and show dependency on pressure and temperature. Mantel and Springer [16] further enhanced the model with time varying properties and conditions. But the major difficulties in these models are the exact determination of the roughness factor. Recently Yang and Pitchumani overcome this difficulty and proposed a model [34-36] by incorporating the volume conservation and representing the asperities of rough tape as an effective fractal surface which is flattened down to ideally smooth by the rigid counter surface (roller). Tracing the change in the contact area between effective fractal surface and the rigid counter surface leads to the equation (2.9) for degree of intimate contact D_{ic}.

$$D_{ic}^{(m)}(t) = \frac{1}{f^m}\left[\frac{5}{4}\left(\frac{h_r}{L_r}\right)^2 \frac{f^{\frac{2mFD}{2-FD}+m+4}}{(f+1)^2}\int_{t_{m+1}}^{t}\frac{P}{\eta_T}dt+1\right]^{1/5} \quad \text{where} \quad t_{m+1} \le t \le t_m \qquad 2.9$$

Where *FD* is the fractal dimension, *f* is the scaling ratio, *m is* the number of asperity generations, L_r is the total length of the cantor set, *P* and *t* are applied pressure and duration under roller, and h_r is the recess depth of the first generation asperity. D_{ic}= 100% represent the state where two layers have flatten down and achieved perfect contact.

As the asperities of the rough surface come into intimate contact, healing of the interface occurs through the polymer chain diffusion and entanglement with the other polymer chains, see Figure 2.16. The phenomenon is largely dependent on the molecular structure of the polymer and factors such as time, temperature, and pressure at interface. According to the reptation theory, weld time t_w should be directly related to the longest molecular relaxation time in polymer melt, i.e. the time required for the polymer chain to completely loose its original configuration. The evaluation of non-isothermal degree of healing D_h with time is given by the equation (2.10) [37]:

$$D_h = \left[\int_0^t \frac{1}{t_w(T)} dt \right]^{1/4} \qquad 2.10$$

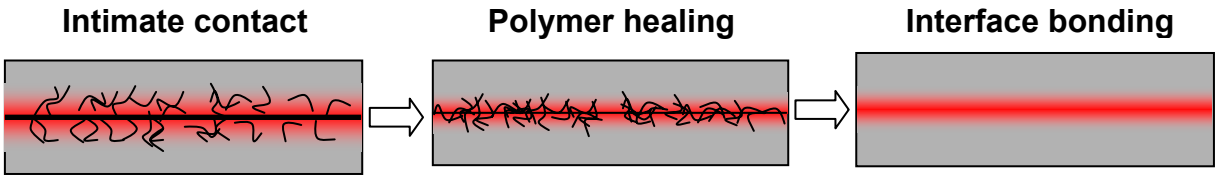

Figure 2.16: Interface heating, polymer diffusion, and bonded material.

Strength development and bonding degree D_b

The consolidation, intimate contact and healing process occur simultaneously during the lay-up process. Note that the consolidation and intimate contact development is pressure and temperature dependent phenomenon, while the healing is solely temperature controlled phenomena [10]. As a result the polymer healing continues to take place even after the roller exit as long as the temperature exceeds the melting point. Mantel [16] describe the term bonding degree D_b based on the intimate contact and polymer healing to trace the extent of bonding level at plies interface.

$$D_b(Simulated) = (D_{ic})(D_h) \qquad 2.11$$

However equation (2.11) is only applicable to an isothermal process. In thermoplastic tape placement process bonding start and end at different times and rates and are also depend on the location in the interface. Ageorges [38] developed a transient approach based on the stepwise calculation to compute the bonding degree. The evolution of the local degree of intimate contact $\Delta D_{ic}(n)$ at step n is shown in Figure 2.17. The corresponding degree of healing is free to develop in succeeding steps till it reaches its maximum value (i.e. 100%). In general the local bonding degree $D_b(n)$ at step n is calculated by the equation (2.12)

$$D_b(n) = \min\left(\sum_{t=1}^{n-1}\left[\Delta D_{ic}(i) \times \min\left(\sum_{j=i+1}^{n} D_h(T_j, t_j), 1\right)\right], 1\right) \qquad 2.12$$

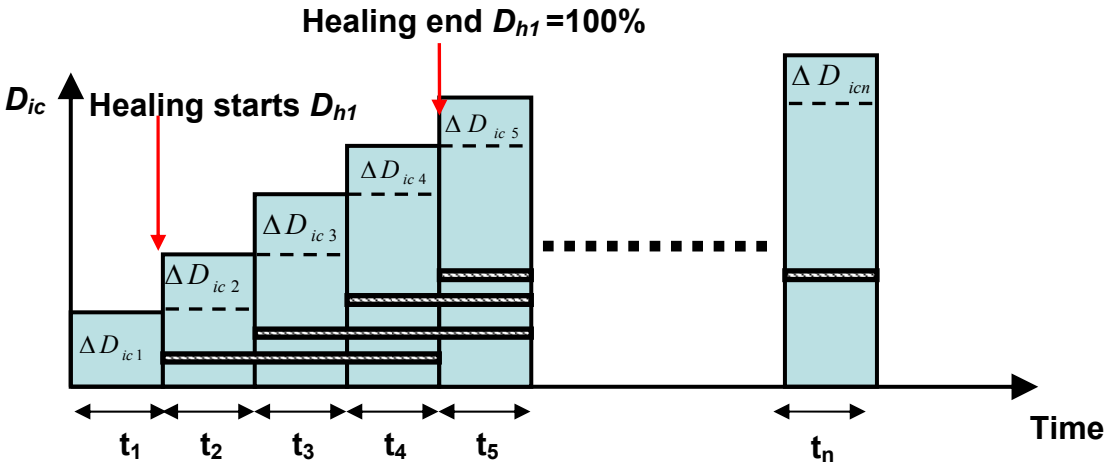

Figure 2.17: Evolution of bonding degree D_b with time in the stepwise computation.

2.4.4 Thermal degradation

PEEK material is normally processed at high temperature around 400 °C due to its high crystalline melting temperature. Hence the thermal stability of the polymer could be limited [39] due to high temperature, long processing duration, and oxidative atmosphere. Such knowledge is necessary to identify optimum process cycles. The

thermal degradation in the process is studied by considering the following two influencing trends.

Thermal stability

Cole [40] found through IR spectroscopy that ether and carbonyl groups in PEEK are less stable in an oxidizing atmosphere. The ether and carbonyl group extract hydrogen from an aromatic ring to form phenol and aldehyde groups respectively. The aryl radicals produced by the loss of hydrogen can then combine to form crosslink between chains, thus causing the changes in the viscosity and in the crystallization behavior. The polymer cross linking rate is experimentally investigated (as in chapter 3) to develop the non-isothermal Arrhenius relation.

$$Rr = A \int_{T340ini}^{T340final} \exp\left[\frac{-E_a}{R_c.T(t)}\right] \qquad 2.13$$

Where E_a and A are the activation energy and pre-exponential component.

Weight loss

In a high temperature oxidative environment the polymer based composite material exhibit complex thermogram. Gupta [41] represent through mass spectrograph that the abundance of oxygen accelerates the weight loss by 50% as compared to non oxidative environment. The activation energy for the kinetic model [42] can also determined through thermogravimetric analysis.

2.4.5 Crystallization

In thermoplastic polymer based composite, crystallinity play an important role in describing the final mechanical properties. As the amorphous thermoplastic polymer never has the crystal, this phenomenon is only happen in semi-crystalline materials. Processing conditions dictate the microstructure, type, shape and size of the crystalline structure in such material. Hence by understanding the crystallization kinetics, processing parameters can be adjusted to optimize the properties of final structure. Several models have been developed for evaluating the crystallinity level during the tape placement process, in the following section an overview is provided about the models that can be used for the tape placement process [43].

Ozawa's model

The model [44] is an extended form of Avarmi equation to explain the process of crystal nucleation and growth for a non-isothermal condition. The relative crystallinity c_r is a function of temperature and cooling rate as:

$$\log\left[-\ln\left(1-c_r\right)\right] = \log\,\phi(T) + n\log\left(\frac{dT}{dt}\right) \qquad 2.14$$

Where $\Phi(T)$ and n can be obtained from crystallinity measurements at different temperature. Due to the absence of the melt kinetic term, the model is not suitable for the clearly describing the melt crystallization as opposed to cold crystallization in dual crystallization mechanism.

Velisaris and Seferis's model

A dual mechanism crystallization (nucleation and growth) model [45] based on two Avarmi expressions show good correlation with experimental data for non-isothermal heating and cooling in tape placement process [46]. The complete expression to evaluate volume fraction crystallinity c is:

$$c = c_\alpha\left(w_1 F_{vc1} + w_2 F_{vc2}\right) \qquad 2.15$$

Where $w_1+w_2=1$; w_1 and w_2 are the weight factors and c_α is the equilibrium volume fraction of crystallinity of the material. F_{VC1} and F_{VC2} represent the normalized volume fraction crystallinity for each crystal growth mechanism namely spherulitic and epitaxial crystal growth.

Choe and Lee's model

Sonmez and Hahn [21] select this model [47] which includes the effect of the temperature of melt from which crystallization is performed. The model is based on the Tobin phase transformation kinetics [48]. The equation for non isothermal crystallization kinetics is given by:

$$\frac{dc_r}{dt} = k_1 \exp\left(\frac{-3E_a}{RT}\right)\exp\left(\frac{-3\psi_1 T_m^0}{T\left(T_m^0 - T\right)}\right)t^2\left[1 - c_r(t)\right]^2$$

$$+ k_2 \exp\left(\frac{-4E_d}{RT}\right)\exp\left(\frac{-(3\psi_1 + \psi_2)T_m^0}{T\left(T_m^0 - T\right)}\right)\left[1 - c_r(t)\right]^2$$

$$\times \int_0^t (t-w)^2\left[1 - c_r(w)\right]dw \qquad 2.16$$

Where k_1, k_2, ψ_1 and ψ_2 are kinetic parameters, E_a is the activation energy and T_m^0 is an equilibrium melting temperature.

2.4.6 Crystal-melting kinetics

An opposite phenomenon to crystallization, it describes the phase transition between the crystalline and molten state. It is also related to semi-crystalline polymers material only. The model [49] can evaluate the degree of melting X_f by relating it to volume fraction crystallinity as:

$$c = c_\alpha(1 - X_f) \qquad 2.17$$

where

$$\frac{dX_f}{dt} = K_m(1 - X_f)^n \qquad 2.18$$

where K_m is described by the Arrhenius relation and n is the kinetic order.

2.4.7 Process induced stresses

Different thermodynamics and kinetics of the process e.g. layup velocity, pressure, temperature and cooling rate may lead to different structures and properties of the processed material. These conditions may lead to process induces defects such as voids, micro cracking, fiber buckling, warpage and / or residual stresses in the final part [50]. The degree of crystallinity achieved also depends on the conditions such as cooling rate, pressure and annealing present during the processing, therefore the

many studies have been carried out in relating the process induced residual stresses to the degree of crystallinity [51-52]. The matrix modulus E_m in composite material can be related to storage modulus E' as:

$$E_m = E' = \frac{J'}{J'^2 + J''^2} \qquad 2.19$$

Where the dynamic mechanical storage flexural compliance J' and the loss flexural compliance J'' can be expressed as a function of the crystallinity [51]. With the updated information of matrix modulus, overall material modulus can also be updated using rule of mixture. Jeronimidis and others [53] shows a method to related process induces (thermal) forces N_x^{CT} and moment M_x^{CT} to mid plain strains ε_i^0 and curvatures k_i^0 using classical laminate theory as:

$$\begin{bmatrix} N_x^{CT} \\ N_y^{CT} \\ N_{xy}^{CT} \\ M_x^{CT} \\ M_y^{CT} \\ M_{xy}^{CT} \end{bmatrix} = \begin{bmatrix} A_1 B_1 \\ B_1 D_1 \end{bmatrix} \begin{bmatrix} \varepsilon_x^0 \\ \varepsilon_y^0 \\ \varepsilon_{xy}^0 \\ \kappa_x^0 \\ \kappa_y^0 \\ \kappa_{xy}^0 \end{bmatrix} \qquad 2.20$$

where A_1, B_1, D_1 are the extensional, coupling and bending stiffness matrices of the laminate.

3 Experimental characterization and testing

The experimental work provides several information regarding the material, process and product quality. Methods and techniques which can lead to proper selection of setup and process parameters are discussed in this section.

3.1 Thermoplastic material

The thermoplastic tape material used in this study is the unidirectional carbon fiber reinforced polyetheretherketone (i.e. CF-PEEK) by Suprem. The reported and the experimentally determined general specifications are shown in Table 3.1.

Table 3.1: Specification for the CF-PEEK material.

Specification	Reported by supplier	Experiment
Thickness	0.13 mm	0.14±0.01 mm
Width	12 mm	11.88 ± 0.025 mm
Density	1.6 g/cm3	1.54 g/cm3
Fiber contents (by volume)	60 ± 3%	58 ± 0.7 %
Matrix contents (by mass)	33%	33± 0.8 %
Glass transition temperature	143 °C	-
Melt temperature	340 °C	343 °C

According to supplier data the grade of the thermoplastic polymer is PEEK 150, therefore following molecular mass values (in Table 3.2) were selected from the literature [18].

Table 3.2: Molar mass details for the PEEK material.

Specification	Number average molecular mass M_n [g/mol]	Weight average molecular mass M_w [g/mol]	Polydispersity index I_p
PEEK 151G	28700	75900	2.6

The thermoplastic material is reinforced with the HEXCEL AS4 high strength carbon fibers with 94% carbon contents and fiber diameter of 7.1 micron. Table 3.3 shows the further technical information [54].

Table 3.3: Properties of Hexcel AS4 12K.

Fiber type	Tensile strength [MPa]	Tensile modulus [GPa]	Elongation at failure [%]	Weight /length [g/cm]	Density [g/cm^3]
AS4	4475	231	1.8	0.858	1.79

The thermal diffusivity and specific heat of thermoplastic material was measured using a NETZSCH model LFA 447 Nano-Flash diffusivity apparatus [55]. The unit used in this testing was equipped with a furnace, capable of operation from 25 to 300 °C. Table 3.4 contains the thermo-physical properties of 2 mm thick CF-PEEK consolidated sample in different directions. The thermal diffusivity decreases and specific heat increases with increasing temperature. Increasing thermal conductivity values at increasing temperature are typical for amorphous and semi-crystalline structures. Significant differences were detected for both directions most probably due to the influence of fiber orientation. The thermal conductivity in fiber direction is approx. 7-8 times higher.

Table 3.4: Thermal properties of CF-PEEK material.

Temperature [°C]	Measurement direction	Thermal diffusivity [mm^2/sec]	Specific heat [J/g.K]	Thermal conductivity [W/m.K]
25	Transverse to fiber	0.575	0.886	0.813
300		0.413	1.803	1.188
25	Parallel to fiber	3.922	0.886	5.542
300		3.256	1.803	9.364

3.2 Thermal mapping under the hot gas torch

Temperature studies in impinging jets reveals its dependency on the Reynolds number, nozzle to plate distance, nozzle geometry, target shape orientation, cross flow, etc [56]. As a result, different advance techniques like cooling ring [57], infra red remote sensing [15] and high temperature thermocouple [58] have been implemented to thermally map the impinging flow around the nip point. Simple and quick setup to use thermocouple encouraged several [13-14, 18] for the hot gas temperature estimation.

The adiabatic temperature of a stoichiometric hydrogen–air flame is approximately 2807 °C. In high temperature impingement, the combustion products diffuse through the boundary layer to the colder surface. Baukal [58] described the drop of heat flux as a function of torch distance from impinging surface. Martin [59] state that for a torch at an angle of 15° the heat transfer coefficient drops by 43% corresponding to ones for the normal impingement. Considering these circumstances the thermocouple method was selected for the temperature measurement. An S-type thermocouple (SAT-24-12 by omega) with wire diameter of 2 mm was used which has the capability to measured up to 1650 °C. Calibration of thermocouple was performed inside the autoclaved and under the hot gas torch with K-type thermocouple up to 1000 °C.

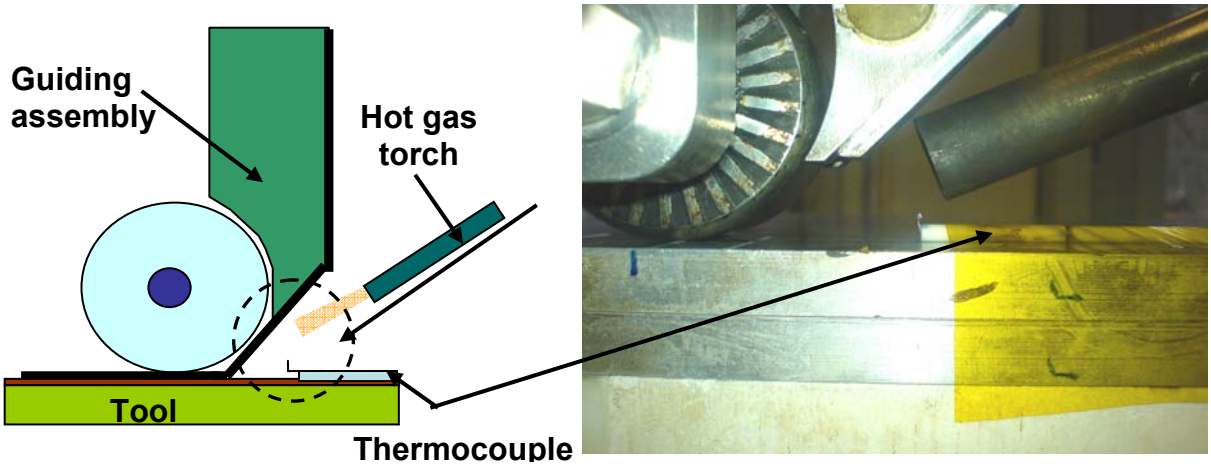

Figure 3.1: Hot gas temperature measurement using thermocouple.

A ceramic tube protected the bare thermocouple wires, exposing only the juncture to the hot gases. First thermocouple was fixed on the tool plate with the help of PTFE tape so that the juncture was about 5 mm above the tool surface. The tool plate was then precisely positioned under the hot gas torch (Figure 3.1) on locations shown in the mapping diagram in Figure 3.2. Although unlimited points can be selected for temperature measurement, as the positioning under hot gas torch was carried out by moving the tool plate, only 18 points were selected over the length of 40 mm as a first approximation. For incoming guide assembly measurement was performed at the centre line L-2 only. Efforts were made to take measurement close to the nip point (roller centre), but the narrow space made it difficult to fix the thermocouple hence forced the first measurement at least 10 mm from the roller centre.

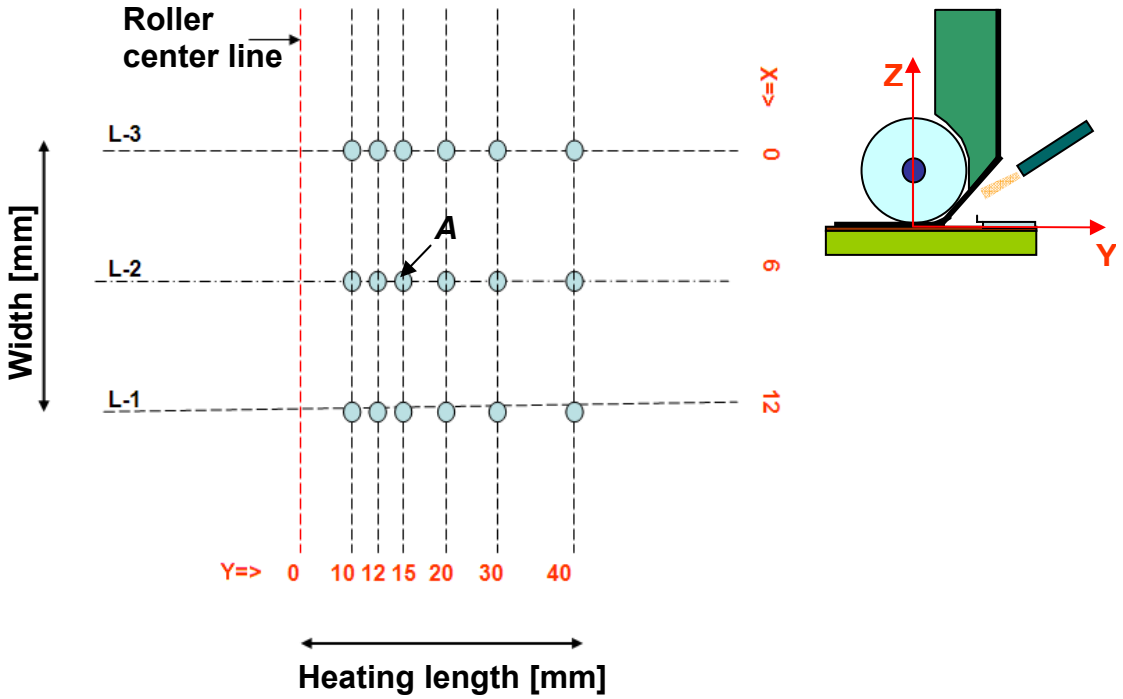

Figure 3.2: Locations over the tool for thermal mapping under the hot gas torch.

Consider the temperature profile in Figure 3.3 at a point *A*, which lie on the middle line L-2 and 15 mm apart from the roller centre (see Figure 3.2). Thermocouple was positioned at this location and hot gas torch was turned on till the temperature reading became stable and reached the steady state condition. Since the thermocouple was stationary at the position, the temperature reaches the steady state value with in few seconds.

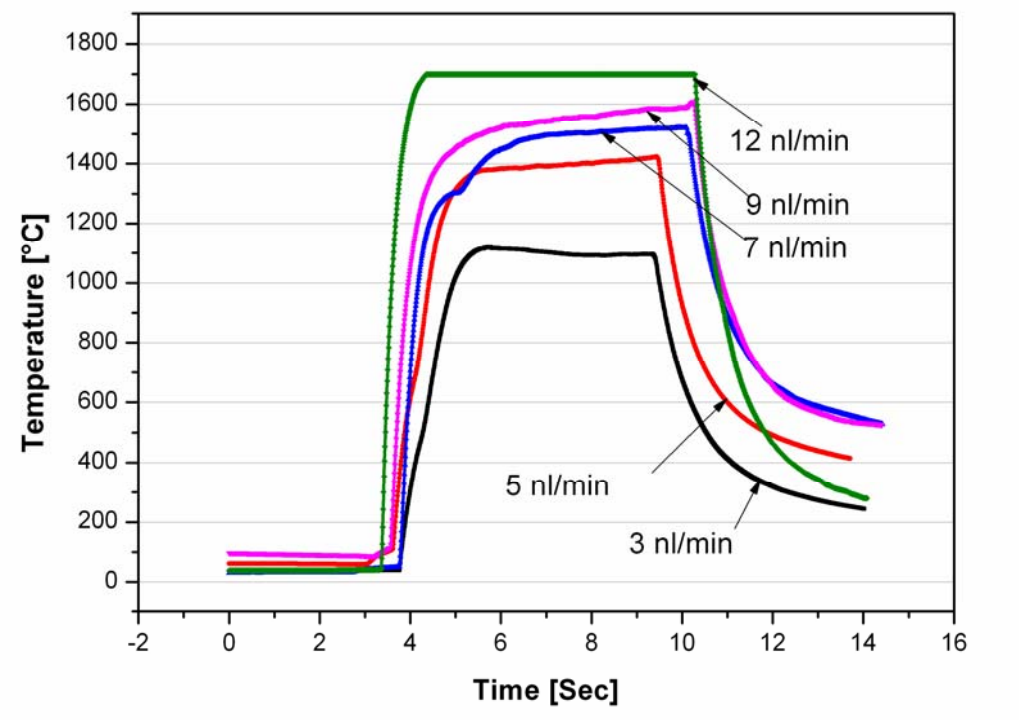

Figure 3.3: Temperature profile 15 mm from nip point (point *A* in Figure 3.2) at different gas volume. Thermocouple is fixed with tool and stationary at this location.

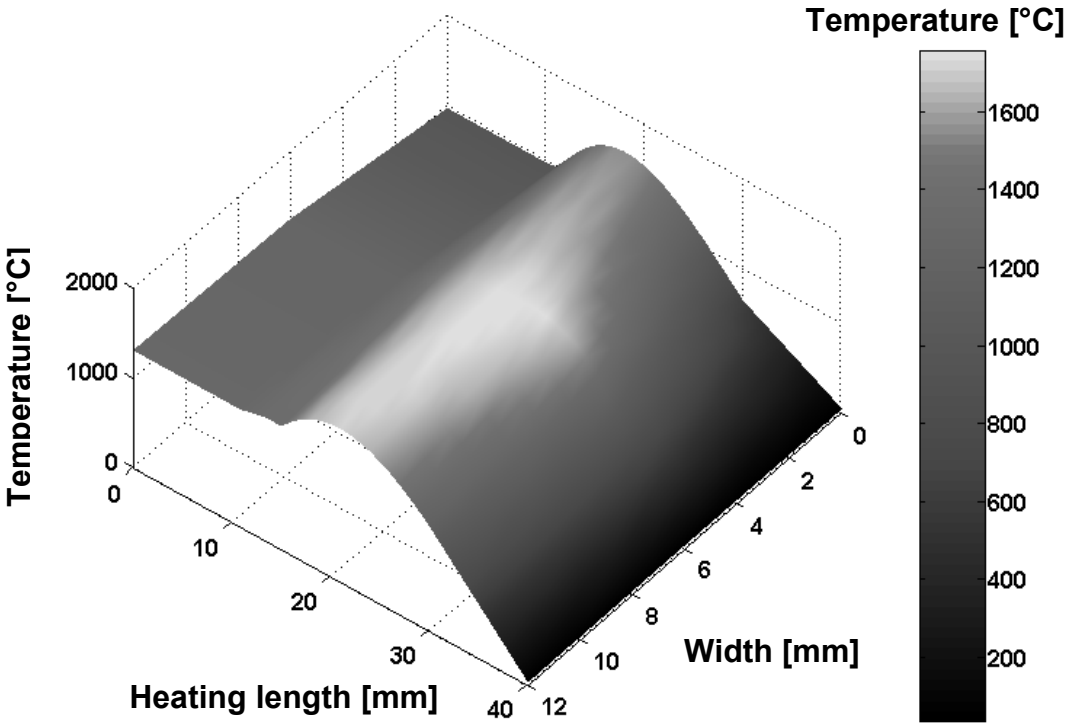

Figure 3.4: Temperature distributions under the hot gas torch for 5 norm liter/min.

Similar data was also collected for other points and interpolated in X and Y direction to generate the map as shown in Figure 3.4. Due to unavailability of the data near the nip point and the expected stagnant condition for the flow in the enclosed space, data is extrapolated up to the nip point region. Resulting temperature distribution is highly variable along the length, while it is seemly constant in the width direction. Location of maximum temperature exists at the mid width and away from the roller centre line. This is in complete accordance with the previous study [59] which states that the point of maximum heat and mass transfer does not coincide with the point of intersection between inclined jet axis and surface. The point of maximum temperature shifts by a length ΔY toward that part of the jet which is being deflected in the acute angle (see Figure 3.5).

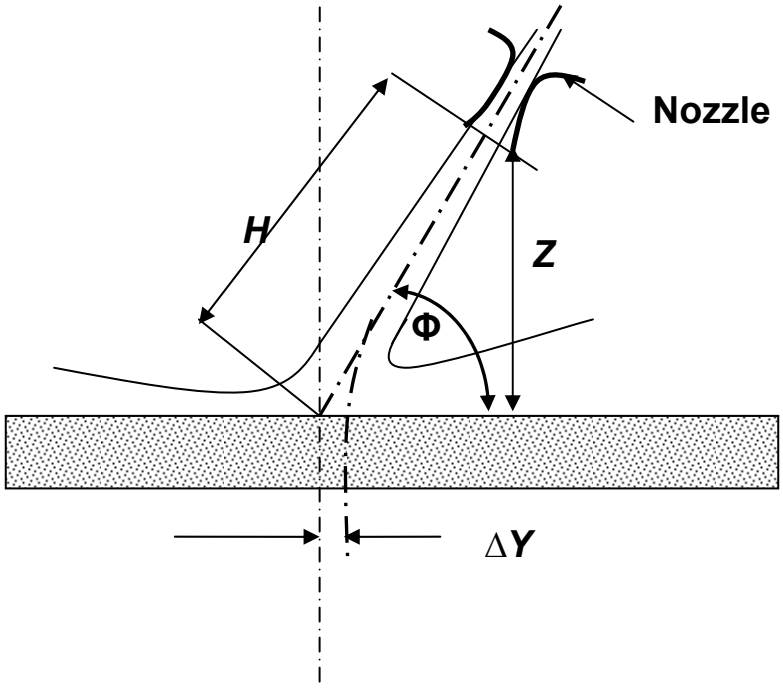

Figure 3.5: Displace location ΔY for the maximum temperature for an inclined impinging jet.

3.3 Equivalent heating length

Although there is also a slight variation of temperature in width direction, but the assumption of uniform temperature distribution in width direction; allow an easy way to estimate the heating length. By considering the points only on line L-2 in Figure 3.2, 3D map in Figure 3.4 can be represented by the points 'abcd' in Figure 3.6(a). Selecting only the point 'e' & 'f', will provide the actual heating length shown in Figure 3.6(b). If T_{max} represent the maximum temperature on the e-f section, then integrating the area under the curve and equating it with the rectangular area will result in an equivalent heating length. With the conservation of total energy and such transformation, a single value of the hot gas temperature can be used as the equivalent heating length.

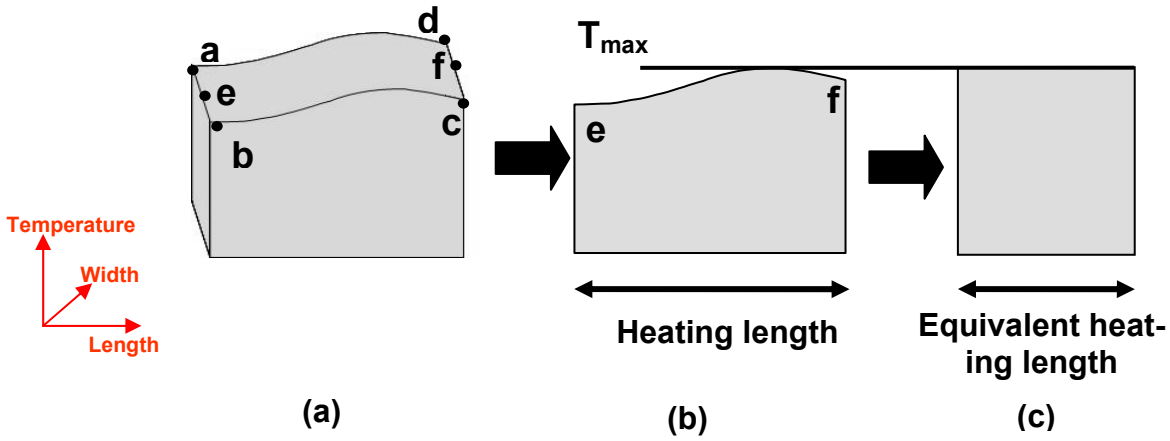

Figure 3.6: Estimating equivalent heating length.

Figure 3.7(a) shows the results for the temperature and equivalent heating length corresponding to selected gas flow volume for the guided assembly. Hot gas temperature rises with the increasing gas volume but the equivalent heating length has constant value. This indicates availability of additional thermal energy at higher gas volume. The scatter in temperature is obtained by observing the variation in measurement at points (L-1 to L-3) on Y=15 in Figure 3.2, which lie in the maximum temperature region. Furthermore to consider the slight temperature variation in width direction, heating length are also calculated for line L-1 and L-3 and represented as the scatter in the same Figure 3.7.

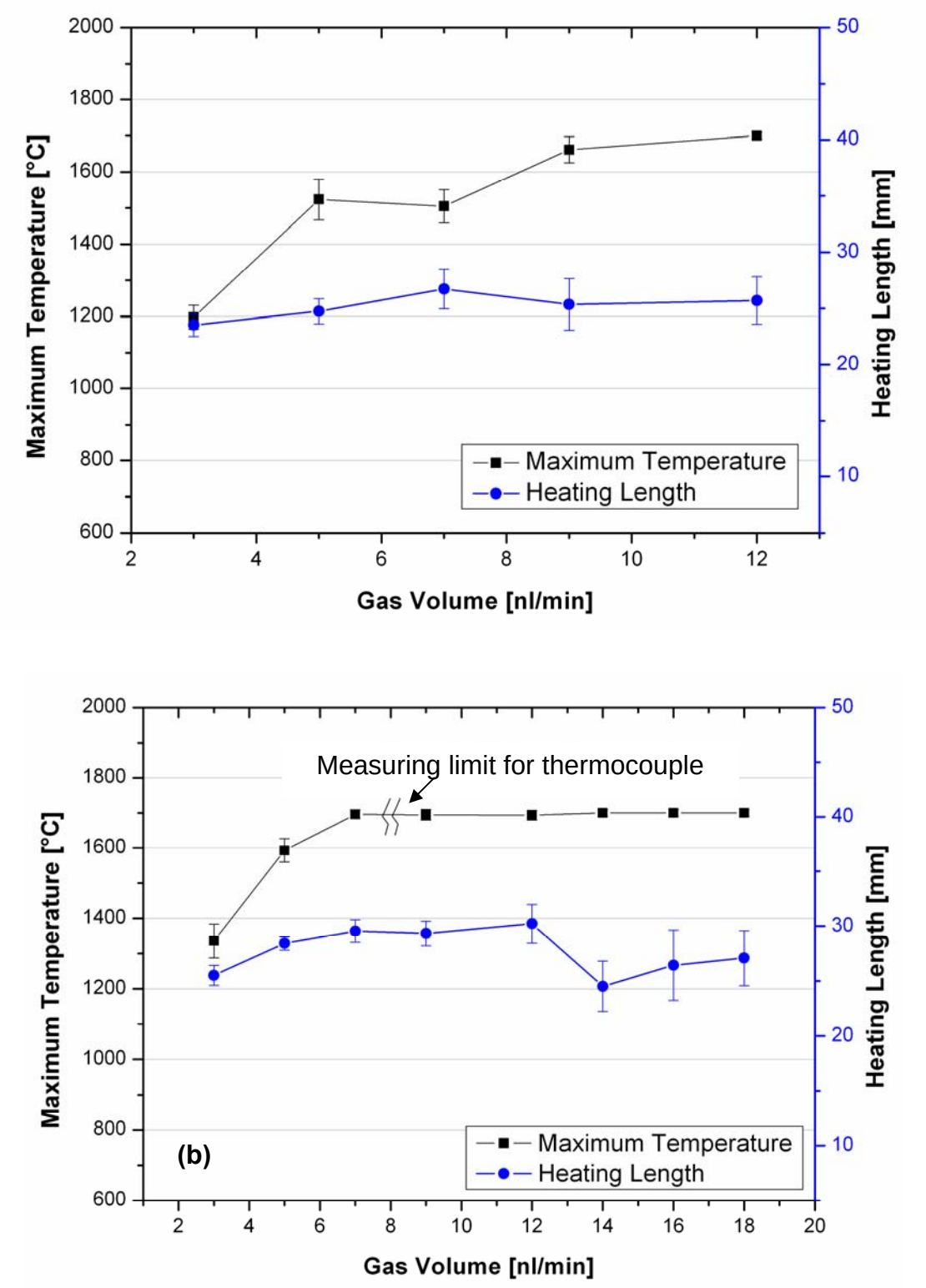

Figure 3.7: Hot gas temperature and equivalent heating length at different gas volume flow for (a) Incoming guide assembly (b) over the tool surface.

A similar trend is also visible for the temperature over tool surface (see Figure

3.7(b)). The temperature rises more sharply reaching maximum measurable limit (1700 °C) for the thermocouple at 9 norm liter/min. Thereafter thermocouple reported this maximum value for further increase in gas volume. The interesting observation is a decrease in the equivalent heating length over 12 norm liter/min. Although no further information is available about the actual maximum temperature, but the measurement shows sharp drop in temperature from points at Y=15 to Y=40 (in Y direction) at higher gas volume. This consequently resulted in smaller heating length for higher gas volume. One possible reason is the concentrated hot gas impingent jet due to high energetic velocity which consequently results in smaller heating length.

3.4 Convective heat transfer coefficient

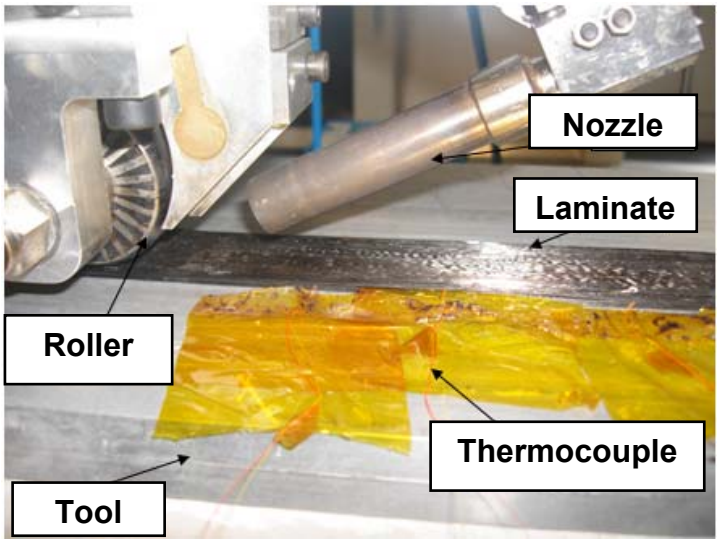

Figure 3.8: Temperature measurement inside the laminate through embedded fine gauge K-type thermocouple.

Heat convection under hot gas torch is thoroughly investigated by several authors and has evaluated distinct values of convective heat transfer coefficient (h_m) for their manufacturing setup. Toso [15] used the infrared picture for the hot gas nitrogen in the vicinity of nip point and found it to be 21 W/m^2 °C. For the same gas Kim [12] assumed coefficients of 900 W/m^2 °C and 250 W/m^2 °C for substrate and incoming tape respectively. Tierney [24] used the mathematical formulation to determine the heat transfer coefficient for impinging nitrogen, no particular value was provided for the reference. Shih [13] obtained a convective heat transfer coefficient of 260 W/m^2°K and Noha [14] determined it to be 350 W/m^2°C for hot dry air by comparing the tem-

perature history from numerical result with experimental work. To determine the convective coefficient of heat transfer, temperatures in three different layers of the 14 layered already placed CF/PEEK laminate were measured with embedded fine gauge K-type thermocouple see Figure 3.8.

A 1D through thickness heat transfer model based on equation (2.1) is used to predict the temperature at these three locations using some estimated value of h_m. Once the predicted temperature profile matches well with the measured temperature at three locations, value of h_m is selected as the heat transfer coefficient for this particular gas flow volume as shown in Figure 3.9.

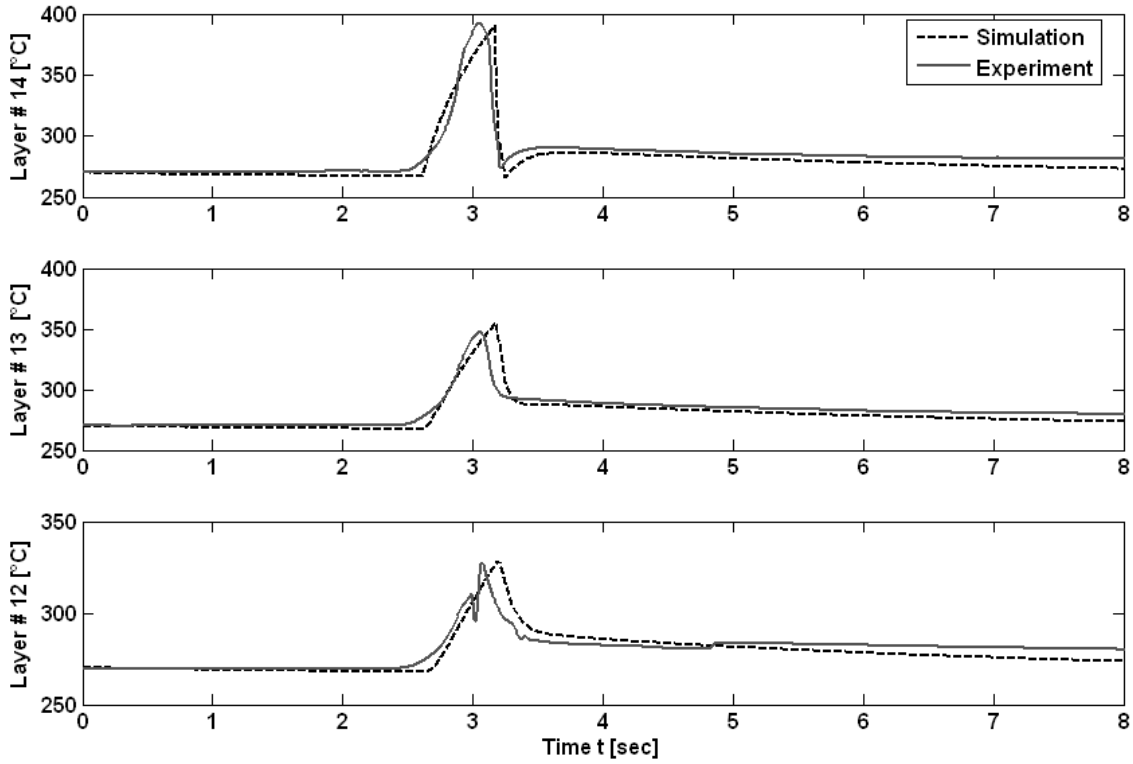

Figure 3.9: Relative comparison of experimental and simulative temperature data under layer 14, 13 and 12 (Gas volume 6 norm liter/min, velocity 3 m/min)

Some interesting conclusions from this study are

- As the combustion gas velocity is much higher compared to the process lay-up velocity, it is realized that there is no significant change in heating length for particular lay-up velocity (i.e. heating length is independent of lay-up velocity).

- Similarly a single value of heat transfer coefficient is found suitable for a particular gas volume, irrespective of lay-up velocity see Figure 3.10.
- General increasing trend is visible in Figure 3.10 at higher gas volume.
- Peak and valley depicts the wavy behavior in Figure 3.10. Peaks correspond to higher temperature measurement within the laminate at low gas volume (e.g. 6 norm liter/min) as compared to higher gas volume (8 norm liter/min). Exact reasoning for this is not available but it might be due to the gases escape. Kim [60] performed the CFD analysis for the flow in nip point region and concluded that flow is stagnant at nip point region and high turbulent afterward. The maximum value of heat transfer coefficient and hot gas temperature are located before the nip point (not at the nip point). The turbulent flow at higher gas volume causes the lateral flow and significant gases to escape from the composite surface.

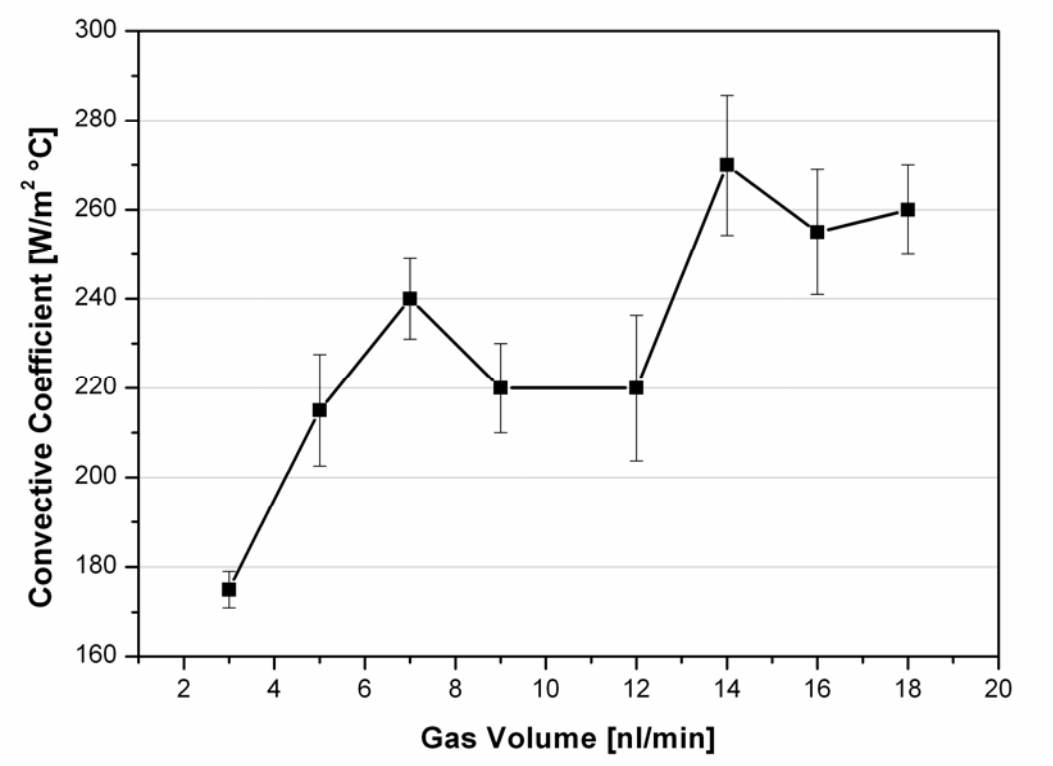

Figure 3.10: Convective heat transfer coefficient between the hot gas and composite surface at different gas volume flow.

Due to small variation around the mean values, it is decided that to use the actual curve for the further analysis and simulation instead of equating it with some linear fit.

The difficulty in positioning the laminate with embedded thermocouples on guiding assembly restricts the similar study for the determination of convective heat transfer coefficient for incoming tape.

The theoretical and experimental study on the variation of roller temperature is also performed. Noticeable temperature variation is found out during the winding process, where roller had continuous contact with hot tool or composite for the extended duration. But the change in roller temperature is negligible for the tape placement process, where the continuous contact exists for the short duration during the lay-up. Experimental testing shows 10 °C rise in roller temperature as it comes in contact with incoming tape and hot substrate material. But it drop down by 5 °C before roller makes the second contact. For continues rotation maximum variation of 10 °C was marked, as the thermal equilibrium established between the roller and the surrounding environment through natural convection. Table 3.5 shows the iteratively obtained values of convective coefficient between roller and composite material by assuming constant temperature over the roller contact length.

Table 3.5: Estimated convective heat transfer coefficient between roller and composite substrate.

Roller Temperature [°C]	Convective heat transfer coefficient [W/m2 °C]
50	65000
60	60000
80	55000
90	55000

3.5 Material deformation

3.5.1 Thickness build-up

Over the glass transition temperature T_g, thermoplastic materials are sensitive to geometrical deformation. Understanding of the thickness build-up and width changes can help the manufacturer to estimate the number of lay-up and expected material requirements for desired laminate dimensions. A laser distance measuring sensor (Weltoc) attached to the placement head was used to measure the thickness with laminate stacking. Exact horizontal location was about 75 mm from the centre of the

consolidation roller, this provide enough lap for any post consolidation changes inside the tape. The device was first calibrated and referenced to zero with respect to tool. The sensor identifies the laser reflection from the newly laid up layer and calculate the distance by comparing from referenced value. Data was then stored through a data logger (spider 8) system into the computer for further analysis. Figure 3.11 shows the data obtained for the lay-up with 9 m/min and 4 norm liter/min.

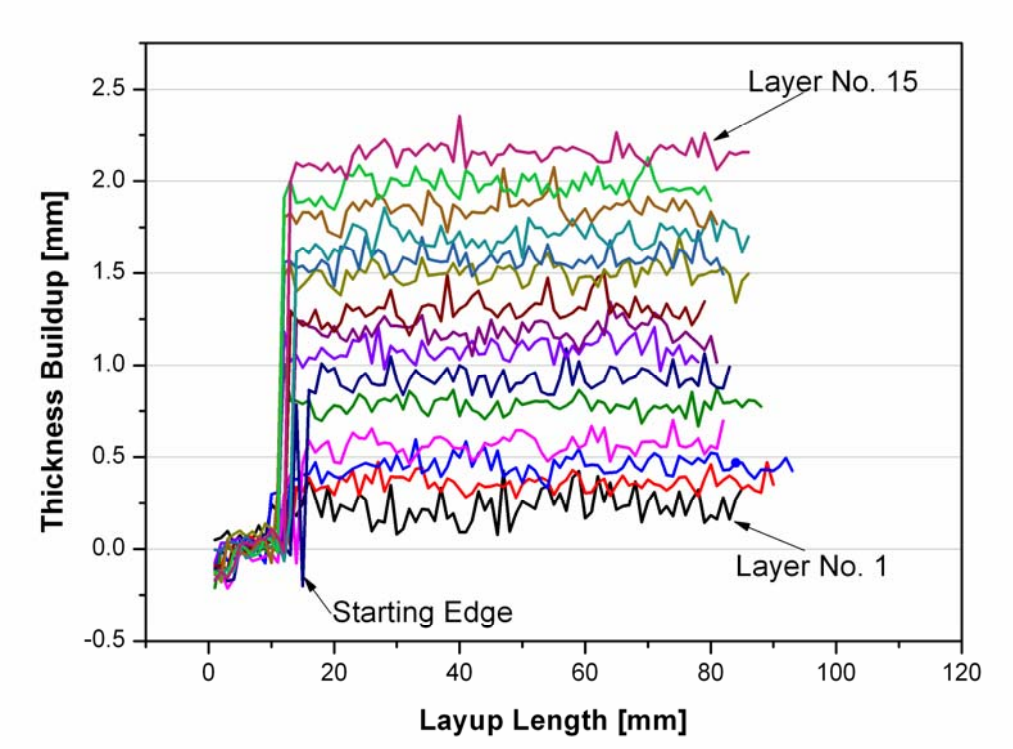

Figure 3.11: Thickness measurement during the lay-up process (Gas volume 4 norm liter/min, velocity 9 m/min).

The data contained the disturbance due to roller dynamics and material surface roughness. FFT filter was used to smooth the data over the lay-up length, and the laminate thickness for additional lay up was determined as plotted in Figure 3.12. Thicknesses build up show the linear relation, with more compaction at higher gas volume.

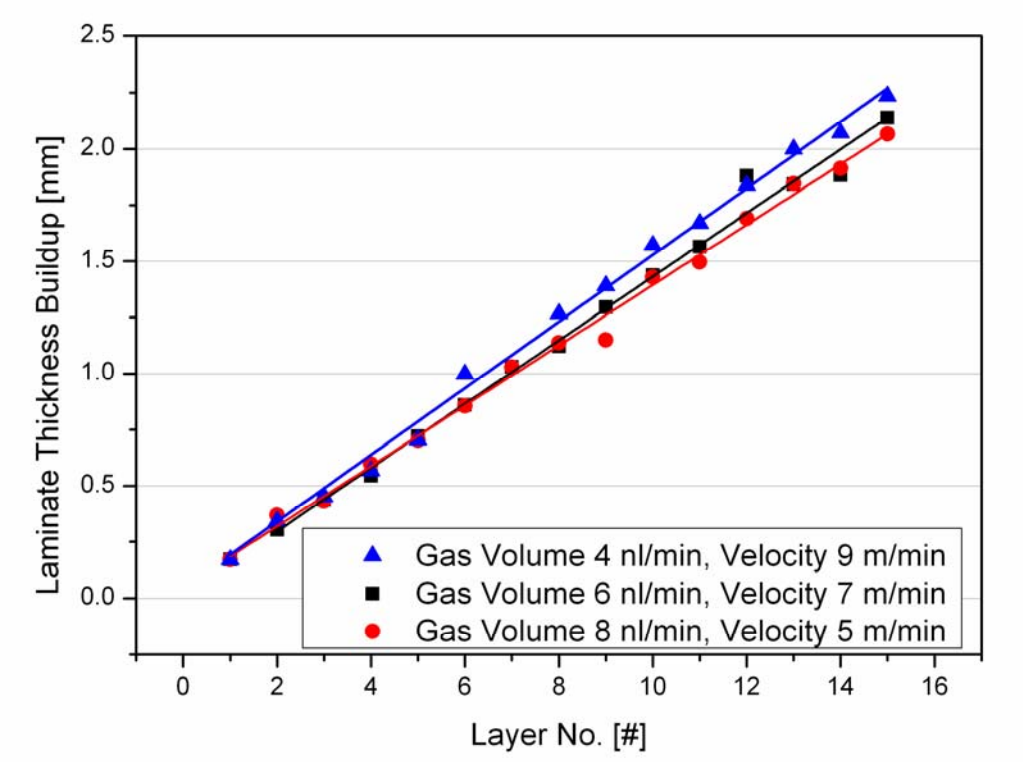

Figure 3.12: Linear trends in laminate thickness build-up.

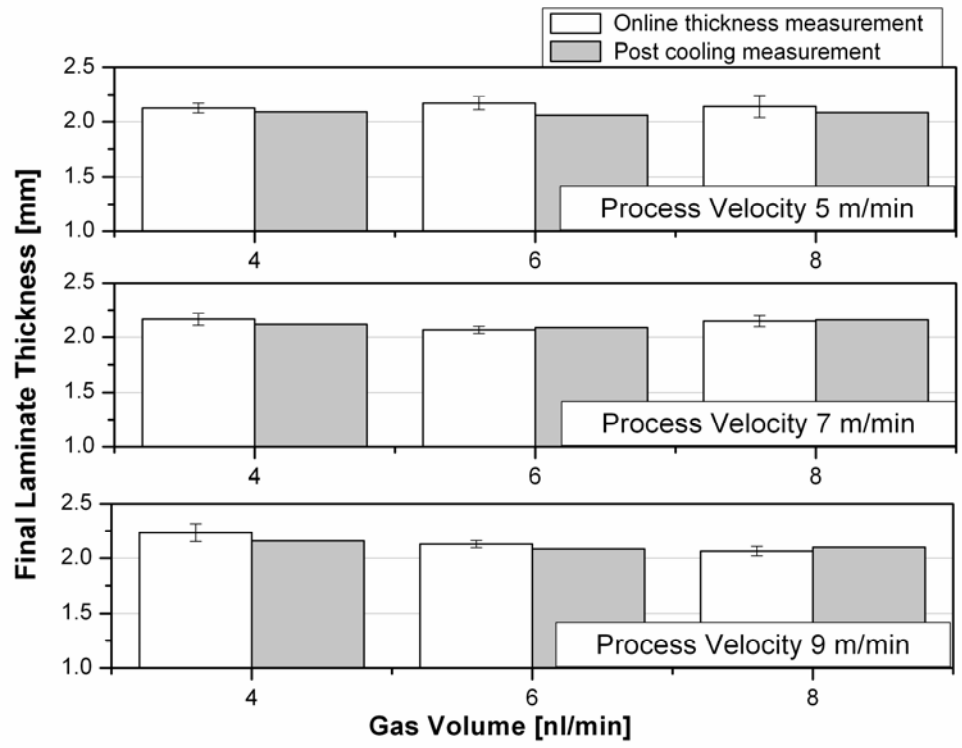

Figure 3.13: Laminate thicknesses before and after cooling.

Manufactured laminates were again measured using micrometer after being cool down to room temperature. The trapped void inside the laminate at tool temperature obeys the natural gas law ($PV_v=nR_cT$) during cooling. The drop of void internal pressure and its volume results in thickness contraction. A further 2-5% decrease in thickness was observed in most of the laminate (see Figure 3.13).

3.5.2 Width change

Assuming a conservation of volume, the variation in tape thickness is directly related to the width change. Experiments were carried out on the tape placement test rig to measure the width change for a single tape. A CCD camera installed behind the consolidation roller as shown in Figure 3.14 captured the images of the deformed tape. A Labview code analyzed the online data and identified the tape edges by differentiating the dark color pixel from white surroundings. For the planned study, tapes were first cut into 350 mm length and scanned under the CCD camera without consolidation to record the initial width. In the next step, the width change was recorded during the lay up of single tape on hot tool. Lay up velocities 3, 5, 8, 10 m/min and hot gas flow volumes of 4, 6, 8, 10, 12, 14, 18 norm liter/min were selected.

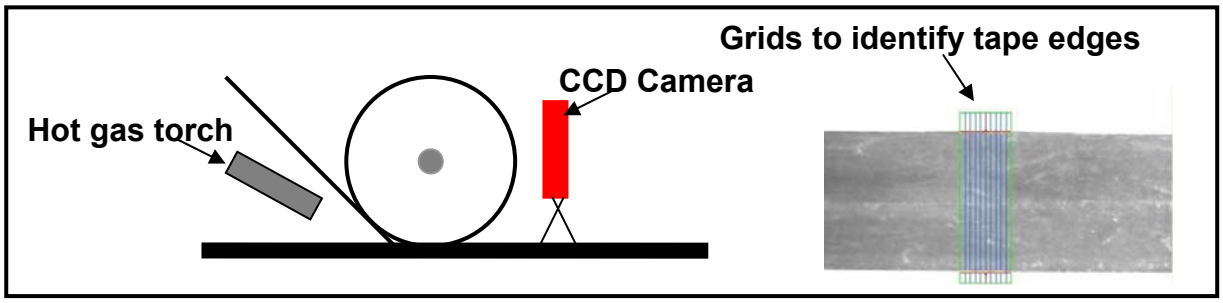

Figure 3.14: Width measurement behind the consolidation roller using CCD camera.

Figure 3.15 shows the initial and final width change data measured through the CCD camera. The variations in the final width data indicate the non uniformity in transverse direction. The fiber and matrix move together in thermoplastic materials. Ideally all the fibers should be arrayed perfectly parallel, but in practice with very fine fibers such as 7 µm diameter carbon fibers; there is some slight twisting in the fiber tows. Hence the transverse displacement along the fiber direction is not similar and results in edge variation.

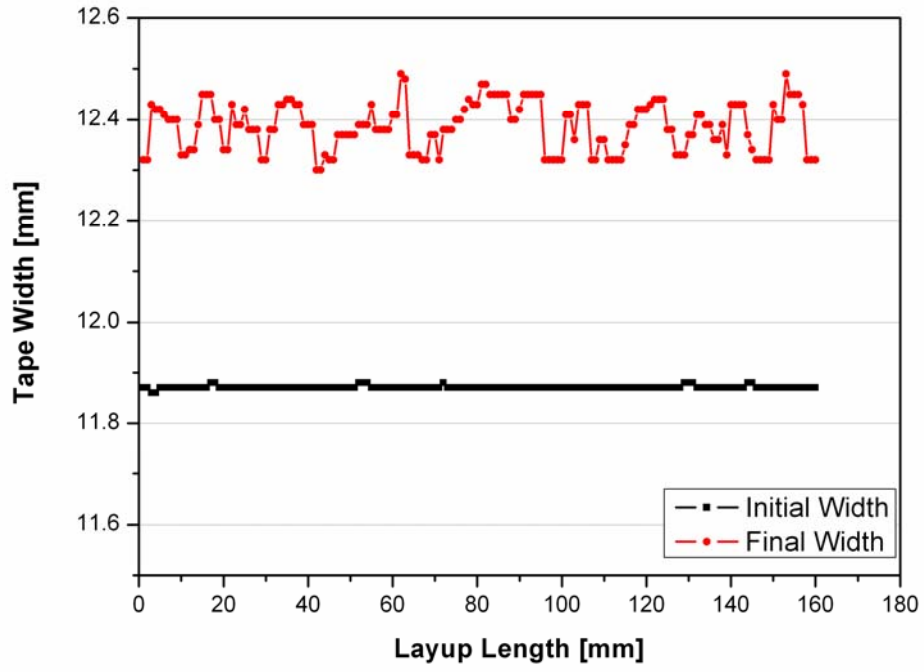

Figure 3.15: Initial tape width before consolidation and final tape width after consolidation (Gas volume 18 norm liter/min, velocity 3m/min).

The complete insight for a width change in a single tape with different lay-up combination is shown in Figure 3.16.

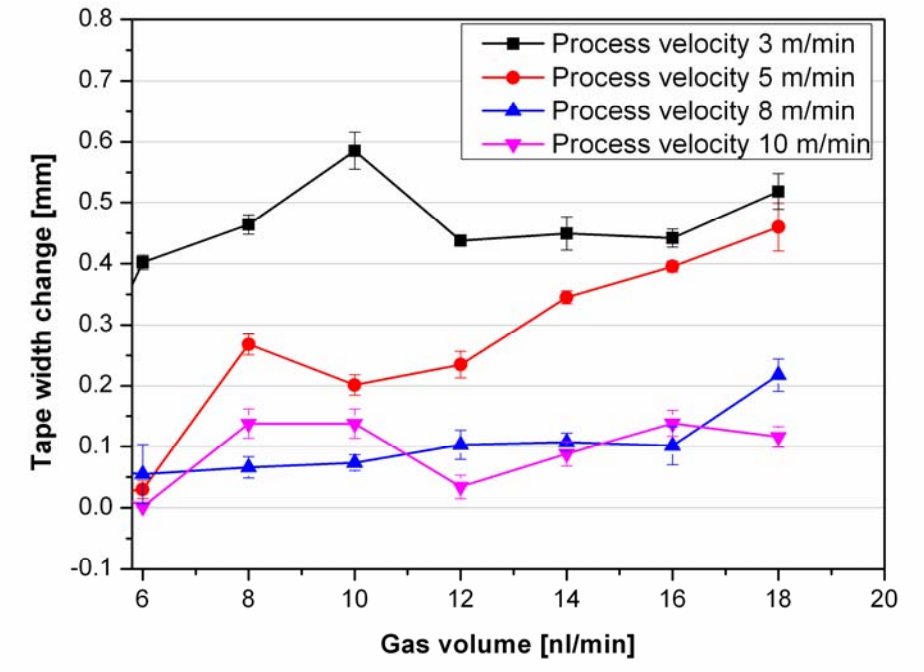

Figure 3.16: Width variations for a single tape at different lay-up configuration.

Large changes (0.5 mm) at low lay up velocity of 3 m/min indicate the high thermal energy input for sufficient deformation. An increasing trend with increasing gas volume at 5 m/min laid up velocity shows the gradual rise in energy input. Similarly small width change (< 0.1 mm) shows lay-up combination with low energy input. Scatter in figure is estimated by averaging the data from five lay up and plot shows marked variation for high energy combinations.

All the laid up tapes were also analyzed under the light microscope. In all combinations tape deformed into three different shapes as shown in Figure 3.17. If the initially rectangular tape edge is designated as type I, then the three shown patterns can be classified as type II, III and IV deformation respectively [61]. The values in the Figure 3.17 indicate the width deformation from the tape's center.

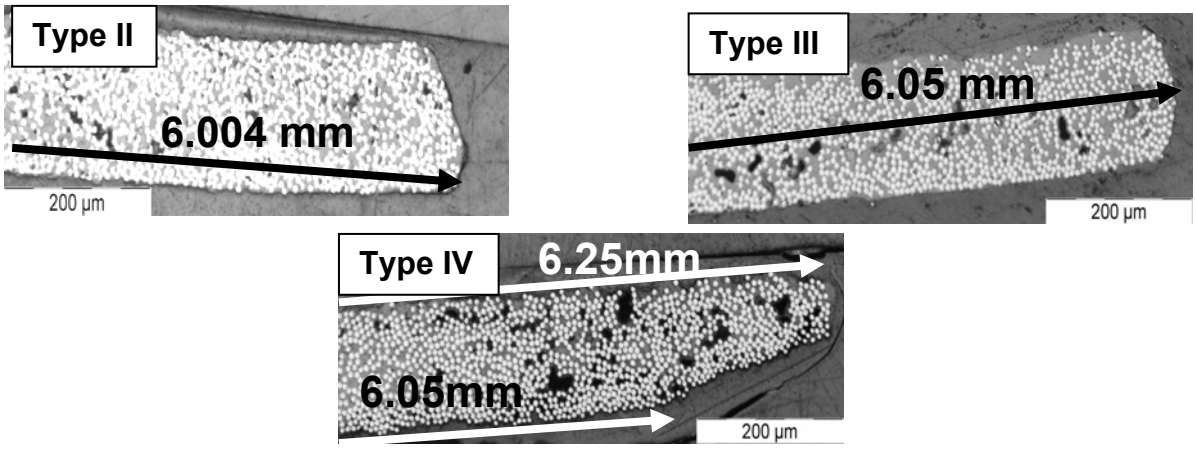

Figure 3.17: Type II, III and IV edges deformation in single tape during tape placement process. Measured half width for each case is also represented.

To further investigate, deformed types are plotted against the lay up velocity and hot gas volume flow in Figure 3.18. Low lay up velocity supplemented by the higher hot gas volume flow generated type IV deformation and symbolizes the high input energy combination. Inversely high lay up velocity with low hot gas volume flow produced type II deformation corresponding to low input energy combination. Transition of type IV to type II was observed by type III deformation through intermediate energy as marked by the solid lines in figure.

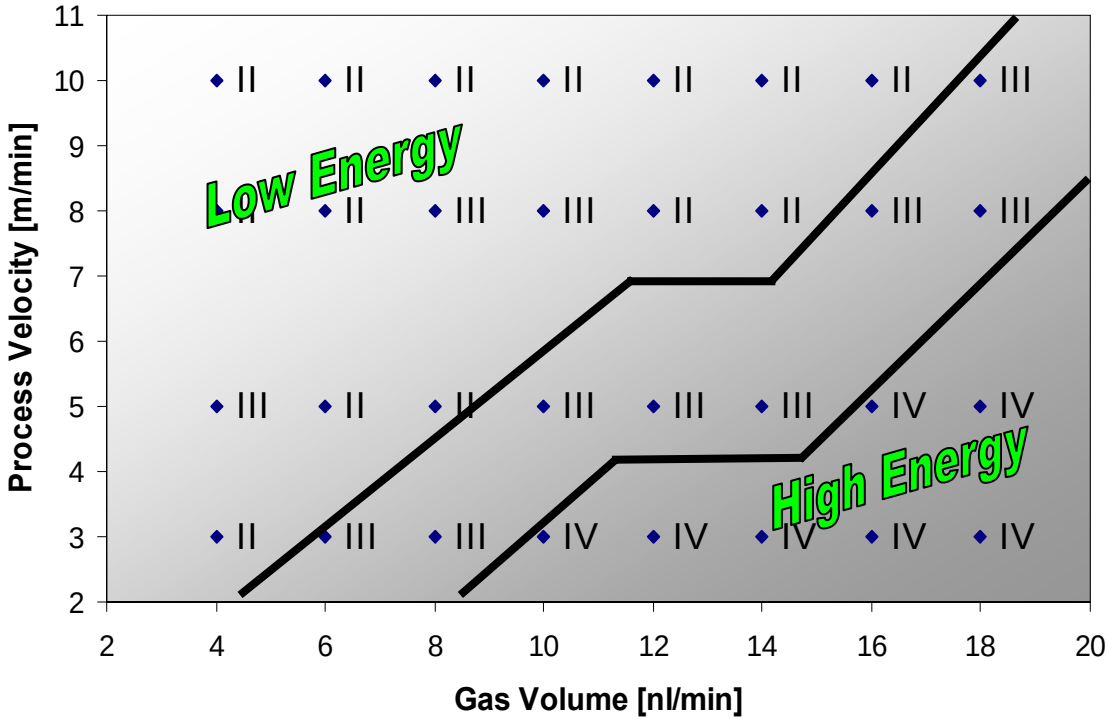

Figure 3.18: Edges deformation with combination process parameters.

3.6 Surface roughness

Techniques which have been used to measured the surface roughness include direct measurement using profilometer or through photomicrograph of tape cross section. Dai [23] demonstrated the use of photomicrograph to estimate the roughness factor. Loos [32] characterized the thermoplastic tape surface topology using Talysurf 4 profilometer. Yang [36] also used the profilometer and for the first time used the method describe by Majumdar [62] to apply the roughness data (in the form of fractal cantor set based description) to the intimate contact development during bonding process. Profile measurements on the thermoplastic tape were conducted on the FRT white light profilometer. The surface of the original thermoplastic tape from Suprem used in this study is modified with diamond coated burr cylinder to generate artificial roughness of four different heights, for evaluating the trend of mean roughness maximum height (R_z) and fractal dimensions (*FD, f)* (see Figure 3.19). Five samples were taken from original and each of the modified tape. Scans were performed over an area of 2x2 mm^2 with 200 evenly distributed points per profile line.

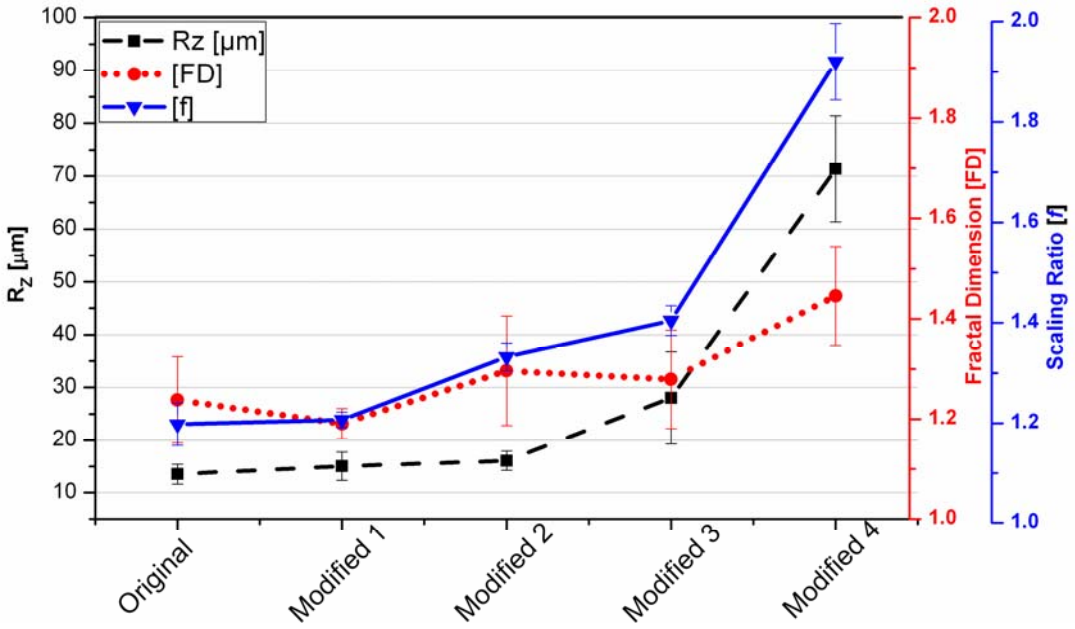

Figure 3.19: Surface roughness for different CF-PEEK tapes showing the relation between roughness parameter R_z and fractal dimensions '*FD*'.

Fractal dimension in all cases is calculated according to the method described in literature [30, 63]. The comparison indicates the direct relation between classical mean roughness parameters R_z and fractal dimensions. An increase in dimension *FD* increases the jaggedness of the surface and therefore the total area of the surface. The *f* parameter controls the absolute amplitude of the asperities height hence shows the similar trend with R_z. Figure 3.20 shows the roughness scans for the original tape (*FD* = 1.3 and *f* = 1.1) and the highly rough case i.e. modified 4 (*FD* = 1.45 and f = 1.9), the second profile represent a relatively rough tape surface.

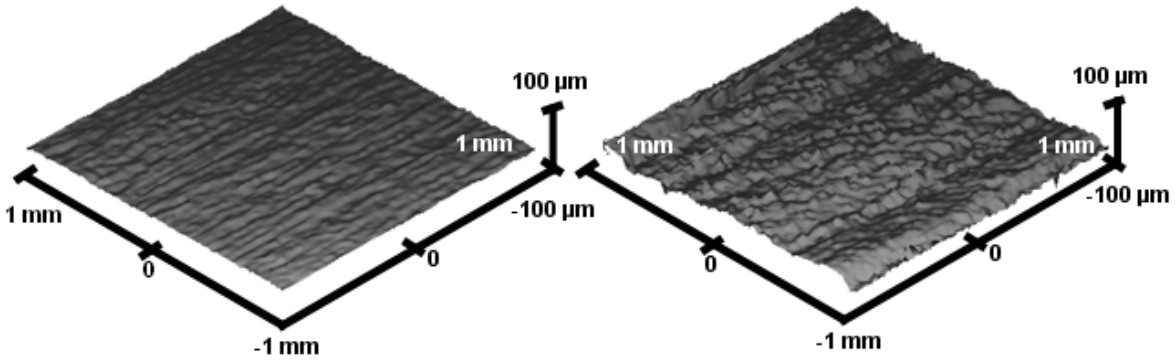

Figure 3.20: Surface profile for the original CF-PEEK tape (left) and modified 4 tape with rough surface (right).

3.7 Rheological properties

3.7.1 Transverse viscosity of unidirectional thermoplastic material

Under the processing conditions, unidirectional thermoplastic materials like CF-PEEK exhibit anisotropic behavior. The inextensible fiber contributes to the higher longitudinal viscosity while the matrix squeeze flow perpendicular to the fibers results in lower transverse viscosity [29, 64-65]. Geometrical deformation during the lay-up process is directly influenced by the transverse viscosity change. A hot press with insulated walls and a precise laser thickness measuring device was used to determine the fiber-matrix viscosity [66-68] (Figure 3.21).

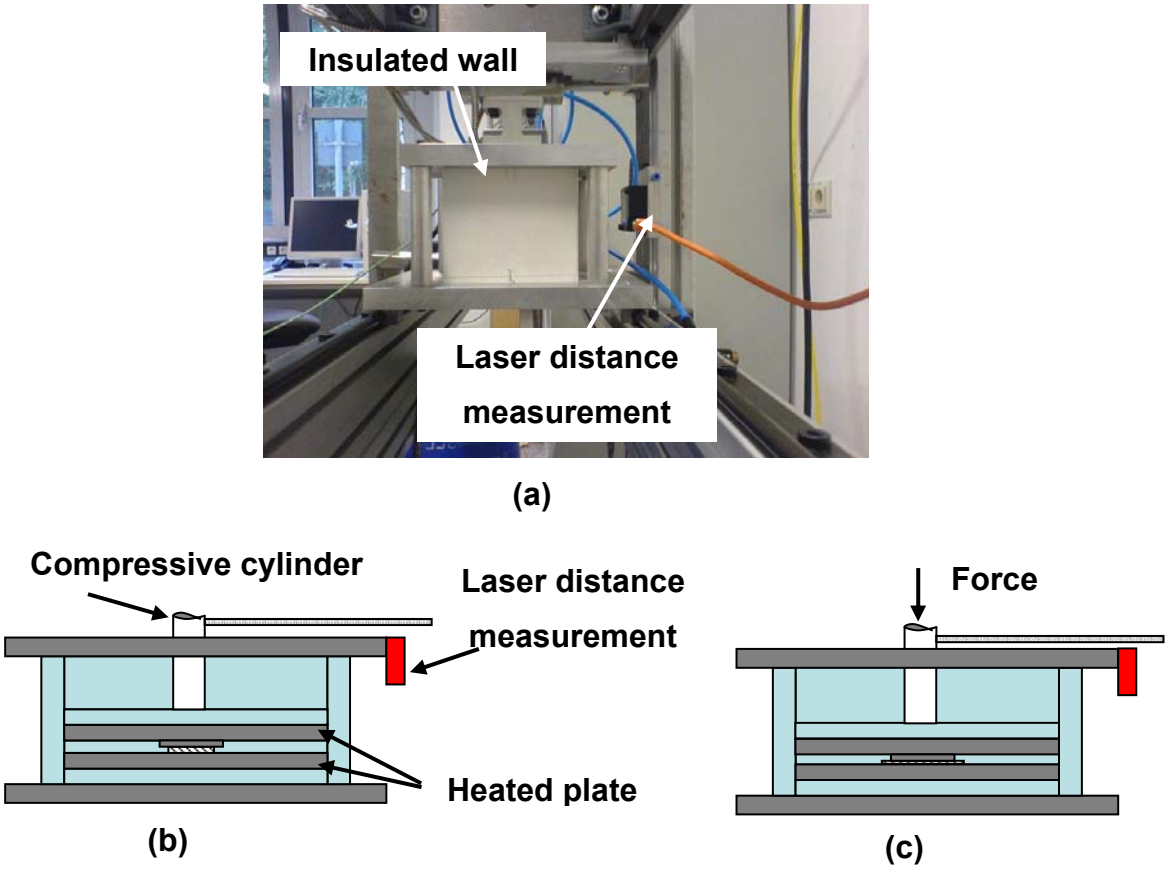

Figure 3.21: (a) insulated hot presses with laser distance measuring device (b) Before compression (c) After compression.

Samples from the 15 plies pre-consolidated unidirectional CF-PEEK laminate were heated for 10 minutes in the temperature range of 340-400 °C and then compressed with a load of 160N for about 120 seconds. For each isotherm the changes in the thickness were captured as a function of time as shown in Figure 3.22.

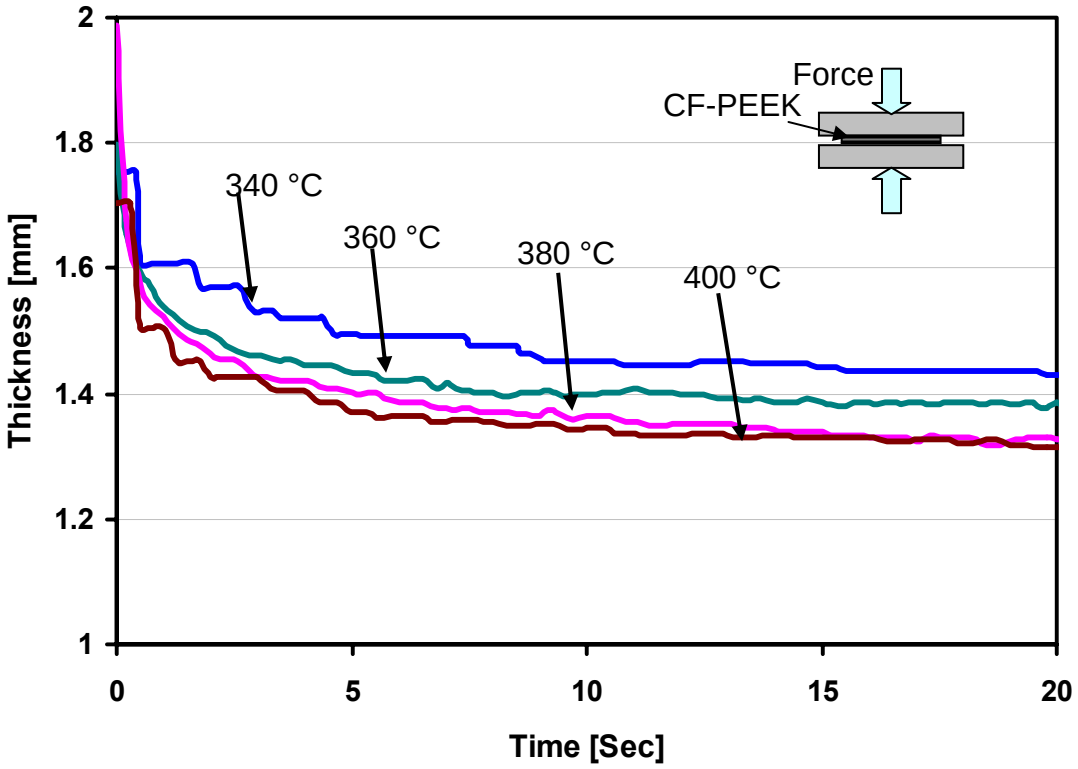

Figure 3.22: Compression of CF-PEEK sample at different temperature (Force 160N).

Bulk reduction in thickness occurs in less than 2 seconds and after 10 seconds no major reduction is noticeable. Although the compression behavior is highly nonlinear but assuming the constant slope $h^{\bullet}$ up to 10 seconds seems to be feasible when dealing with quick processing technique (like tape placement process) where the consolidation occurs in very short span. The viscosity of the unidirectional CF-PEEK thermoplastic material is then estimated at several temperatures by the procedure described in [63] and can be represented by the following Arrhenius relation.

$$\eta_T = A \exp^{B/T} \qquad 3.1$$

where A = 0.0037 N.sec/m^2 and B = 11115 °K.

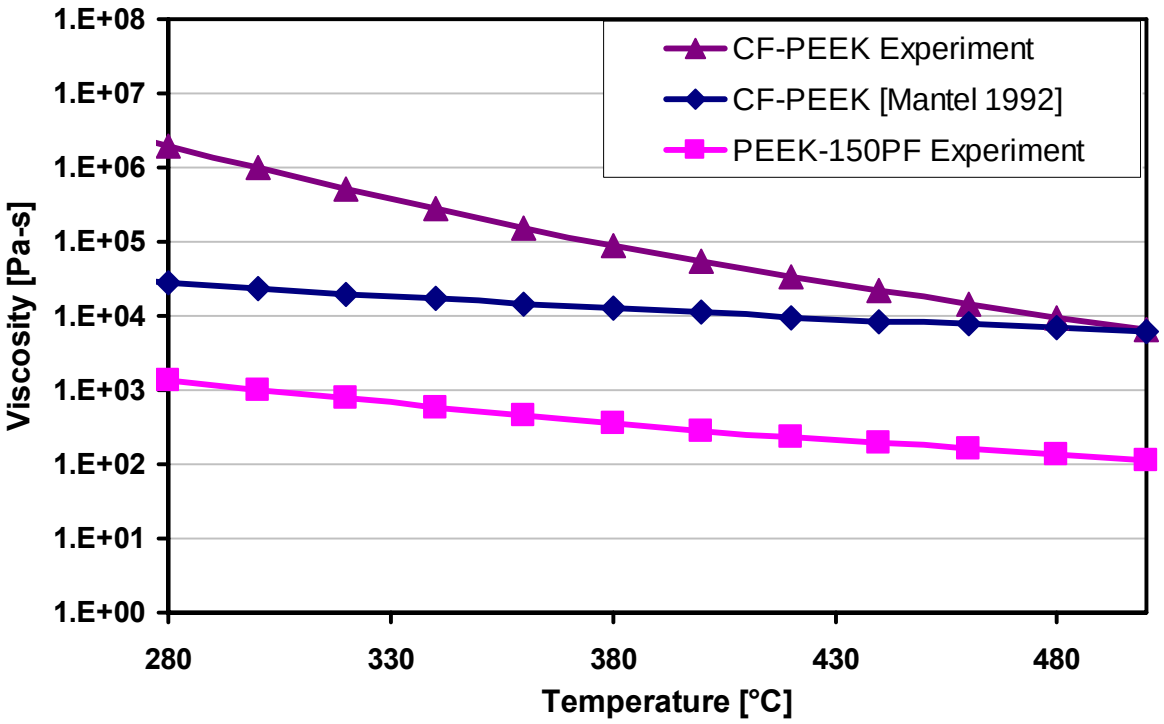

Figure 3.23: Viscosity of unidirectional thermoplastic CF-PEEK and PEEK material.

Figure 3.23 shows the comparison of experimentally determined viscosity with the most cited relation [16]. No information is available about their method of characterization but the viscosity values are lower compared to the material under investigation. Scobbo [69] also report lower values for the CF-PEEK laminate through parallel plate rheometric experiment. Investigation [70] reveals that simple shear deformation method is not suitable for the sample reinforced with the long fiber. The resin rich layer formed between the plates and laminated sample in these experiments. Also the complex deformation involving both axial and transverse interply shear makes it difficult to interpret the viscosity from such test. Other methods [70-71] report magnitude somewhat comparable to this study in MPa-sec range. Relative comparison with pure PEEK 150 matrix material indicates that the unidirectional fiber reinforcement increased the viscosity by many folds.

3.7.2 Polymer relaxation time (Weld time)

Lee [33] used the CF-PEEK lap shear specimens, manufactured at various consolidation temperatures and times in hot press. By comparing the bonding strength in the form of degree of healing with consolidation time $t^{1/4}$, he extract the weld time for different isotherm. Polymer healing is solely a matrix dependent phenomenon. Instead of visualizing a large scale diffusion of polymer across the interface, the fusion bonding between the similar polymers can be considered as the relaxation of the surface molecules only. The relaxation time can be extracted from stress relaxation measurements using dynamic mechanical experiments [72]. But for semi crystalline polymer melts, DMA experiments become difficult to conduct at high melt temperature, since the sample cannot be adequately supported in the instrument due to excessive resin flow [73]. Neglecting the polydispersity effect, the relaxation time for the polymer at melt can also be extracted from the viscosity / shear rate data obtained in steady state shear experiments (Figure 3.24).

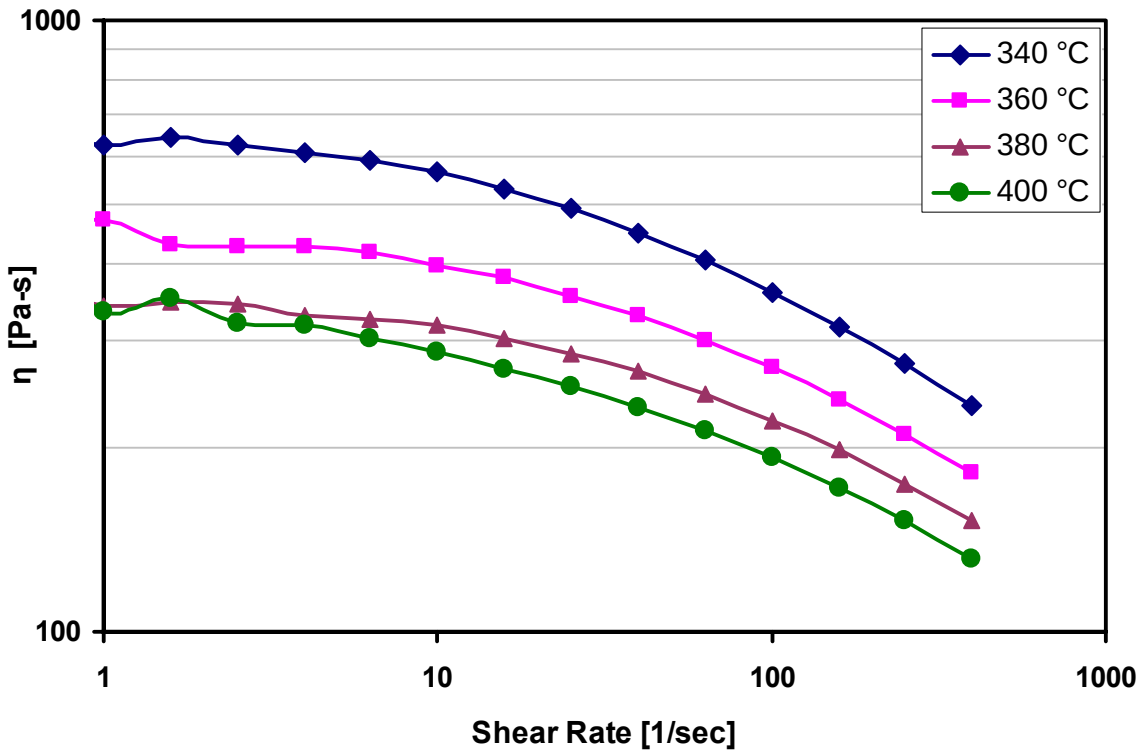

Figure 3.24: PEEK 150PF viscosity at different shear rate and isotherm.

The viscosity of the melted polymer follows the Newtonian behavior at low shear rates, but then beyond a particular shear rate it begins to decrease. Experiments were carried out with PEEK 150PF grade material on a parallel plate rheometer (Rheometric Scientific ARES) for the determination of weld time above the melt temperature at 340, 360, 380, and 400 °C with 2% strain (Figure 3.24).

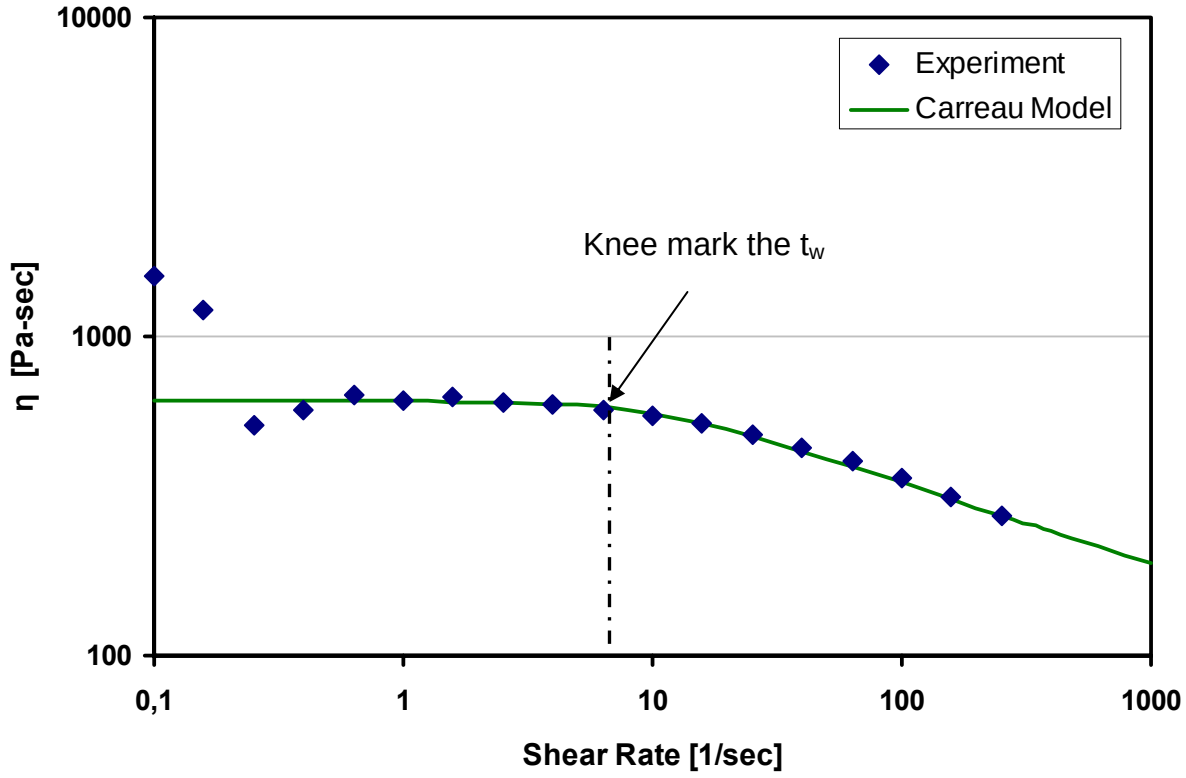

Figure 3.25: Carreau model describing the viscosity and weld time for CF-PEEK at 340 °C.

The viscosity curve displays a Newtonian plateau at low shear rates at all the temperatures, and then follows a logarithmic decrease with increase in shear rate. Experimental data was then fitted with the Carreau model [74]. The position of the knee in the model determines the onset point t_w (Figure 3.25). An Arrhenius relation develops by linearly relating the log (t_w) with *1/T* plot is shown in Figure 3.26.

$$t_w(T) = 2\times10^{-5} \exp^{\frac{43000}{R_c T}} \qquad 3.2$$

where R_c is the universal gas constant.

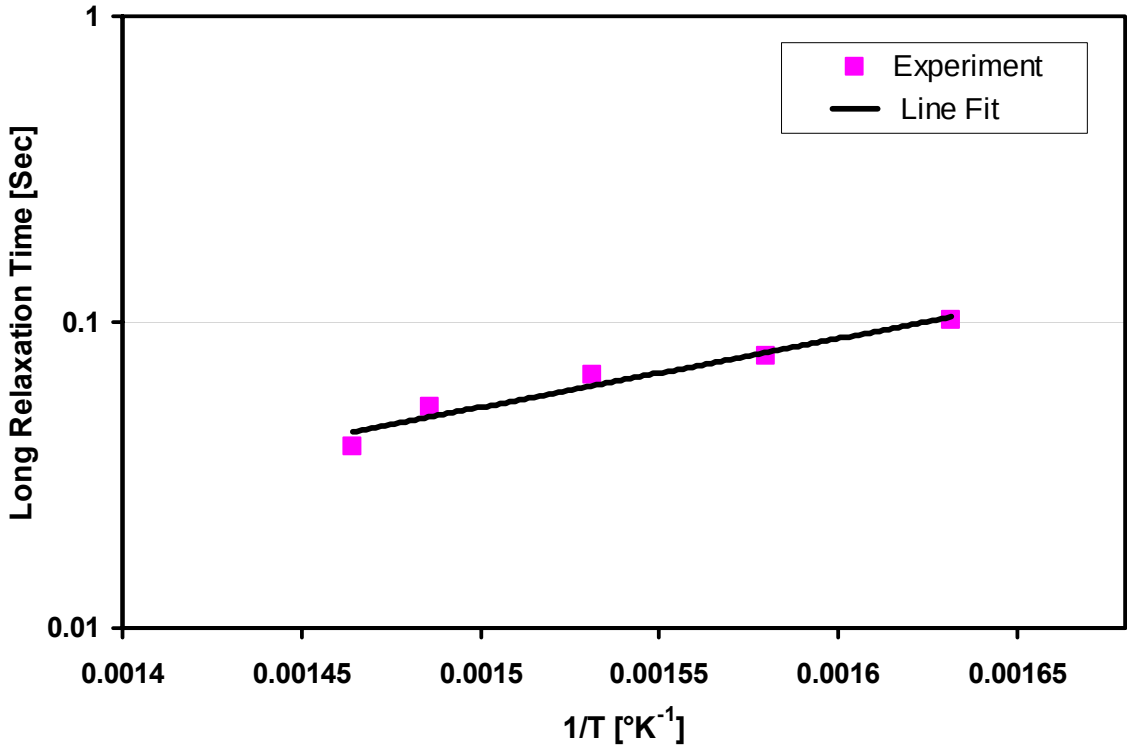

Figure 3.26: Weld time (or long relaxation time) for CF-PEEK material at different temperature.

3.7.3 Polymer crosslinking

Thermal stability of the PEEK material in air was characterized by monitoring the changes in its viscosity with time through rheological experiments at different isotherm with 2% strain and at 2.5 rad/sec shear rate. Figure 3.27 indicates the increase in the dynamic viscosity *η'*, which is related to permanent morphological changes in the resin properties.

As suggested before, the mechanisms responsible for the increase in viscosity consist of a random chain scission process, producing radicals that attack the neighboring polymer chain to form branches and finally crosslink. Once the crosslinking phenomena started it hinder the polymer healing (diffusion) with increased viscosity. The crosslinking concentration R_r (mol/g) for non-isothermal condition [18] is given by the equation (3.3)

$$Rr = A \int_{T340ini}^{T340final} \exp\left[\frac{-E_a}{R_c.T(t)}\right] \qquad 3.3$$

Where A = 5x10^{13} mol/(g-sec) and E_a = 276 KJ/mol. The detail of evaluating R_r is omitted here but can be found out in literature [63]. The equation (3.3) traces the crosslinking rate for the polymer as long as it held above the melt temperature (340 °C).

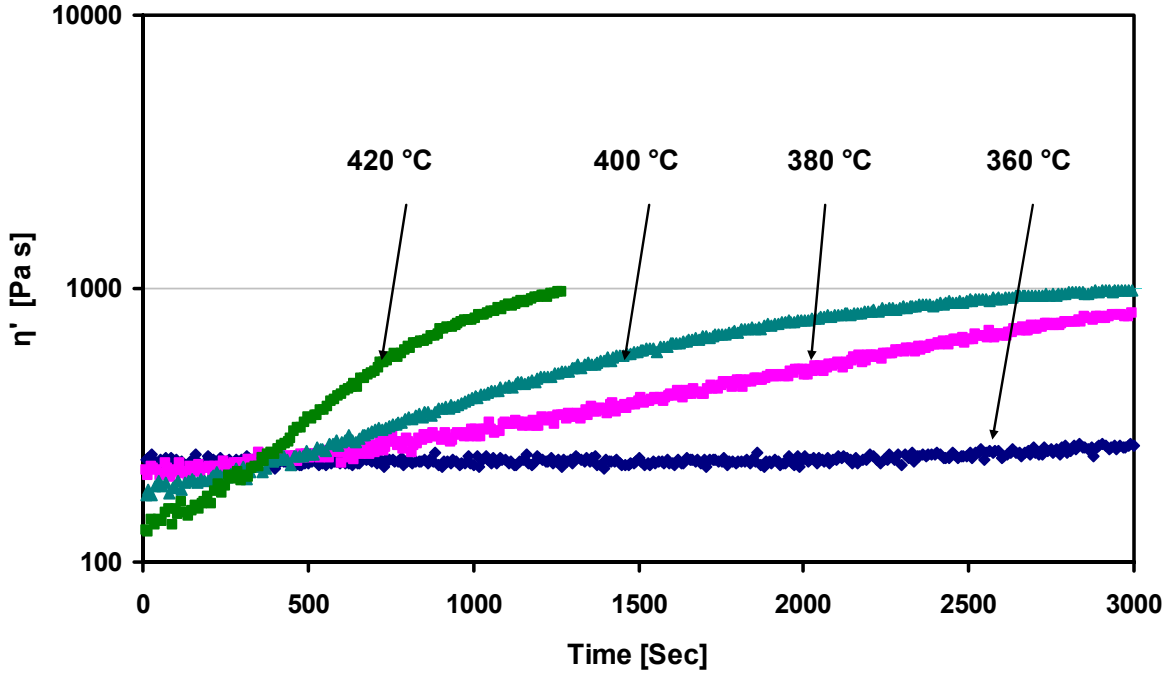

Figure 3.27: Increase in PEEK 150 viscosity with time at different isotherm (strain 2%, shear rate 2.5 rad/sec).

3.7.4 Thermo-gravimetric properties

Thermo-gravimetric analysis (TGA) was used to determine the temperature range where weight loss due to thermal degradation is dominant. Figure 3.28 shows the TGA scan performed on the CF-PEEK sample at different isotherm with air environment for overall duration of 220 minute. Heating rate was set to 10 °C/min on the DTG-60 thermal analyzer by Shimadzu Scientific Instruments, Inc. Material experienced negligible loss of weight (up to 2 %) when exposed to 450 °C but noticeable over 600 °C. For example, the exposure at 700 °C degraded the material at higher rate and negligible weight residual indicates the complete decomposition within 180 min.

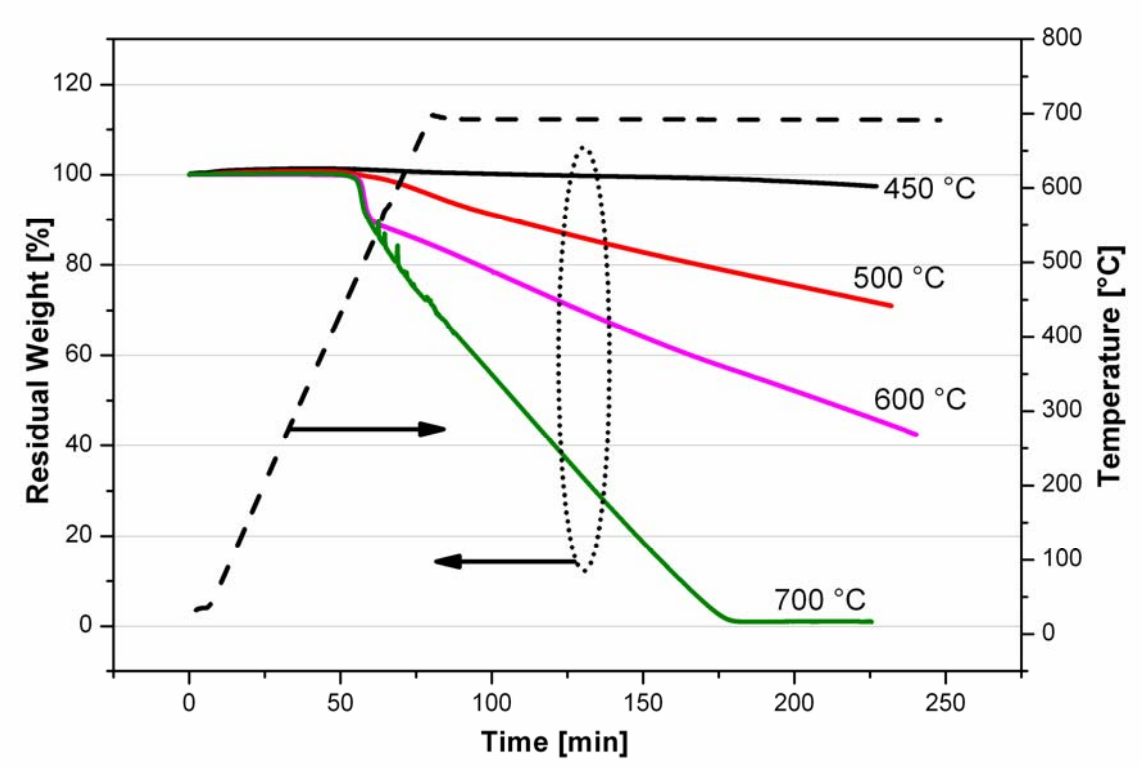

Figure 3.28: TGA scan for CF-PEEK material in air at different isotherm, heating rate 10°C/min.

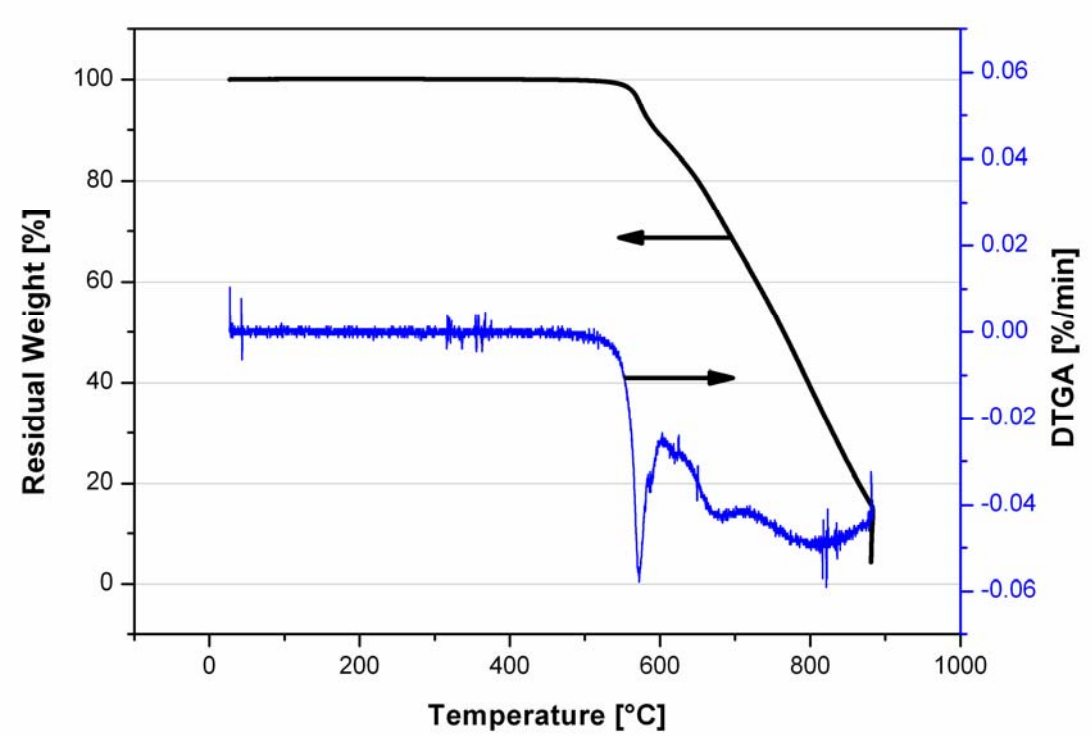

Figure 3.29: Comparison of weight loss (TGA) and its derivative (DTGA) thermograms of CF-PEEK in air. Heating rate 10 °C/min

Further details are available in Figure 3.29, which shows the thermal scan up to 900 °C. The onset temperature at 550 °C marks the beginning of the degradation step and the derivate DTGA shows that the maximum rate of decomposition is around 5.8 %/min. The thermal degradation kinetics is represented by equation (3.4) [42].

$$\frac{d\alpha}{dt} = A\exp\left[\frac{-E_a}{R_c.T(t)}\right](1-\alpha)^n \qquad 3.4$$

Where α is the fractional decomposition of the sample, t is the time (s), A is the pre-exponential factor (1/s), E_a is the activation energy (J/mol), R_c is the gas constant, and n is the reaction order (assumed to be 1). Studies [41, 75] have been carried out based on different kinetic modeling techniques to classify the activation energy and pre exponential factor for the PEEK material. TGA scan similar to Figure 3.28 were performed on CF-PEEK material with different heating rate (10, 20 and 50 °C/min) to calculate the kinetic parameter based on the dynamic model proposed by Park [42]. As shown in Figure 3.30, the overall activation energy is little affected by heating rates, hence can be represented with respect of conversion level and independent of heating rate.

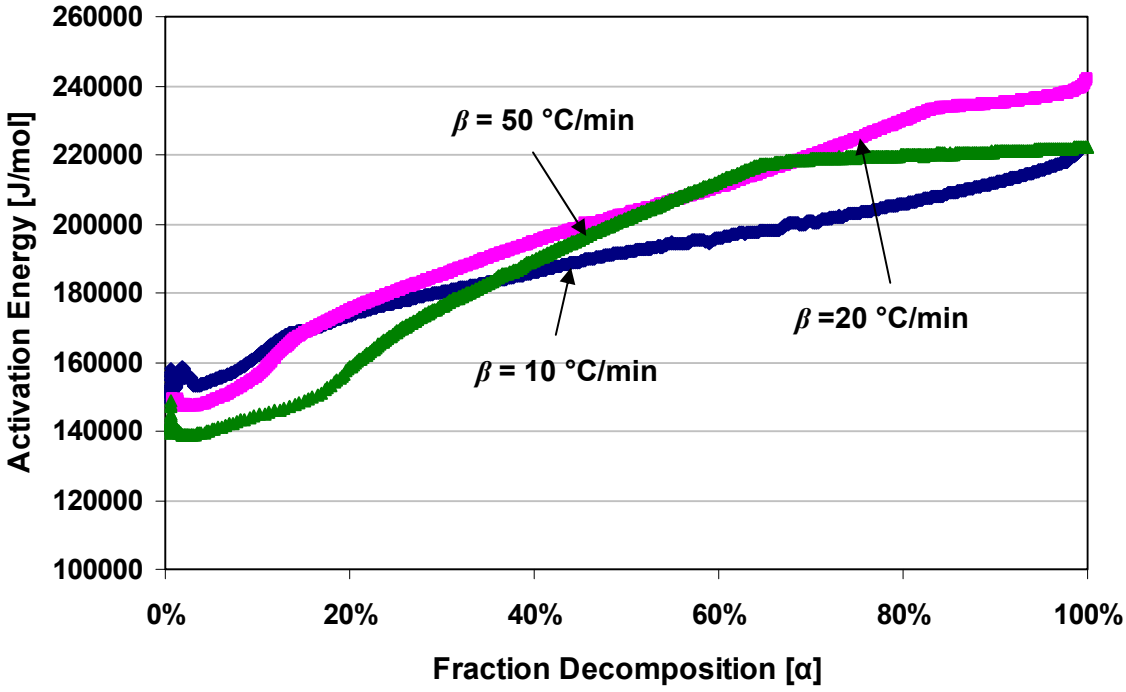

Figure 3.30: E_a in case of CF-PEEK's thermal degradation in air at different heating rates β.

Table 3.6 summarizes the values of kinetic parameters with respect to different conversion level obtained in this study with the values found in literature.

Table 3.6: Activation energy at different conversion level for PEEK material.

Conversion level [%]	Activation energy [41] E_a [KJ/mol]	Activation energy E_a [KJ/mol]	Log A [1/min]
5	111.4	156.6	5.27
10	160.6	159.9	8.7
15	172.1	163.9	9.57
20	175.9	167.8	9.91
25	178.3	171.8	10.41

3.8 Mechanical testing

In this part different test methods are presented to characterize the mechanical properties of the CF-PEEK laminate. In case of laminated structure major interest for designer and manufacturer lies in the evaluation of interlaminar bond strength, as it influences other strength values and failure mechanism. The standard method for measuring the interlaminar fracture toughness of laminated composite material is the double cantilever beam test (DCB). This test requires a specimen thickness of between 3 and 5 mm, which translate into 24 to 40 plies and additional time for specimen preparation. Also, the testing and result interpretation take considerable time. Considering these circumstances, simple and faster testing methods were selected for the qualitative and quantitative evaluation of the interlaminar bond strength. For qualitative purpose peel resistance testing was selected, like DCB which also gives a measure of the quality of the interlaminar bond between the layers. For quantitative testing, interlaminar shear strength (ILSS) method was selected to investigate the response of composite materials against delaminating loads.

3.8.1 Peel resistance

Double ply wedge peel testing requires simple specimens and gives a quick measure of the quality of the interlaminar bond strength [76-77]. The test specimens were manufactured for the combination of lay-up velocities and gas volumes by consolidating two unidirectional tapes over a hot tool maintained at 280 °C. A 0.5 mm thick

Kapton film was placed on top of the first tape to initiate delamination of peel testing. Five samples were manufactured for each combination with an average length of 300 mm. Each as-placed double ply sample was then tested on the fixture illustrated in Figure 3.31 incorporating a 1.5 mm thick stainless steel wedge. A grip fixture attached to the crosshead was used to clamp the sample plies. The crosshead was then actuated and pulled at a rate of 20 mm/min. Load data was recorded by the logger software over an average length of 150 mm.

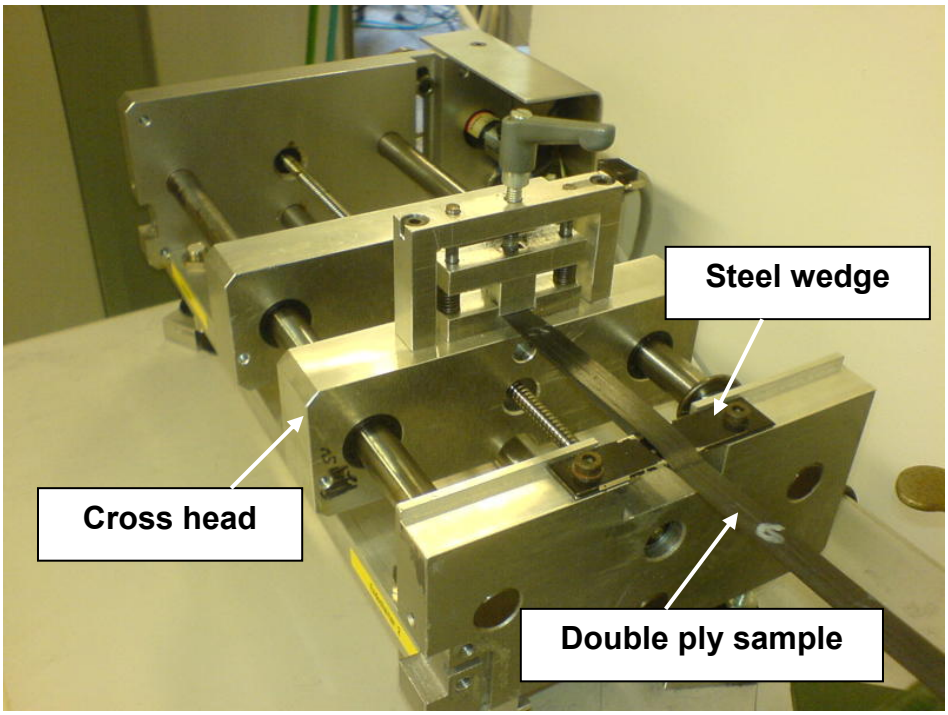

Figure 3.31: Wedge peel test setup.

The typical peel force curve (see Figure 3.32) involves several peaks. Researchers have [78] correlated the peaks with the fracture propagation at fiber-matrix interface while the region outside these peaks is dominated by the pure matrix fracture. Unlike the DCB test, which gives one initiation value per sample, the wedge peel test provides several hundred data points. Averaging this data over several points gives an estimate of the relative strength of the interlaminar bond. Mean peel resistance for each combination of process velocity and hot gas volume is obtained by first discarding the early data up to 20 mm of the test length and than averaging all the data points on the data range. Standard deviation is also calculated over the data range.

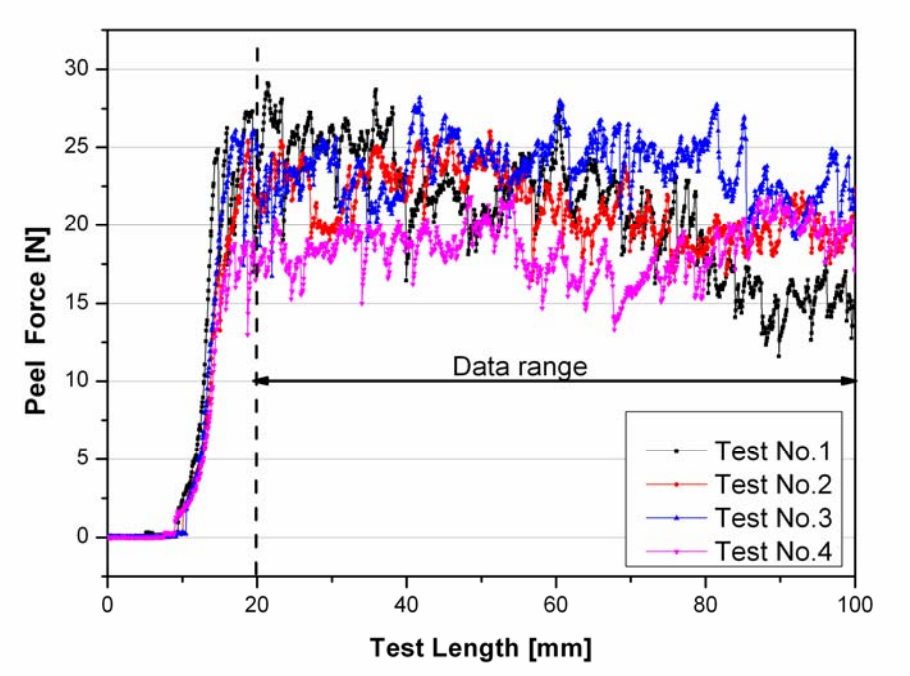

Figure 3.32: Measured forces as the fracture propagate in peel sample. (Gas volume 14 norm liter/min, velocity 3 m/min).

Figure 3.33 gives the complete overview of the peel resistance test for the sample manufactured.

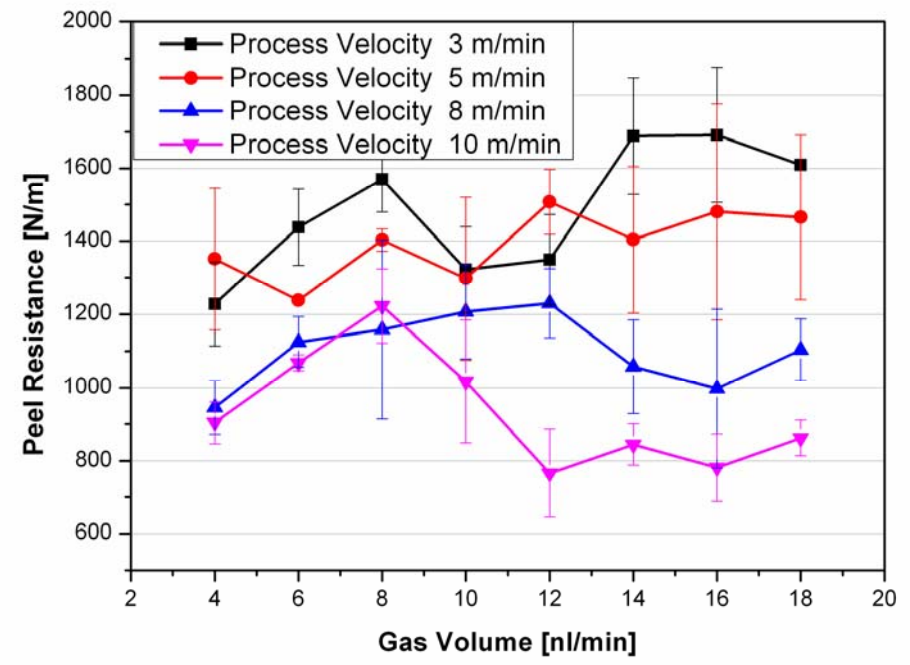

Figure 3.33: Peel resistances for the combination of lay-up velocity and gas volume.

High bonding strength at low lay-up velocities (3 and 5 m/min) indicates the adequate healing and resin flow at the plies interface. Peaks and valleys denominate the variation of interlaminar bond strength with increasing gas volume. The trend is quite similar to the convective heat coefficient plot in Figure 3.9. Hence the thermal energy transports to the tape interface are the possible reason for such variation. Also the large scatter is present in the data which is identified as a result of fiber bridging [77]. Graph also shows that the peel testing is just adequate to get a general idea about the influencing manufacturing parameters, but it is inadequate for estimating the laminate's final quality. As in tape placement process the bond development within the laminate's interfaces is a result of repetitive consolidation during successive lay up, hence it is necessary to evaluate the mechanical performance of fully laid up laminate.

3.8.2 Interlaminar shear strength (ILSS)

The mechanical properties of the processed unidirectional laminates were characterized by means of flexural test apparatus (DIN EN 2563). The method consists of determining the resistance to delamination under shear forces parallel to the layer of the laminate. For this purpose a specimen of rectangular cross section is tested in flexure on two supports. The load is applied at the centre of the specimen by means of a loading nose midway between the supports. Several 15 layered laminated plates were manufactured with the combination of different process velocities and hot gas volumes flow. Samples from these plates were tested for the ILSS. The tests were performed on Zwick universal testing machine at room temperature with a 5 KN load cell.

Ten samples were tested for each plate as shown in Figure 3.34, to obtain a satisfactory average and standard deviation. The first maximum load was recorded as the failure load. The shear strength is calculated from the following equation:

$$\sigma = \frac{3 \times P_R}{4wh} \qquad 3.5$$

where P_R is the failure load, w is the midpoint width, and h is the sample thickness.

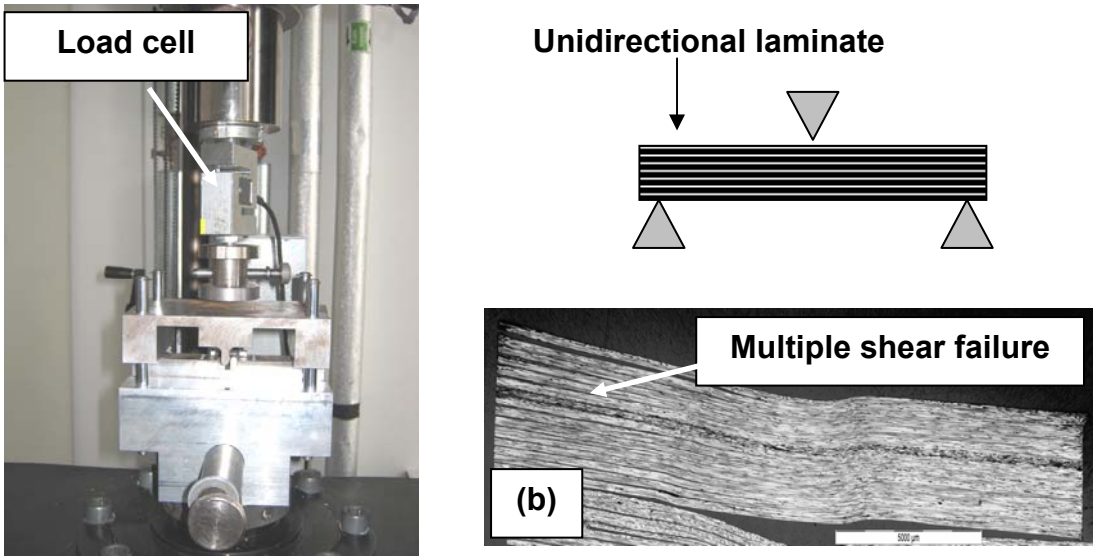

Figure 3.34: (a) Fixture for ILSS test (b) Typical multi-shear failure in sample.

Figure 3.35 represents the curve for the interlaminar shear strength as a function of applied force and strain. The curve can be essentially distinguish into two regions, the first quasi straight part before the maximum load and the post peak part after the maximum load. The quasi straight part extends up to the maximum load, which represent the shear failure at the matrix fiber interface in the sample. The post peak part attributes to the multi cracking / shear of the sample.

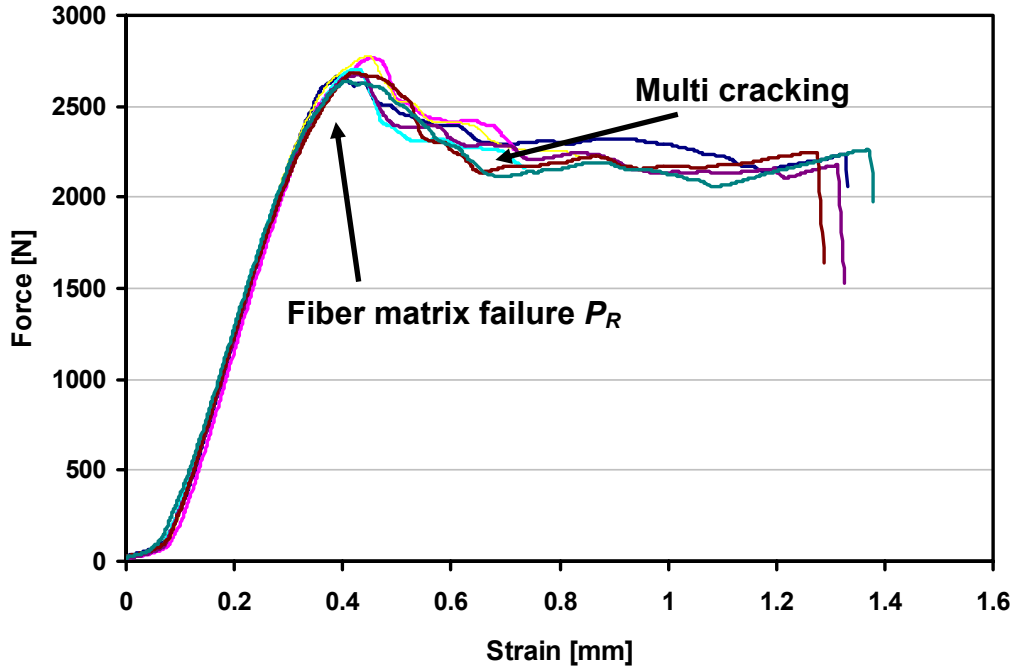

Figure 3.35: Flexural test curve for unidirectional CF-PEEK sample (Gas volume 10 norm liter/min, velocity 3 m/min)

It is evident (see Figure 3.36) that lower process velocity generates laminates with higher ILSS, but after achieving some maxima in each case, the ILSS starts to drop down with increasing gas volume. Again this trend is similar to the peel resistance curves except that ILSS values depict no wavy nature for low lay-up velocity combinations. Multiple passes during the laminate stacking (thickness build-up) generate repetitive consolidation for the underneath layers, thus allowing more time for polymer healing and bond strength development.

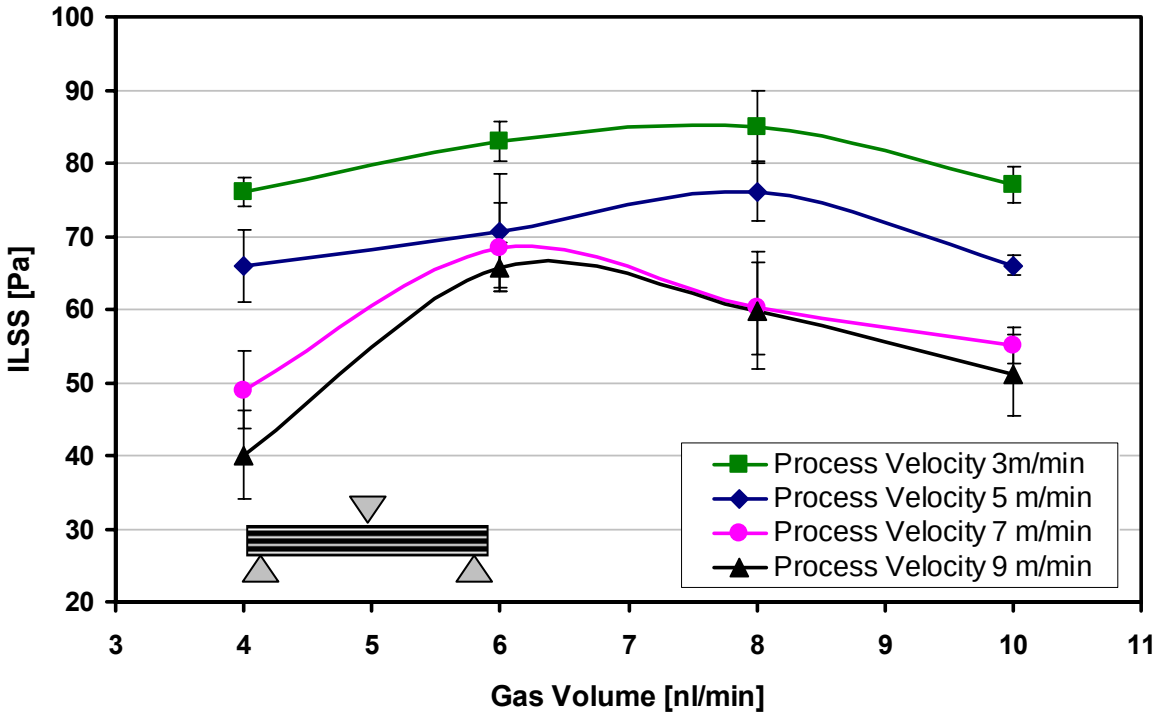

Figure 3.36: ILSS values at different processing parameters.

3.9 Reference plate and experimental bonding degree D_b

To obtain some reference values for relative comparison of tape placement process, two 15 layered unidirectional CF-PEEK laminate were manufactured with autoclaved process. For the first plate, thermoplastic tapes were laid up in a tool plate manually with hand and then consolidated inside the autoclave. For the second plate, laminate was manufactured with high velocity laid up (gas volume 12 norm liter/min and velocity 6 m/min) and then reconsolidated inside the autoclave. Automatic tape laying ensured exact positioning of the tape in second laminate.

Both laminate were consolidated inside a tool to restrict the edge expansions with the cycle shown in Figure 3.37. Samples were then cut out for the ILSS and microscopic examination.

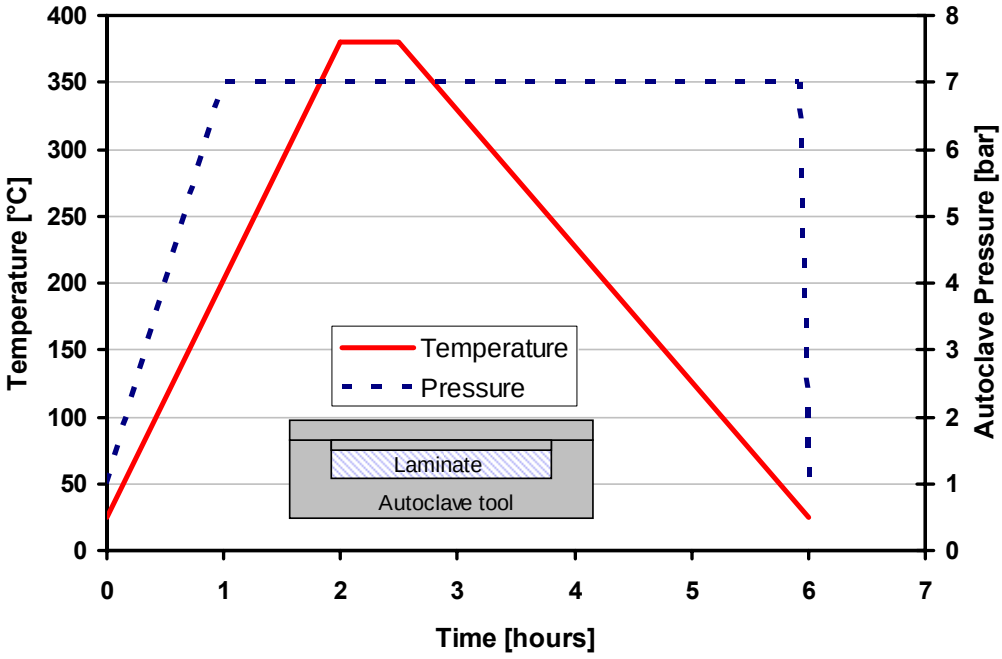

Figure 3.37: Pressure and temperature cycle for autoclaved reference plate.

Figure 3.38 shows the strength development in these two plates, the hand laid up plate has the mean ILSS value of 92 MPa while the tape placed plate with reconsolidation has the mean ILSS values of 94 MPa. Increase in the strength value for the second laminate is quite understandable, as the bonding between the tape had been initiated during the tape placement process, and the autoclave consolidation ensure complete bond generation between the properly align tape interfaces. The void content in these laminate has values less than 0.3 %.

At this point, in order to estimate the capability of the tape placement process, ILSS and void content graph are also compared with the laminate manufactured through tape placement process. It is quite evident that, high strength laminate can be obtained through tape placement process, as the pure laid up laminate (gas volume 8 norm liter/min, velocity 3 m/min with standard parameters Table 4.1) has the mean ILSS value of 85 MPa.

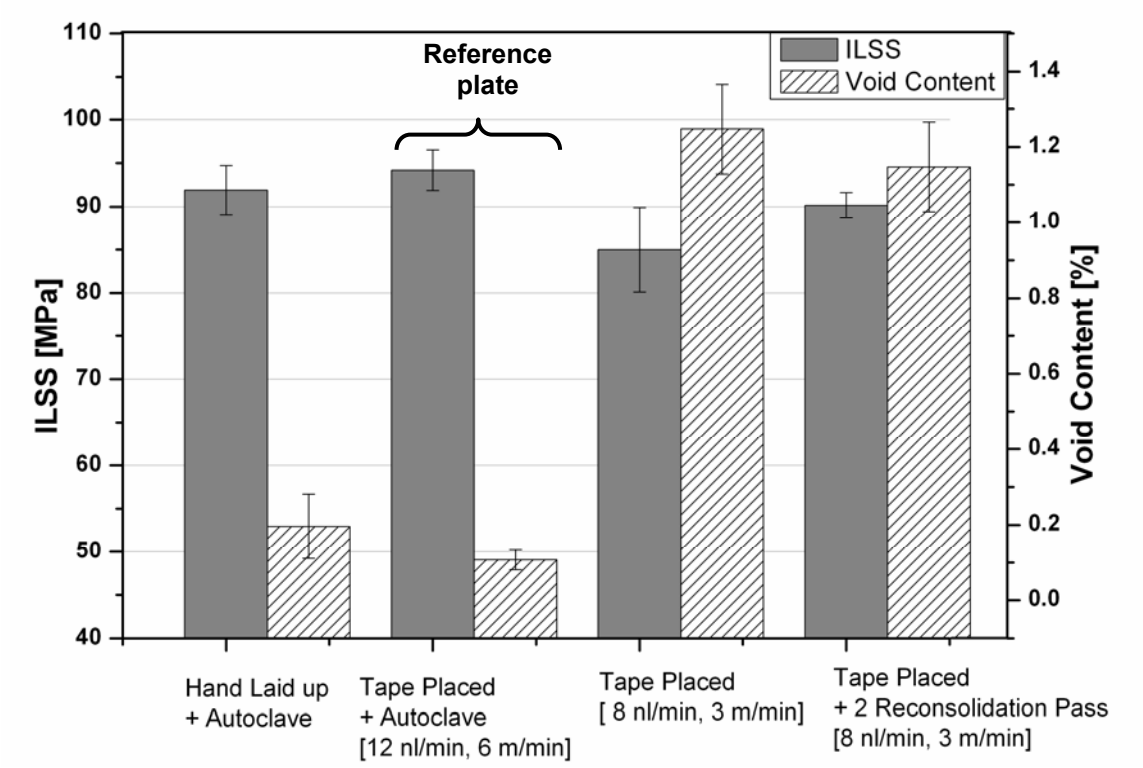

Figure 3.38: ILSS reference values for autoclave and tape placed plates.

An improvement in strength was obtained, when the laid up laminate was reconsolidated with two additional pass without further lay up, to improve the bonding level in the top layers. This resulted in much better mean ILSS value (90.3 MPa) and along with the scatter range it reaches the pure autoclaved consolidation level. This reconsolidated laminate also show better void content percentage as compare to purely laid up laminate. But still the void value is higher than that of autoclaved consolidated plate. Hence one of the objectives of this study is to find out the reasoning and a way to eliminate the difference (ILSS value and void content) between autoclave and tape placement consolidation processes.

Degree of healing may be defined as the ratio of instantaneous interfacial bond strength to the ultimate bond strength [33]. The same statement holds true for the bonding degree D_b with only pre requisite of 100% developed intimate contact between the layers. During this study the photomicrograph and tomography analysis carried out for the tape placed laminate which is reconsolidated in autoclaved, show complete interfacial contact. Also the sufficient hold time (> t_w) ensure complete polymer diffusion for the development of interfacial bond. Thus ILSS and void content

values for such a laminate represent the reference values, see Figure 3.38. The relative comparison between the ILSS values from the tape placed sample with the autoclaved sample provides a percentage fraction of the actual bond strength i.e. *D_b(Experiment)*

$$D_b\,(Experiment) = \frac{\sigma}{\sigma_\alpha} = \frac{ILSS_{Tape-placed}}{ILSS_{Autoclaved}} \qquad 3.6$$

Figure 3.39 represents the transformation of ILSS values (from Figure 3.36) to D_b experimental. The data representation in this format is more meaningful. Although as discussed before tape placement process can challenge the autoclave consolidation level but still some improvements are required to reach the reference (tape placed and autoclaved post consolidated) strength level. For example, for the selected lay-up combinations in Figure 3.39, the D_b(experimental) values are less 100 %. The pattern of values also indicates the trend of strength improvement and then decrement with increasing gas volume at particular lay-up velocity. Explanation to these factors will be discussed in next chapter.

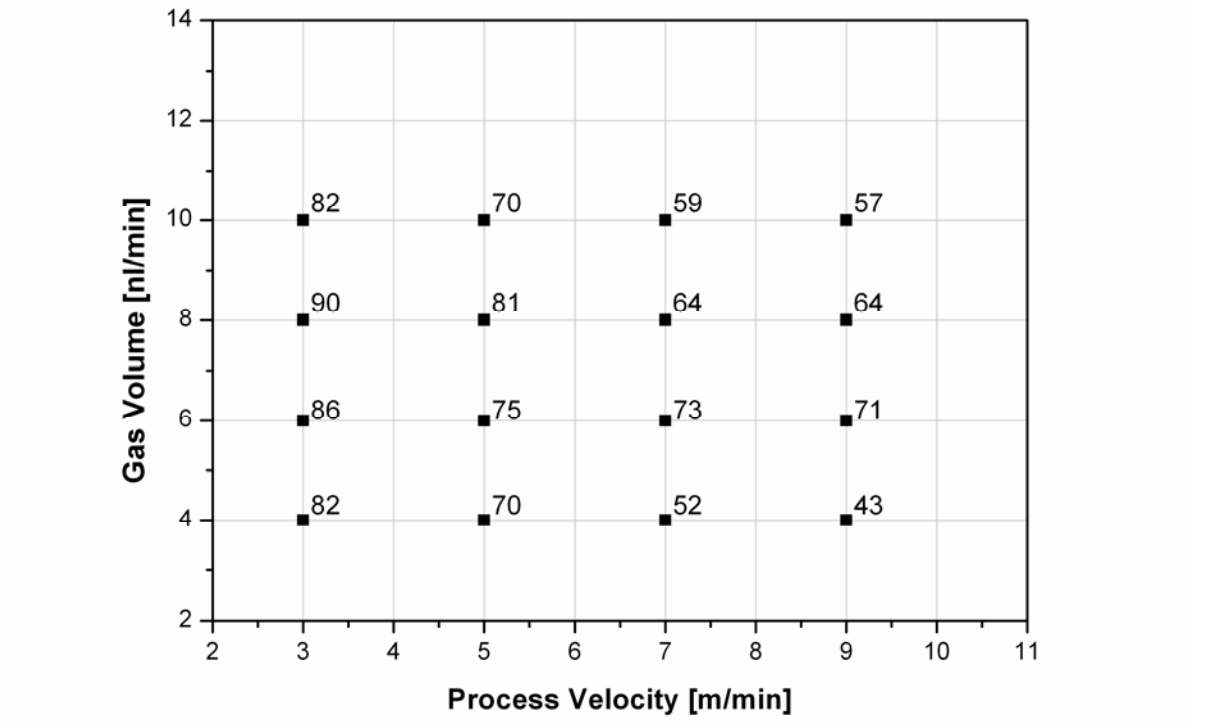

Figure 3.39: Experimental bonding degree D_b (Experiment) for the samples manufactured with combination of lay-up parameters without any post consolidation.

3.10 Void contents characterization

The plates manufactured for ILSS testing were also analyzed under the light microscope for fiber matrix distribution, tape edges effect and for the determination of volume void content. Plates were first trimmed off from the edges and 15x25 mm^2 samples were cut out with diamond cutting wheel. Samples were then cured in resin at 2 bars, grinded, polished, and prepared for light microscopic examination. By taking three gray scale pictures over the thickness as well as along the width and by using the image analysis software, the average void content of each sample was estimated by identifying the black spot areas, see Figure 3.40.

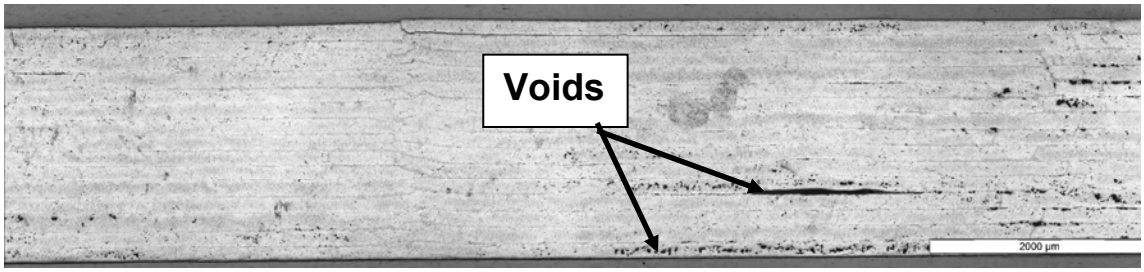

Figure 3.40: Photomicrograph for void content analysis.

Although the photomicrographs have been used for determining the fiber, matrix and void contents. Accuracy level of this method demand large number of readings and expertise to correctly identify the visible objects in the micrograph. In order to verify the sufficiency of number of readings and method accuracy, void content results were compared with the Thermo-gravimetric Analysis (TGA) method [79-80]. Fiber and resin mass contents determined by the TGA method is then used to determine the volume void content in a sample as per ASTM D 2734 standard.

The comparison in Figure 3.41 shows that mean values from two methods are in accordance in most of the cases except plate 7 & 8. TGA method calculates the global void content for the sample, while in the photomicrograph analysis void content are calculated at different location on each sample to get the overall value. As a result the photomicrography method shows large variation (±1%). Despite large advantages of TGA method, the photomicrograph analysis is found suitable for this study due to its simplicity, quick analysis and availability of bulk information regarding laminate microstructures.

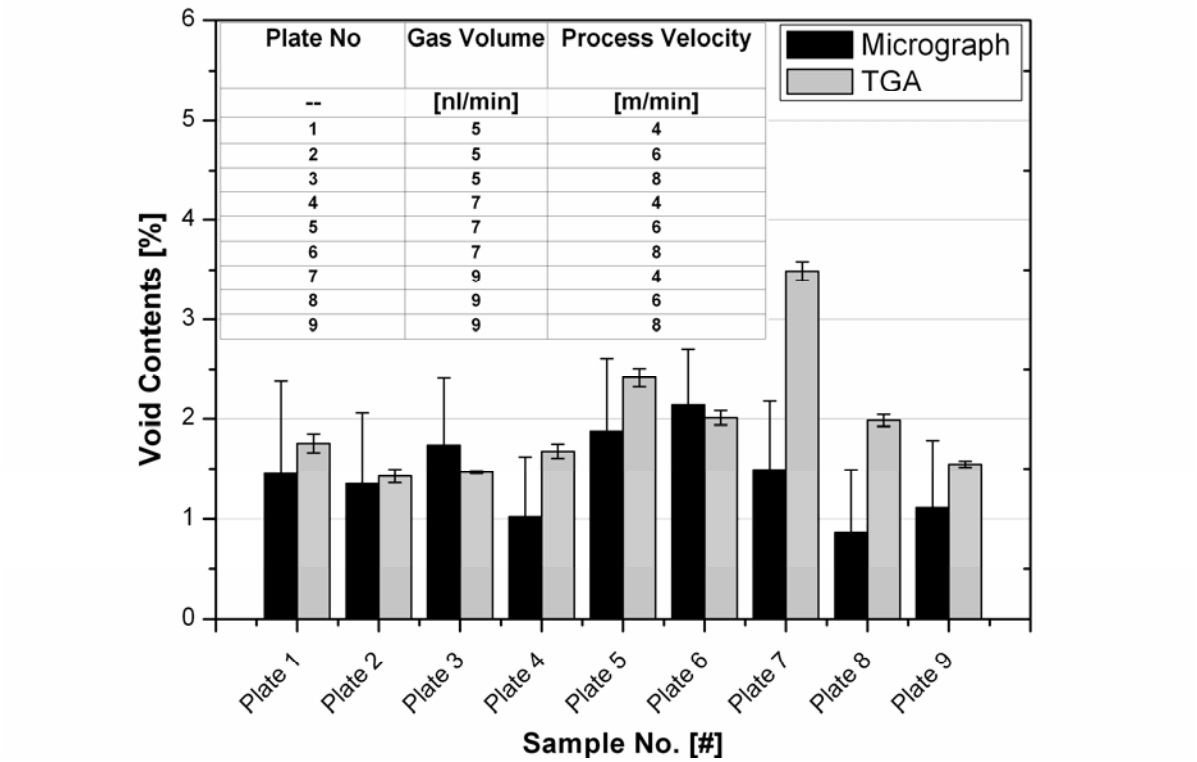

Figure 3.41: Void content measurements for different plates by photomicrograph and TGA method.

4 Process simulation and parameter study

4.1 Modeling thermoplastic tape placement process

Theory explained in chapter 2 provides the sufficient information about phenomenal occurrence during the tape placement process. A sequential implementation of these models could result in a simulation code, which can be used to identify major influencing factor for the process, predicting the final structure quality and optimizing the process. The following model (as shown in Figure 4.1) describing the process dynamics and welding had been selected and implemented for the thermoplastic tape placement process. Figure also show the data flow between different model / sub models and their interdependency. The material is pre-impregnated tapes; hence the impregnation process is not accounted in this study. Similarly the crystallization and process induced stresses [31] needs data from other sub model and hence their implementation is considered for next level of study. In the foregoing section a brief detail of each model is provided. The detailed explanation has been published in the literature [25, 30, 63, 81-82].

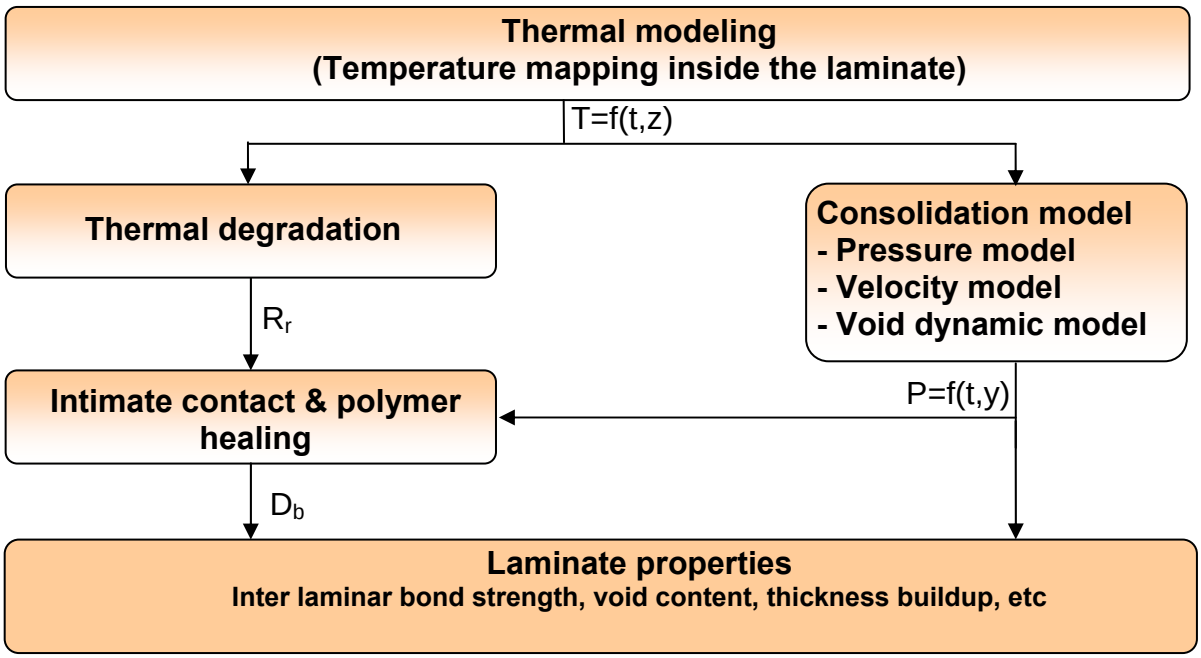

Figure 4.1: Consolidation scheme of thermoplastic composite material.

Thermal model: Although sophisticated modeling techniques are available (as shown in Table 2.1) but for this study thermal gradient inside the laminate was analyzed with the 1-D (through thickness) model. Considering small temperature variation under the hot gas torch in tape's width direction and assuming heat transfer by the high velocity hot gas impingent flow through nozzle is much larger than that of heat conduction through material along the lay up direction due to low thermal conductivity, eliminate the need of complex and time consuming heat transfer calculation in width and length direction. Also Toso [15] found through DSC measurement that for high heating rates (over 1000 °C/s) a consideration of heat generated results in an overestimation of temperature at the nip point by approximately 5 °C. For this reason heat generation/sink effect is not considered in this study. The energy equation (2.1) is simplified for 1 D heat transfer and implemented as:

$$\frac{\partial T}{\partial t} = \frac{k_z}{\rho C}\frac{\partial^2 T}{\partial z^2} \qquad 4.1$$

where *z* is the spatial coordinate in thickness direction. Convection is identified as the main source of heat transfer in the process by several authors [14, 17, 83].

$$k_z \frac{\partial T}{\partial z} = -h_m (T - T_m) \qquad 4.2$$

Where h_m and T_m in equation (4.3) represents the convective heat transfer coefficient and temperature surrounding (air, hot gas or tooling) the lay-down laminate. The incoming tape enters into the domain with room temperature, while the substrate is initially assumed at tool temperature. The equation (4.1) is solved for the incoming tape, substrate and composite section (see Figure 2.12) as describe in the literature [25].

Consolidation model: Thermoplastic tape placement process is highly non isothermal in nature. Moreover, an exact pressure distribution is necessary to determine the void compression / elimination and geometrical variation within the laminate. Referring back to Table 2.2, modeling technique based on transverse squeeze flow method only fulfill all these requirements, hence selected for this study. As input, be-

sides manufacturing setup detail, model also needs the temperature mapping data from the thermal model. The output of the model includes the information about pressure distribution, final intraply void content and change in tape's width / thickness.

Thermal degradation: Experimental testing in section 3.74 shows that PEEK polymer is quite stable up to 360°C, but over this temperature polymer crosslinking results in an increase in viscosity. Already explained thermal stability model (in section 3.73) is selected for the process simulation along with the experimentally determine activation energy and pre exponential components. As input model require thermal exposure history of every layer and output results in the crosslinking rate R_r to show the extent of polymer crosslinking.

Intimate contact and polymer healing: Surface profilometer scan in section 3.6 shows roughness profile in incoming tape is highly random in fashion. And it cannot be represented by the single factor, therefore fractal dimensions were determined and equation (2.9) is used for intimate contact development. Similarly equation (2.10) is selected for no isothermal healing along with intimate contact development to determine the overall bonding degree using mathematical strategy describe by equation (2.12).

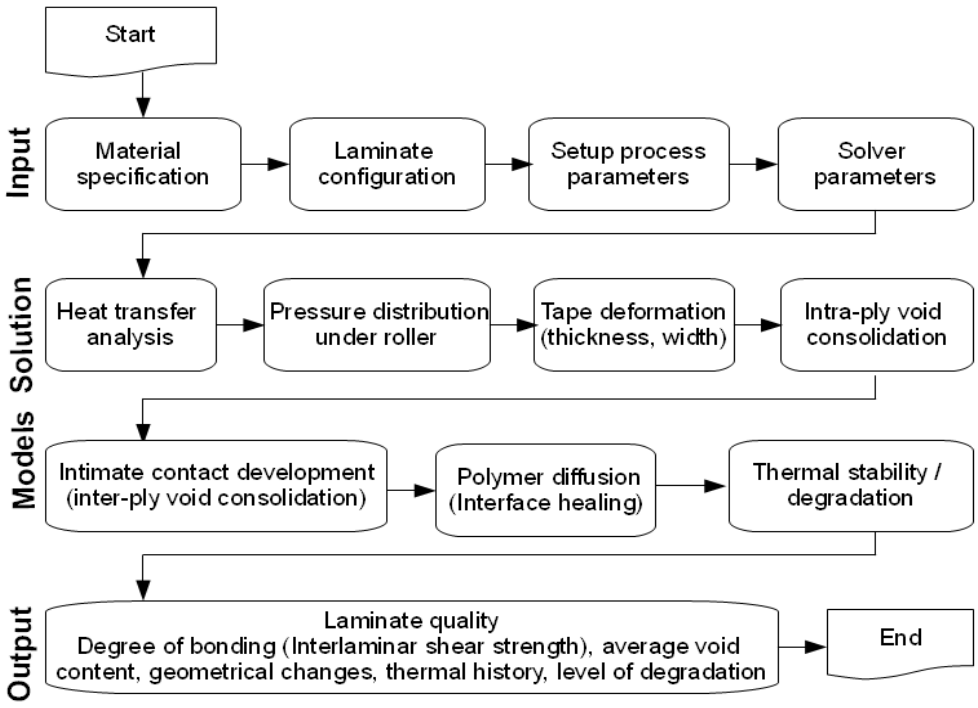

Figure 4.2: Schematic for the ProSimFRT code.

4.2 Model implementation

A process simulation code for fiber reinforced thermoplastic (ProSimFRT) is developed using the Matlab platform for this purpose. Built in numerical functions in the Matlab software are capable of performing high speed calculation by maintaining the accuracy. Three implementation levels of ProSimFRT as shown in Figure 4.2 are Input, Model Solution and Output section.

Input section (see Figure 4.3) serves as an interface to communicate between the user and the solver. Different aspects of the problem starting from material details, lay-up configuration and process setup can be defined in this part. Beside this the instructions to the solver like the solution time, geometrical descritization of the problem, selection of appropriate models and control to the output can also be defined here.

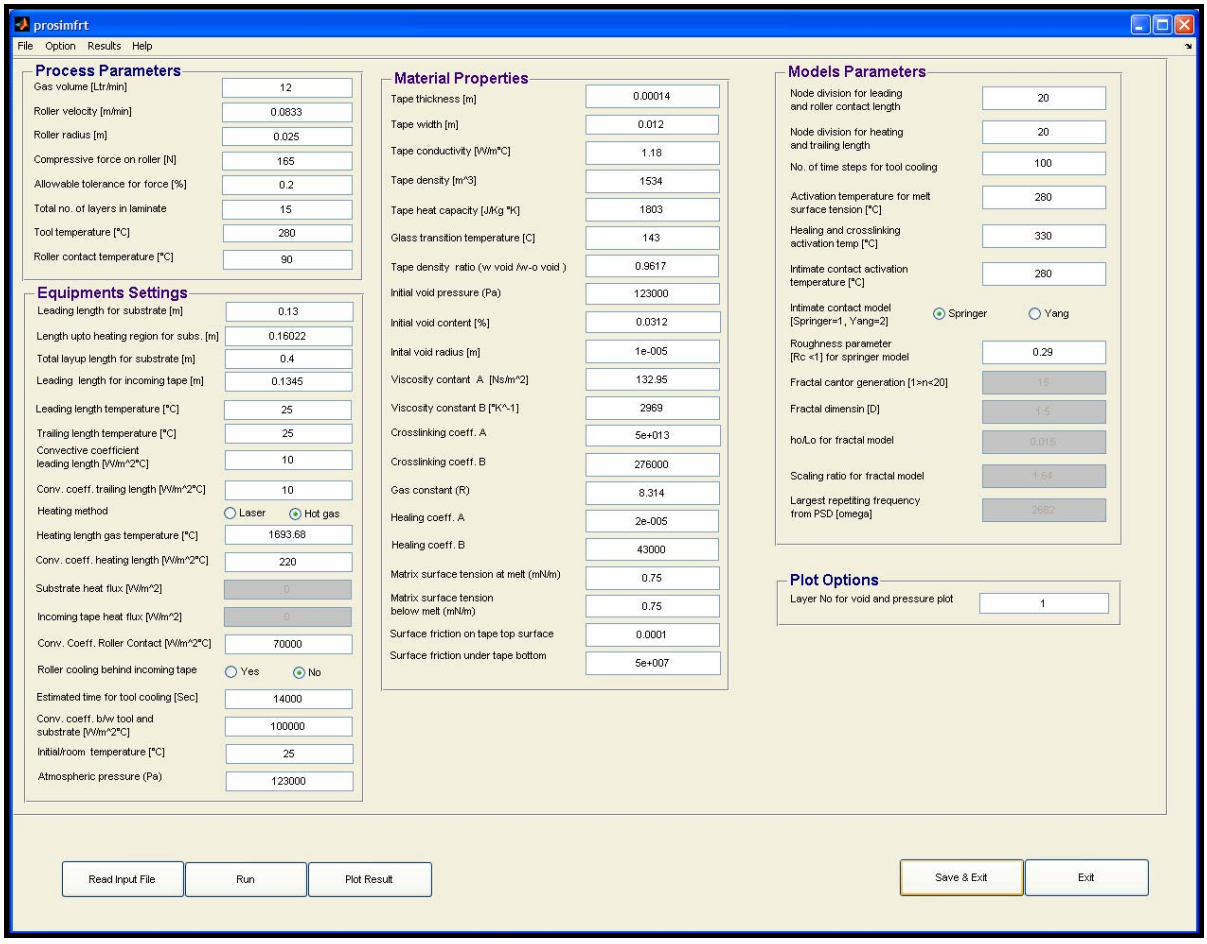

Figure 4.3: Input windows for the simulation code.

Solver section is the collection of numerically implemented theoretical models; solution from each model is available to the succeeding model as an input. Simulation begin with the heat transfer model, and then with simultaneous solution of consolidation and strength development models. Effect of polymer degradation and thermal stability is also calculated through out the lay-up process. Material characteristic are updated at every solution stage to represent the actual state.

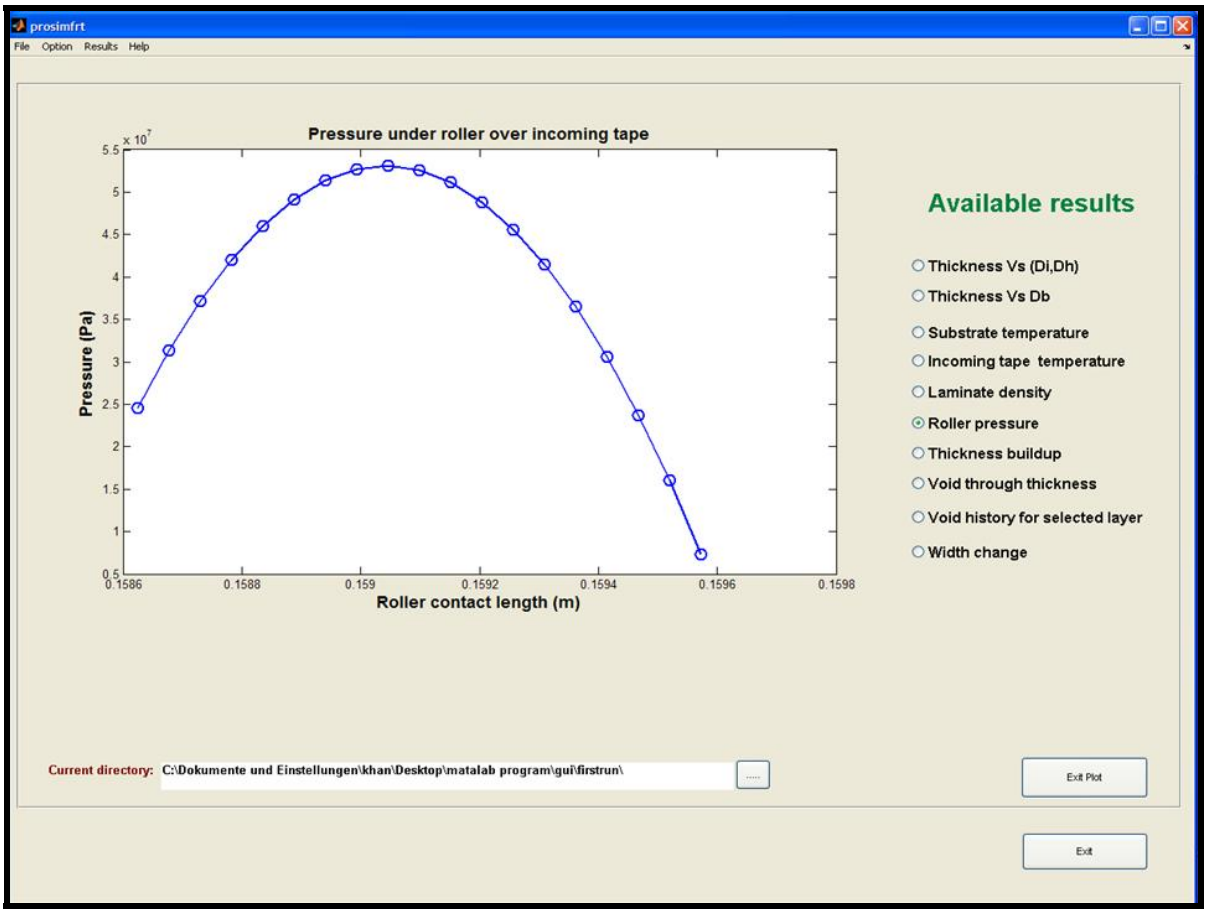

Figure 4.4: Post-process windows for output section to view the results.

Generated outputs as per predefined format in input section are available at the end of the solution. Results can be directly viewed through the software see Figure 4.4 or by using spreadsheet program like Excel or Origin. Extensive information can be extracted from several data files created during solution. An ‘overview.xls’ data file describes the overall laminate quality in terms of degree of intimate contact, healing and bonding. The user can visualize the combine effect of several processes by combining the available results.

4.3 Process simulation

In the foregoing section simulations were performed with different processing conditions and then compared with the experimental results to estimate the accuracy. ProSimFRT code is formulated by considering the IVW tape placement setup. But several other setups (multiple roller, line compactor etc) can be simulated by defining the inputs. A standard process simulation requires the detail of several input parameters, which has been determined in chapter 3. Table 4.1 shows the summary of the standard parameters used in most of simulation ahead.

Table 4.1: Standard Input parameter used in simulation.

Parameters	Detail
Setup	Single roller
Material	CF-PEEK
Tape initial void content	3.1 %
Tape thickness	0.14 mm
No. of plies (layers) in laminate	15
Roller diameter	50 mm
Roller temperature	90 °C
Consolidation force	165 N
Tool temperature	280 °C

4.4 Thermal simulation

Simulation for the 15^{th} lay-up over the laminate is carried out with standard parameter for the lay-up velocity of 6 m/min and hot gas flow volume of 3 norm liter/min. Temperature distribution in the incoming tape and the substrate material (already placed layers) can be numerically calculated and contour can be plotted as shown in Figure 4.5.

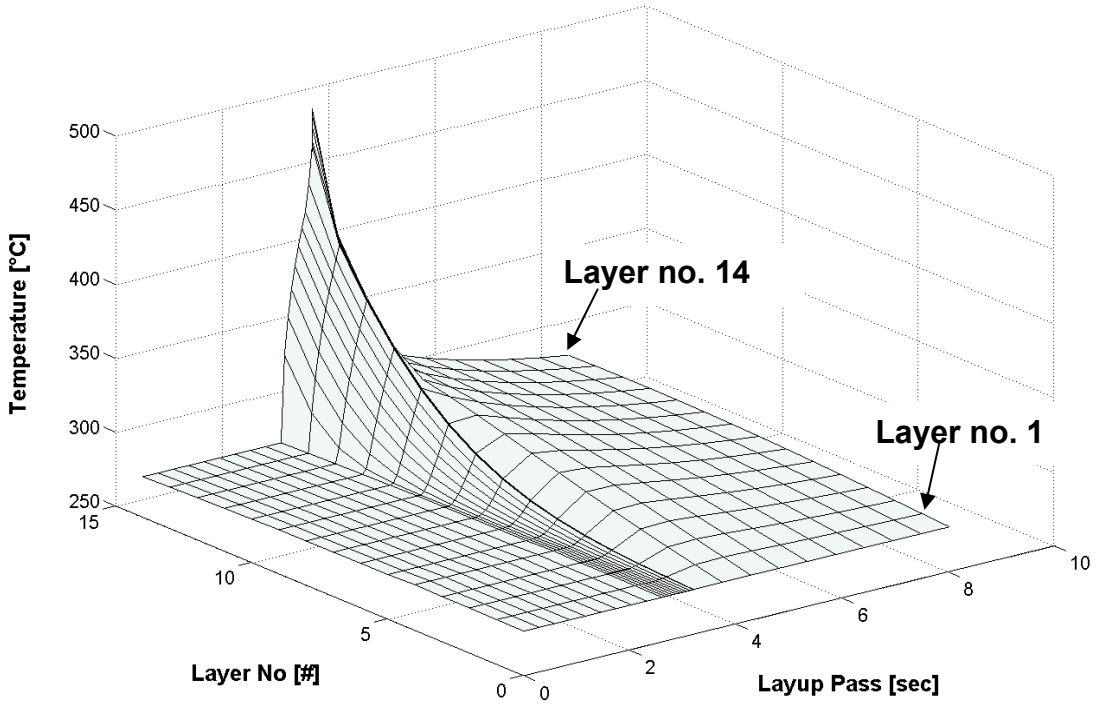

Figure 4.5: Temperature history for the substrate layers with typical hot gas torch heating (Gas volume 6 norm liter/min, velocity 3 m/min).

The top surface of the substrate (layer no. 14) which is directly exposed under the impinging hot gas flow attain very high peak before the nip point, where temperature rises up to 500 °C, high above the melting temperature of PEEK polymer. Thereafter a drop of temperature occurs under the roller which is followed by the cooling through natural air convection. Underneath layers also shows a similar behavior with different temperature magnitude. For example the maximum temperature rise in layer no. 13 is 427 °C which is around 73 °C less than the top layer. For this particular lay-up configuration, the heating effect becomes negligible to the layer no. 8 where it just raises to the 340 °C. Layers close to the tool experience heat sink effect and do not show big temperature gradient between them.

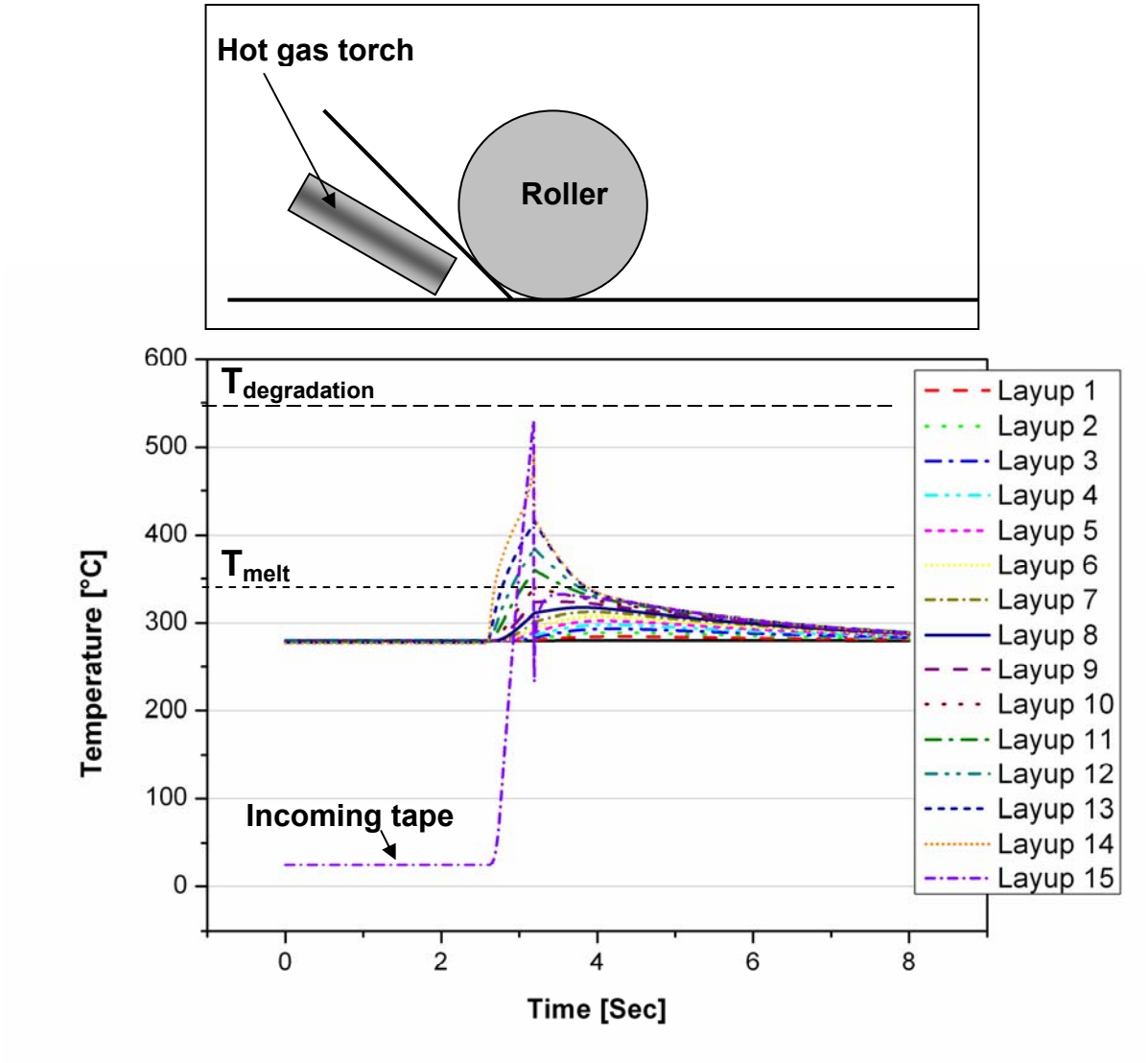

Figure 4.6: Layer by layer temperature during lay-up process (Gas volume 6 norm liter/min, velocity 3 m/min).

Special interest lies in heating of the incoming tape. For the under consideration case, incoming tape enters the heating region at room temperature and has a constant line contact with the cold roller on the back side as shown in Figure 4.6. Even with these conditions, temperature rise in the incoming tape is comparatively higher then the substrate surface. Although the temperature drops sharply under the roller due to direct cooling and even fall below the tool temperature but rises again due to the high substrate temperature and then follows the same cooling trends.

It is not possible to directly measure the nip point temperature using K-type thermocouples, as they could be destroyed under the influence of high gas temperature. Hence it was decided to measure the temperature one layer beneath the top surface during the final (15th) lay-up. The thermocouple captured the temperature distribution under the 14th layer and Figure 4.7 shows the comparison between the measured and simulated histories.

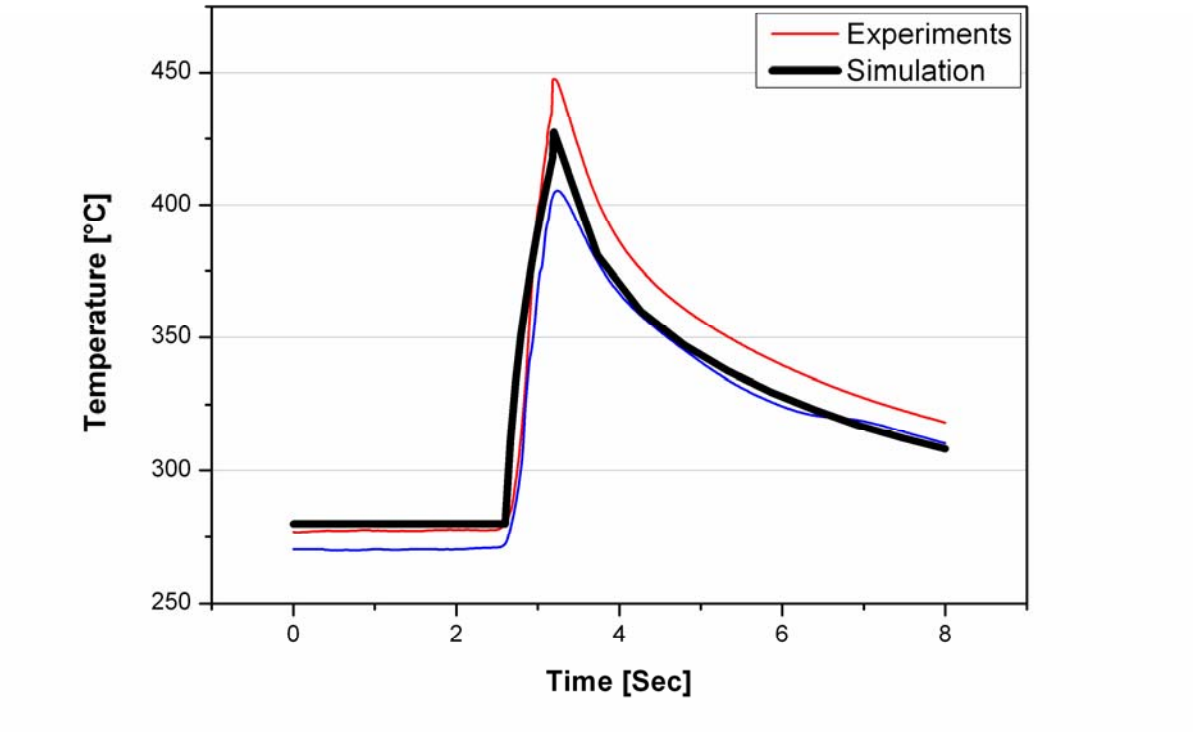

Figure 4.7: Comparison of simulation and measured results under the 14th (Gas volume 6 norm liter/min, velocity 3 m/min).

Differences in the measured histories are found sensitive to the exact positioning of the thermocouple juncture on the tape and variation in tool temperature (±5 °C). Results showed good correlation with the measured ones by capturing the approximate peak temperature. Nevertheless the overall prediction captured the transient heating rather well.

4.4.1 Surface temperature

Thermal histories play an important part in the tape placement process. Large heat input upstream to the roller, could generate thermal degradation / crosslinking in the

laminate, while low heat input could result in high viscous material, which restrict the intimate contact and polymer healing within the laminate. As the Incoming tape and the substrate surface experiences high thermal exposure; at this point it is interesting to know the maximum temperature of the two surfaces. See Figure 4.8 for substrate surface temperature. Two important aspects are visible here: firstly low lay-up velocity could raise the temperature of the CF-PEEK material up to thermal degradation level (>550 °C) and secondly the wavy behavior, which corresponds to the variation in the surface temperature for different gas volume.

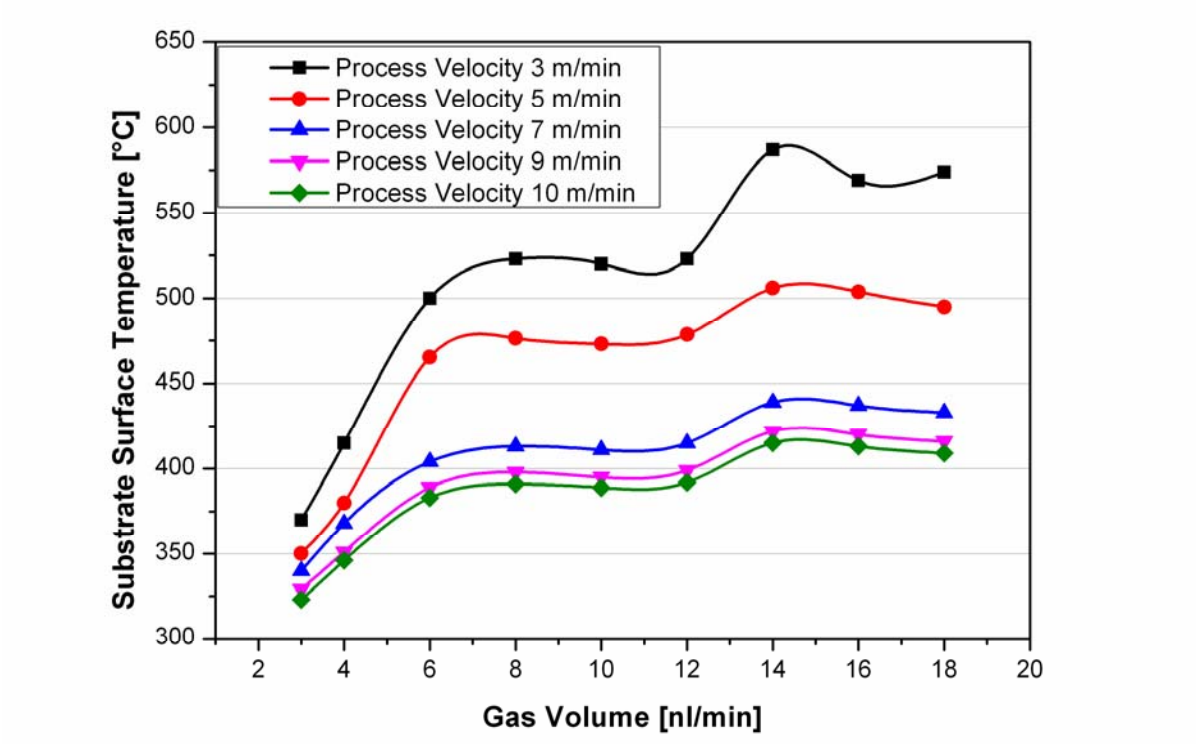

Figure 4.8: Maximum temperatures on the substrate surface through simulation for combination of process velocity and hot gas volume flow.

4.5 Simulation for consolidation and strength development

The consolidated laminate is mainly described by the overall void contents and the interlaminar bonding strength. Predicting the laminate quality through simulation is an efficient way to optimize the process. The models describing the consolidation process in the code are evaluated by simulating different manufacturing conditions and by comparing results with the experimental testing.

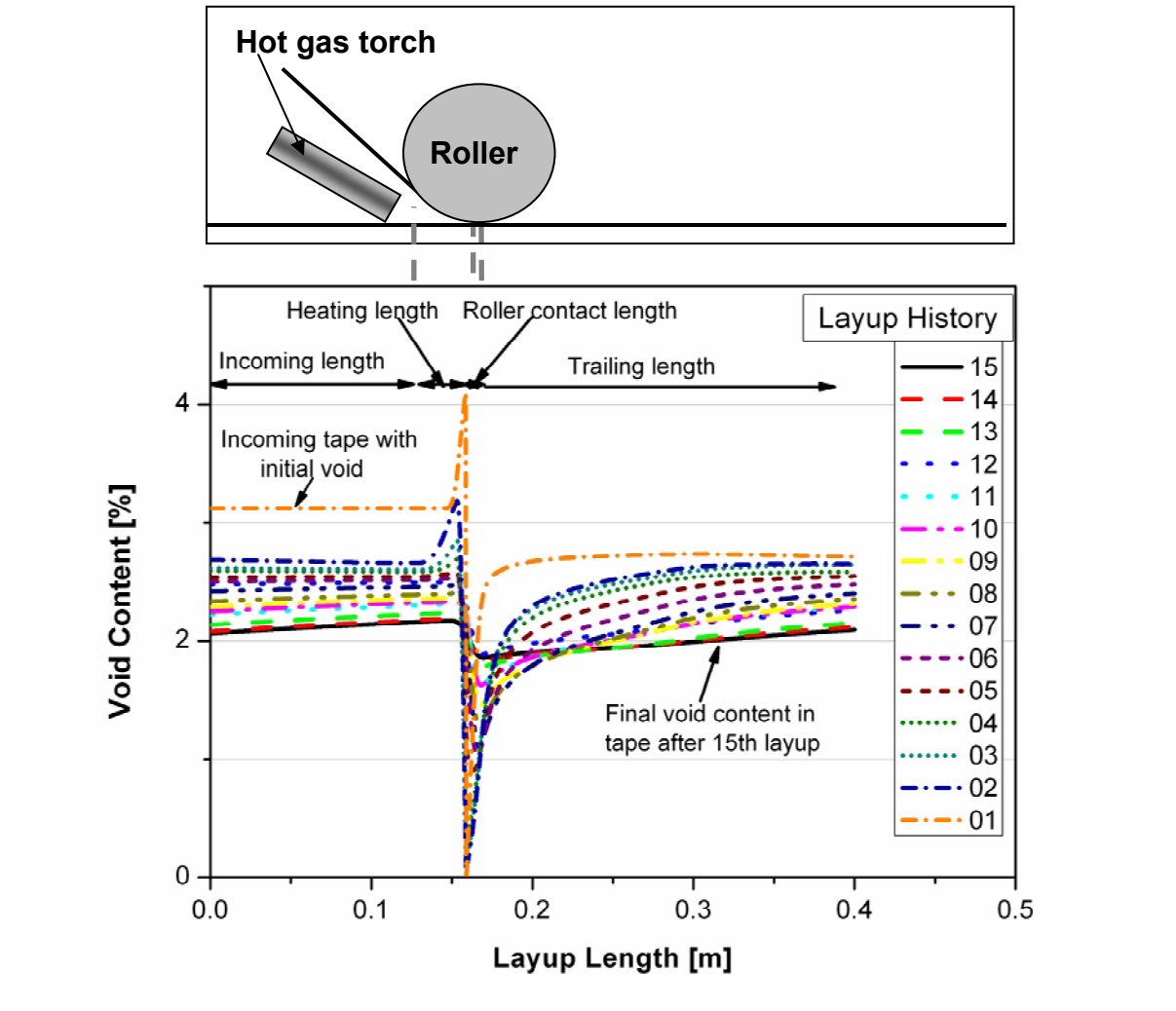

Figure 4.9: Void consolidation in first layer during successive lay-up (Gas volume 8 norm liter/min, velocity 5 m/min.

4.5.1 Void consolidation

Thermoplastic tapes inherit trapped voids and these voids contribute to intra ply void contents inside the laminate. Figure 4.9 shows how the intra ply void in a layer reaches its final consolidated value in several lay-up passes. During the first lay-up (#1) initial void inside the tape is first deconsolidated under hot gas torch in heating section and then consolidated under the roller. Such compression increases the internal void pressure. Since the material leaving the roller have very low viscosity, a

sudden expansion of void is inevitable. Balancing of internal with external void pressure in trailing section determine the final void content for the pass. For the successive lay-up, the value of void content from the previous lay-up acts as an initial void content. Further laminate build-up continues the void consolidation process in the layer 1. Although the scale of void consolidation drops down once the layer is buried inside and with substantial build-up (lay-up 11 in this case) void content reaches their final values for the layer 1. No further improvement is visible for further lay-up.

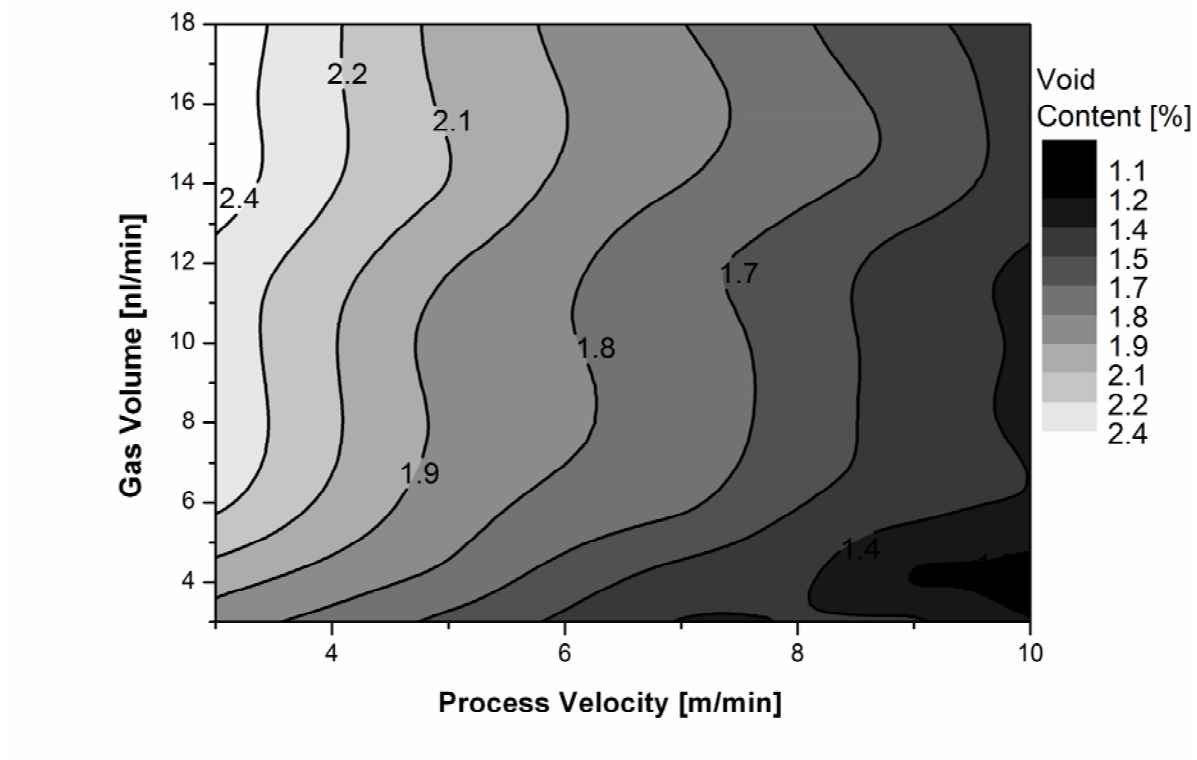

Figure 4.10: Simulated void contour at different processing conditions.

Simulated contour in Figure 4.10 indicates better void consolidation at higher lay up velocities and in all cases final void contents are less than the initial void percentage in the tape. This is in complete agreement with the consolidation mode described above that is final void content in the layer reached after several successive passes. Effect of processing velocity is also visible in this figure, with large void percentage at higher velocity. Since the consolidation of layer is a function of temperature and resulted viscosity, higher velocity limits the heat diffusion into the material. Lack of viscosity reduction due to low temperature restrict the void deconsolidation in the underneath layers.

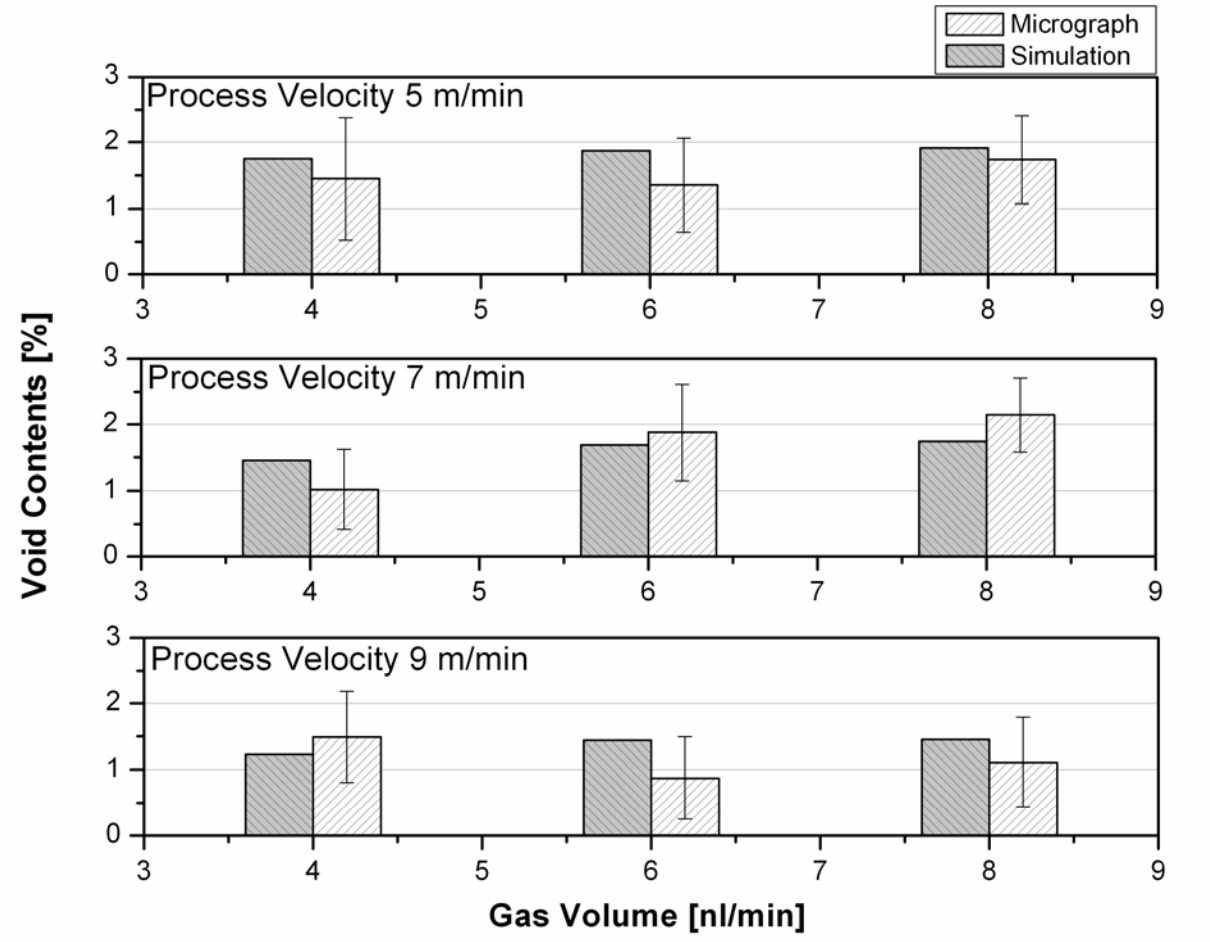

Figure 4.11: Comparison between measured and simulated void contents for combination of process velocity and hot gas volume flow.

Figure 4.11 shows the simulated void content for the 15 layered laminate manufactured with combination of lay-up velocity and hot gas flow. Standard inputs were used for defining the remaining parameters in code. For low lay-up velocity of 5 m/min void variations are not noticeable due to sufficient condition for the void deconsolidation at the roller exit at all gas volumes. But for high lay-up velocity 7 m/min a trend of increasing void contents is visible with higher gas volume. For lay-up velocity of 9 m/min, energy input to the tape in heating section is just sufficient to facilitate the consolidation under the roller and roller extract the reaming thermal energy by solidifying the material at its exit, preventing the void expansion. In all cases simulated results are comparable to measured values.

4.5.2 Geometrical deformation

The simulated thickness build-up for the 15 layered laminate is shown in Figure 4.12 which shows a linear relation between the lay-up no. and laminate thickness. The results show good correlation with the online laser measurement up to 10 layers, a slight deviation for higher lay-up could be a possible cause of the thickness variation in original tape (0.14±0.01 mm).

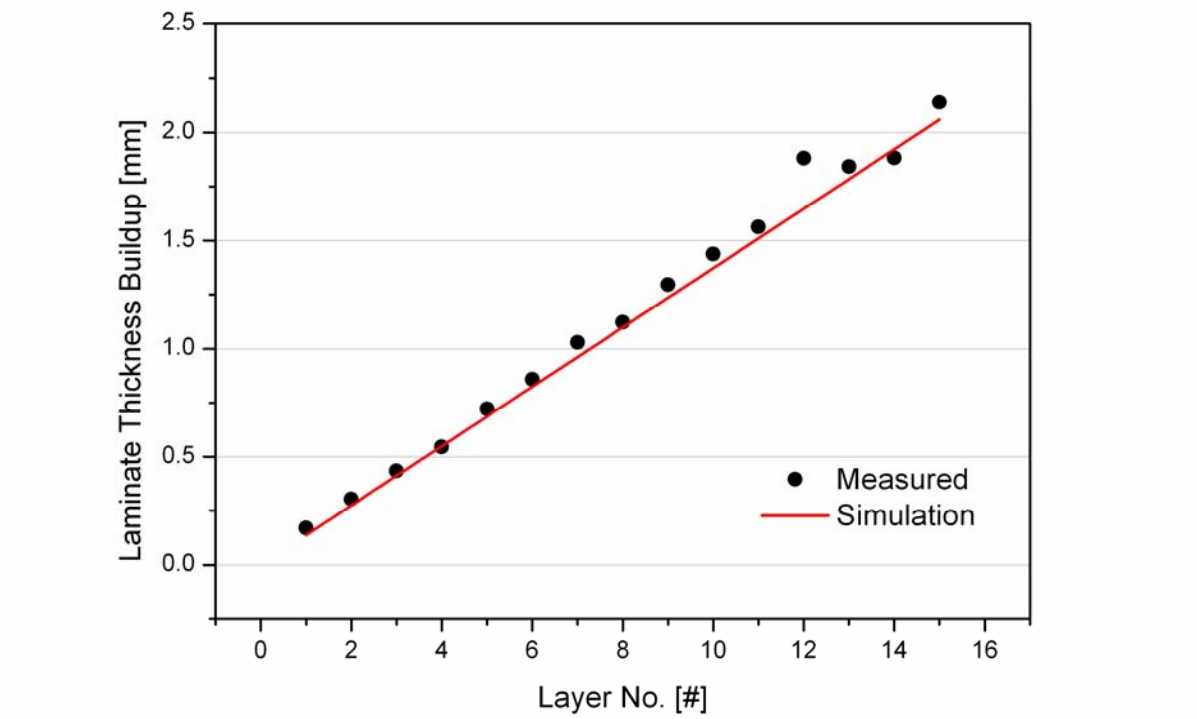

Figure 4.12: Thickness build-up vs. layer no (Gas volume. 8 norm liter/min, velocity 5 m/min).

Width deformation for a single tape on a hot tool also shows an increasing trend at higher gas volume (see Figure 4.13). Higher thermal energy softens the material and results in larger width change. Curly (wavy) behavior in the simulated width change resembles with the incoming tape surface temperature. With the available information of width deformation, transverse positioning of the placement head for the next adjacent tape with different overlaps can be calculated. Figure 4.14 shows the contour generated for 0.1 mm overlap with initial tape width of 12 mm. At lower gas volume, the tapes placement distance is less than the initial tape width but at higher gas volume the placement head should be positioned at larger distance by accounting the incurring width deformation in the tape.

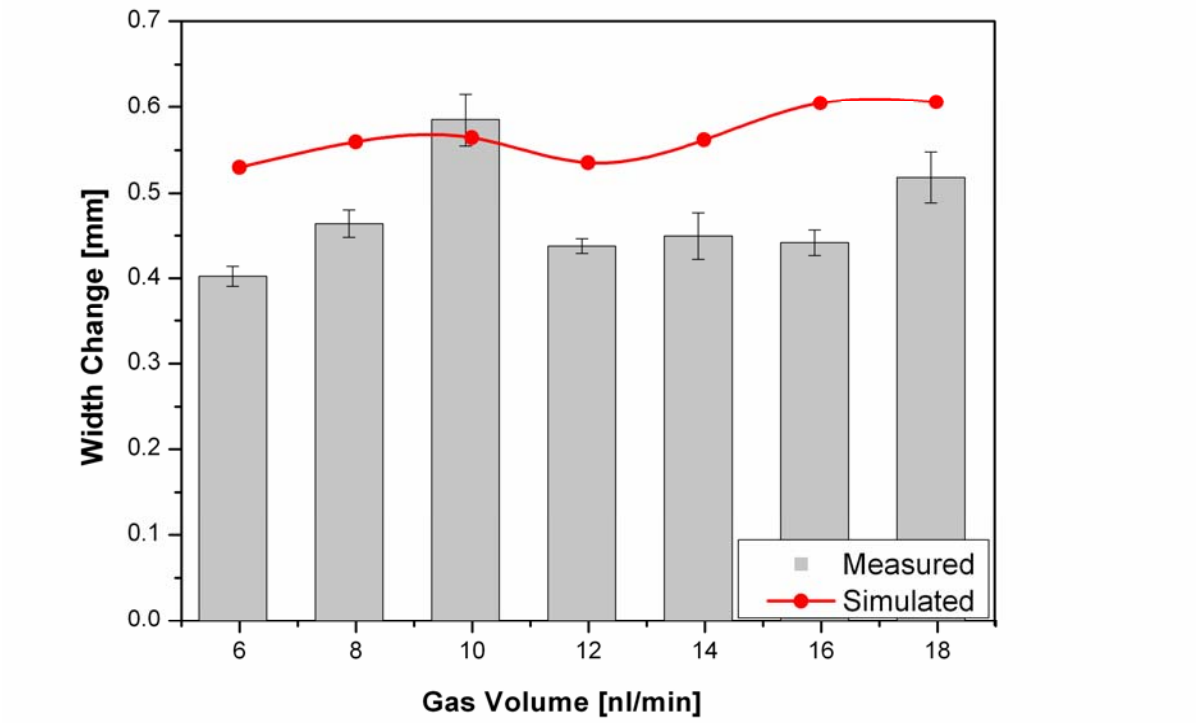

Figure 4.13: Width change prediction vs. measured (velocity 3 m/min).

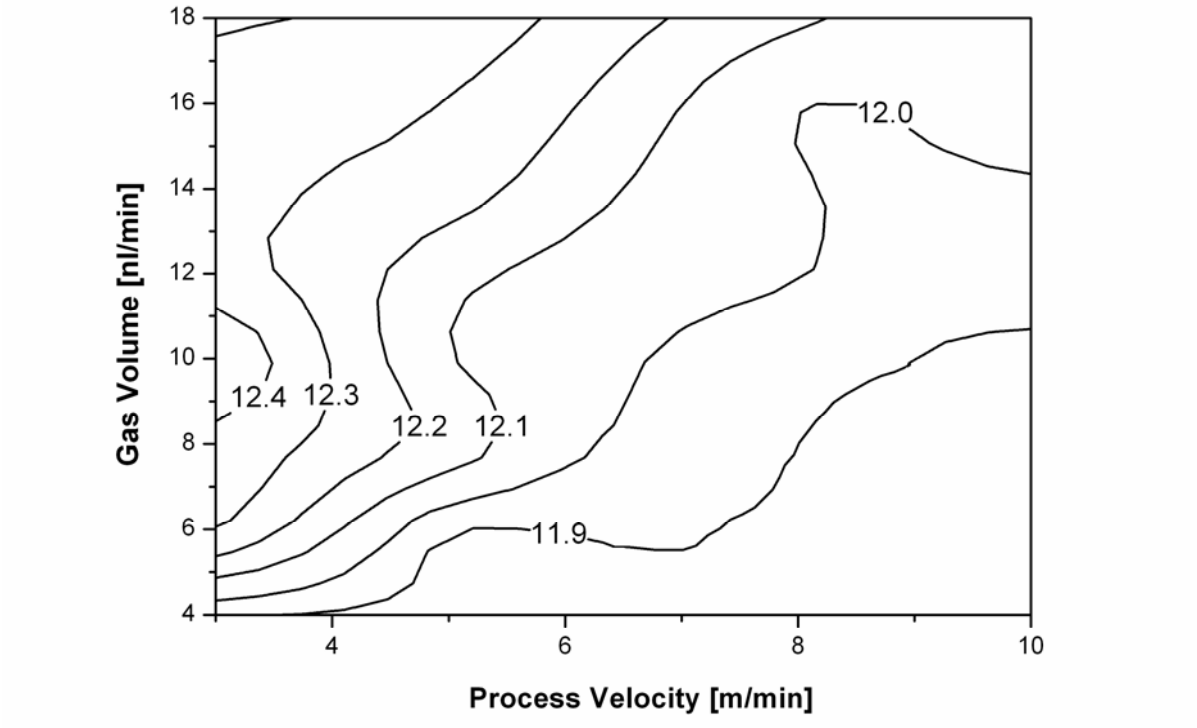

Figure 4.14: Distance for positioning next adjacent tape with 0.1 mm overlap for combination of process velocity and hot gas volume flow.

4.5.3 Prediction of interlaminar bonding

With the available temperature histories from the thermal model, the lay-up process can be simulated by tracing the intimate contact development and polymer healing between the plies. The combine effect as described in chapter 3, defines the level of bonding degree D_b within the laminate. D_b values can be compared with the double ply peel test or with the experimental D_b values from interlaminar shear strength test.

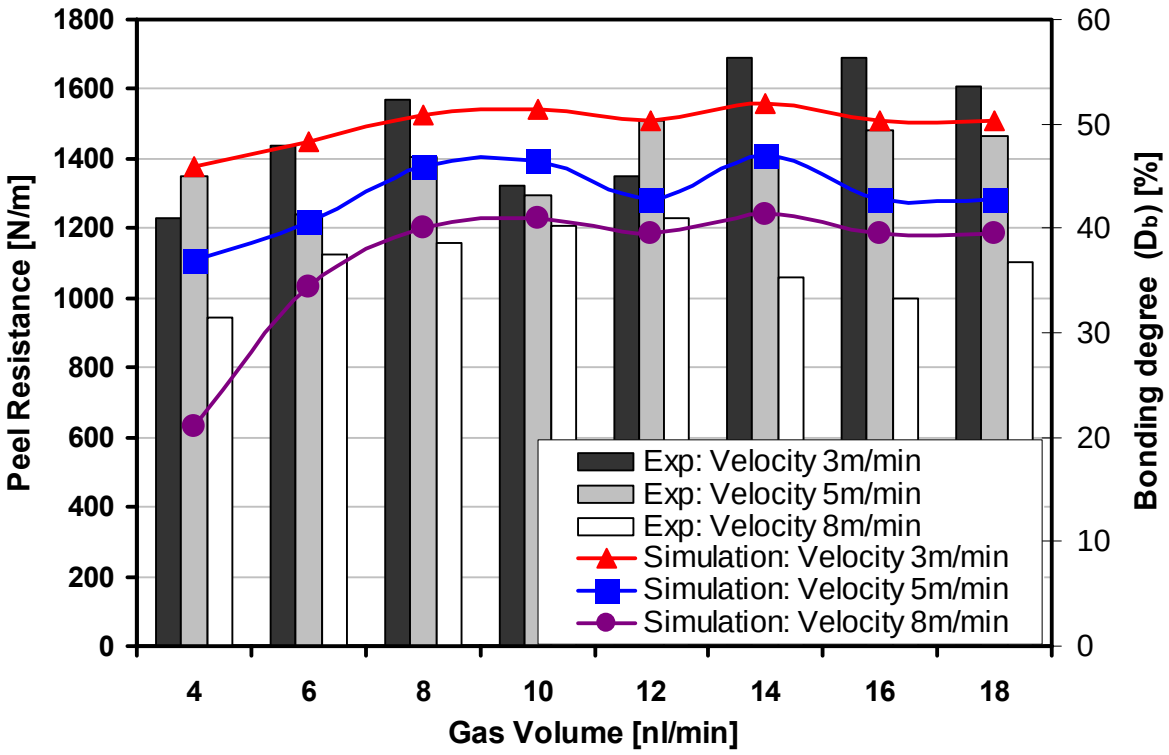

Figure 4.15: Peel strength vs. simulated D_b values for combination of process velocity and hot gas volume flow.

Although peel resistance cannot be transformed into experimental D_b values but indirect comparison with the simulated D_b values as shown in Figure 4.15, gives a way to explain the interlaminar bond development between the plies. At this stage it is possible to explain the sinking effect in peel resistance with increasing gas volume. The temperature distribution under the hot gas torch and consequent surface temperature in the incoming material and substrate material during the lay-up are responsible for this behavior. The gas volume flow which generates the peak in the surface temperature corresponds to better bonding within the laminate. Therefore it is very important

to exactly map the temperature variation in the vicinity of hot gas torch. Overall trends depict an increase in the peel resistance (or simulated D_b) with the low lay up velocities.

Similarly D_b simulation for the complete 15 layered laminate (see Figure 4.16) explains several interesting strength development aspects. The surface temperature variation marks the large influence on the contour shape. The contours in Figure 4.16 show the comparatively wide range to manufactured laminate with high interlaminar bond strength (i.e. D_b>90%) at larger gas volume. The contour converges sharply at low gas volume and shows high variation in D_b. The lay-up velocities over 8 m/min appear to be not suitable for the existing setup due to lack of availability of sufficient energy to the complete bonding process. Simulation [25] indicates that the time to achieve full intimate contact is significantly longer than the time required for full polymer healing at the interface. On the other hand for low lay-up velocity and at higher gas volume flow, the viscosity of the PEEK matrix reduces significantly and the surface irregularities disappear rapidly by allowing easy and swift polymer diffusion for strength development.

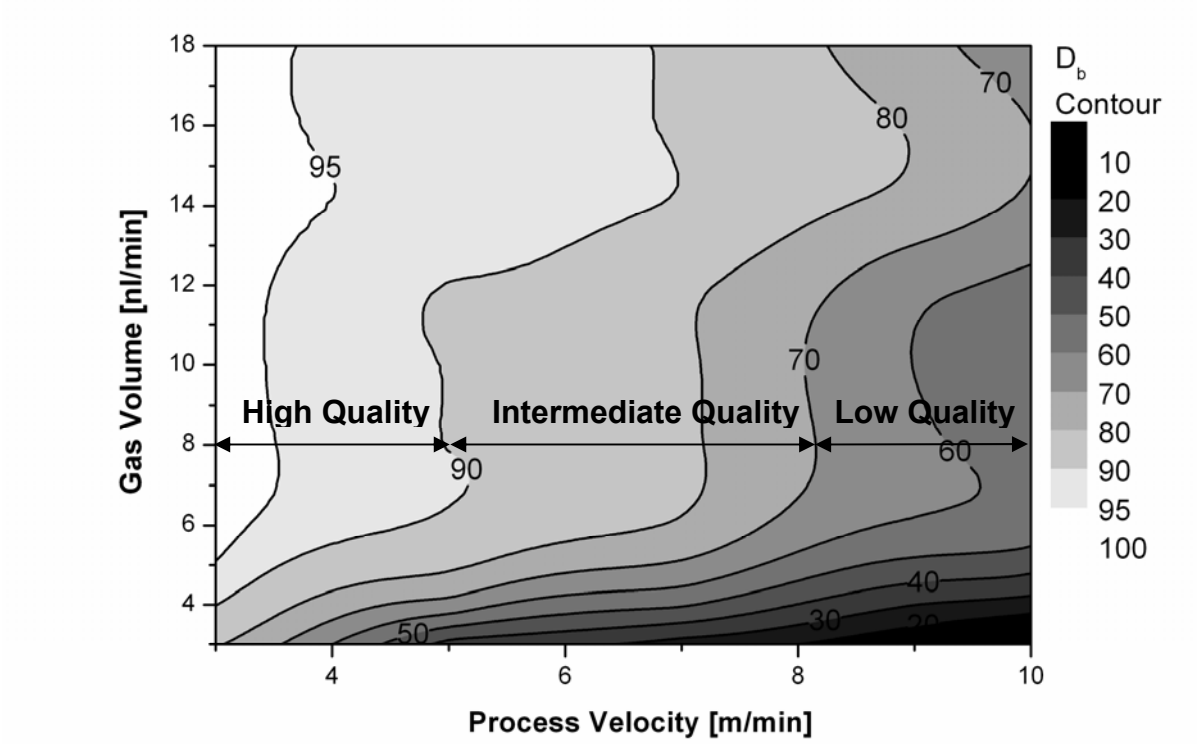

Figure 4.16: Simulated D_b values for combination of lay-up parameters.

4.6 Process parameter study

Industry demands high laying speeds by maintaining the higher laminate quality. The goal of this study is to describe the influencing processing parameters which can result in higher interlaminar bonding strength and minimum void content inside the laminates. As the task of parameter study involves several inputs, pure experimental testing is time consuming and economically not feasible. With the availability of proper simulation tool, unlimited number of process parameter can be verified in faster fashion. A combine strategy is adopted in which extensive simulation is combined with selected experimental testing to achieve the goals (see Figure 4.17).

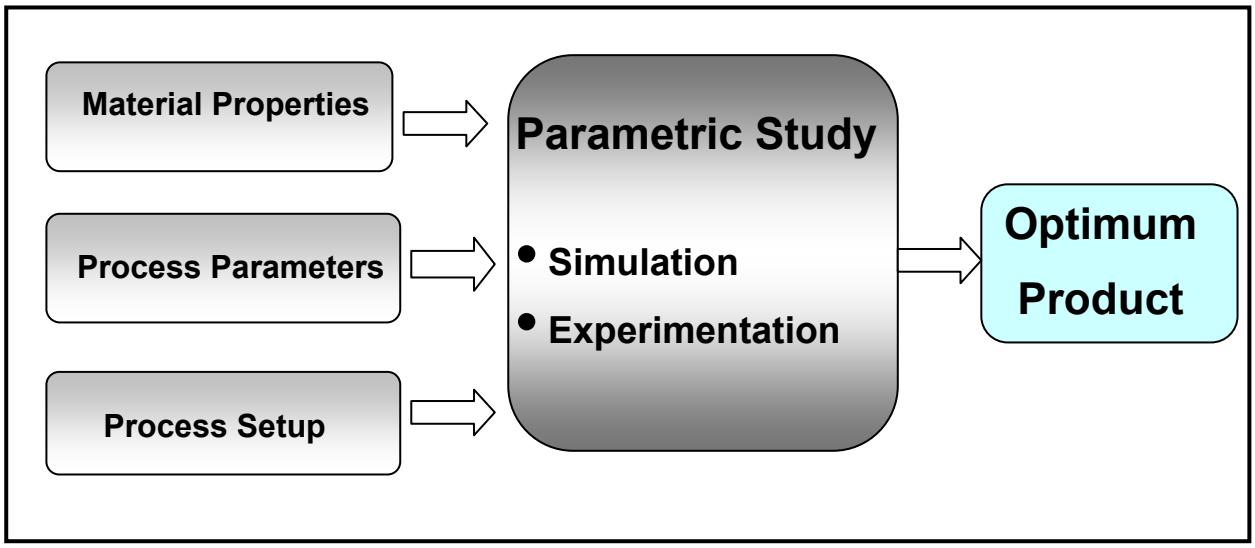

Figure 4.17: A schematic of the process parameter study for tape placement.

Inputs for the study are classified into three categories material properties, process parameters and process setup (see Table 4.2). A total number of 16 parameters are selected for the study and at a time variation of one or two variables are carried out by keeping the other as standard inputs. The values are even varied over the existing limit of the manufacturing setup to see their effects. For the sake of clarity a concise detail of few variations are presented here while the remaining results are summarized at the end of section.

Table 4.2: Selected process inputs for parameter study, for standard input parameters see Table 4.1.

Process Parameters	Process Setup	Material Properties
Gas volume	Multiple roller	Low viscosity
Lay up velocity	Additional torch gas volume	Initial tape void
Roller diameter	Force on additional roller	Surface roughness
Heating length	Line compactor with high forces	
Consolidation force		
Tool temperature		
Roller temperature		
Reconsolidation pass		
Laminate thickness		

4.6.1 Effect of consolidation force

Increase in force is considered to result in obtaining better consolidation. Figure 4.18 shows the change in the bonding degree D_b and void content with the variation of force from 50 to 5000 N. For the low lay-up velocity of 3 m/min, even a small force 50 N is capable to produce the bonding degree over 95%, while a slight higher force 165N is well enough to bring it up to 98%, further increase does not seem to be beneficial. On the other hand at higher lay-up velocities, even the 5000 N of force is unable to bring the D_b to 80%. The reason is incomplete intimate contact and less residence time under the consolidation roller at higher lay-up velocities which results in insufficient energy to initiate good bonding.

Void consolidation curves on other hand present the inverse picture. At lower processing velocity void deconsolidation phenomena upstream to the roller demand very high consolidation force and must be supplemented by the sudden cooling under and beyond the roller to freeze this state. But in all cases deconsolidation downstream to the roller is apparent. Contrary to this fast lay-up velocity causes less void deconsolidation in the heating section hence overall low void contents inside the laminate.

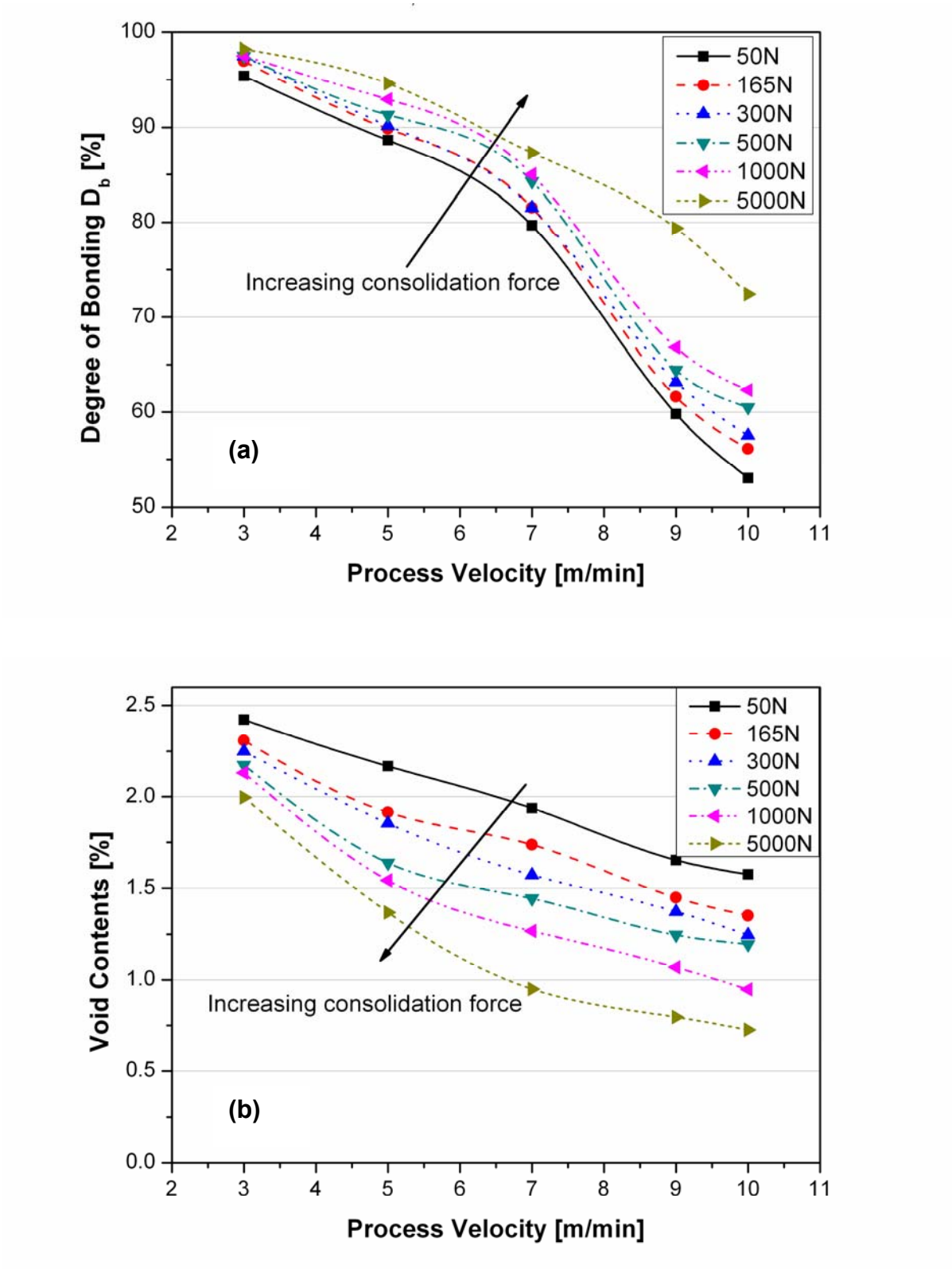

Figure 4.18: Effect of consolidation force on the degree of bonding and laminate's void contents. (Gas volume 8 norm liter/min).

Indeed the consolidation force under the roller is directly related to the interlaminar contact development but it also increases the internal pressure of the trapped void. Thus, very high forces are required for the significant improvement making the construction of a tape placement head assembly heavier. Plates were manufactured and tested to verify the improvement in D_b with the increase in consolidation force and ILSS tests were carried out for the plates manufactured at 100, 160, and 225 N to examine this effect and it shows (Figure 4.19) good correlation with the simulation.

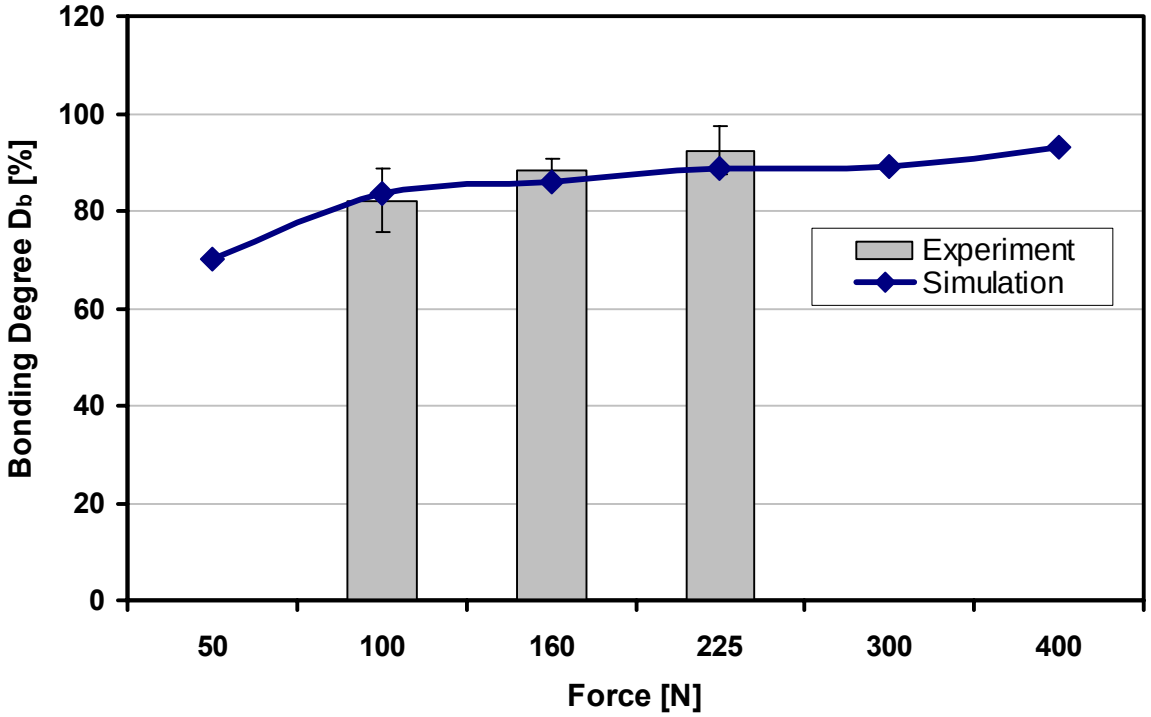

Figure 4.19: Degree of bonding vs. force (Gas volume 6 norm liter/min, velocity 3 m/min).

4.6.2 Effect of number of plies (layers) on laminate quality

Simulations are also performed to investigate the plies (layers) stacking effect i.e. laminate's thickness build-up process. The results are shown in Figure 4.20 as a function of lay-up velocity and as a number of plies in the laminate.

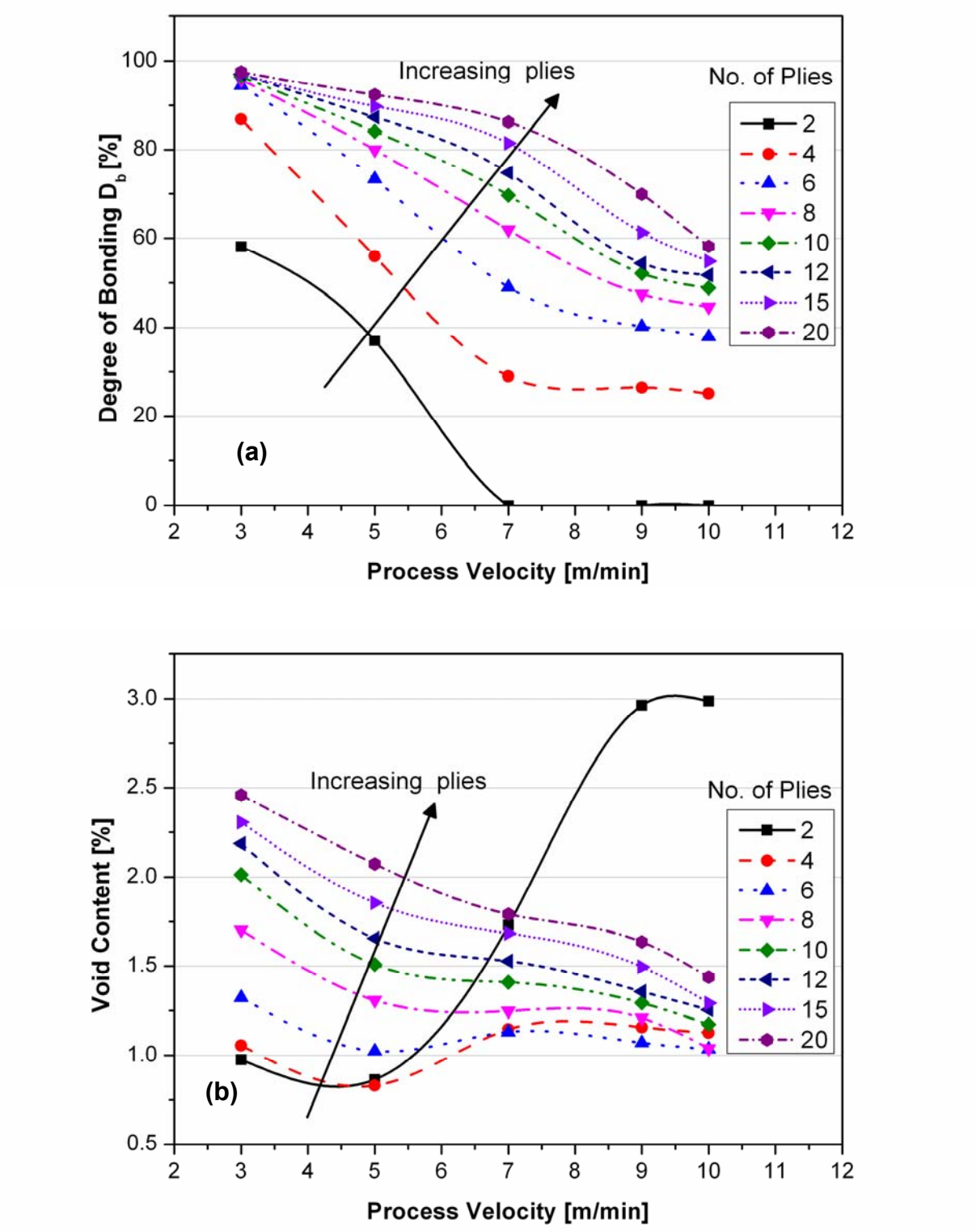

Figure 4.20: Effect of number of plies on the laminate's (a) degree of bonding and (b) void contents. (Gas volume 8 norm liter/min).

Laminate with less plies (<6) are unable to attain bonding degree over 60%. Heat sinking effect by the tool is dominant in these laminate which hinder the bond development process. For thick laminates the plies near to the tool act as a thermal insulator by blocking the direct heat flow. Resulting laminate shows better values for the degree of bonding. Results for the void content simulations also show sensitivity to the number of plies.

Consider the lay-up velocity of 3 m/min, for the thin laminate (less plies) tool behaves positively by freezing the consolidating state under the roller. But for the thick laminates, already placed layers act as insulation and restrict the faster heat flow towards the tool, thus causing large void deconsolidation for the newly placed top layers and increasing the laminate overall void content. On the contrary for the high lay-up velocity of 10 m/min, laminate has less residence time under the hot gas torch owing to less energy inside and the subsequent voids deconsolidation beyond the roller is not effective. For the case of laminate with only two plies, the insufficient heating and heat extraction by the tool even does not initiate any void change in the original tape.

4.6.3 Effect of tool temperature

Simulation results for the degrees of bonding D_b with different tool temperatures are plotted in Figure 4.21 (see next page). The cold tool (<250 °C) behaves as a heat sink and restricts the bonding process. The black regions in the contour plot represent the laminate with improper bonding. With the increased tool temperature (280 °C) significant improvement is visible, some lay-up combination even bring the Db up to 98%. With the tool at 330 °C, this is closed to the melt temperature (340 °C) of PEEK polymer, most of the combinations could result in perfectly bonded laminate. Plates were manufactured with different tool temperatures (250 °C, 280 °C, 300 °C) and tested for the ILSS (in Figure 4.22) also indicate better values at higher temperature. The increasing strength tendency is appreciable until 280 °C (which is the cooling crystallization temperature) to achieve complete bonding, after that no major improvement is noticeable.

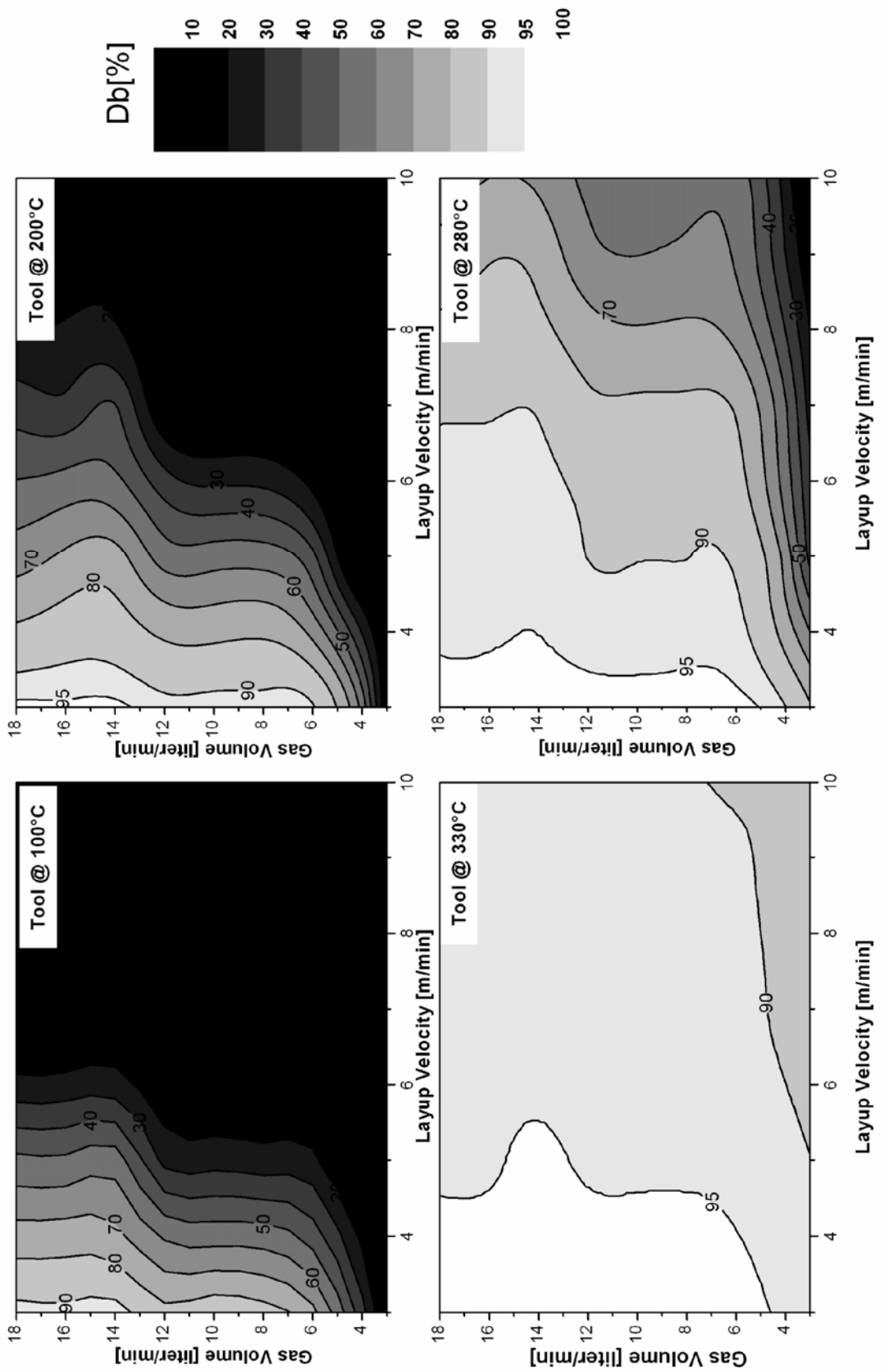

Figure 4.21: Simulated D_b values with different tool temperature.

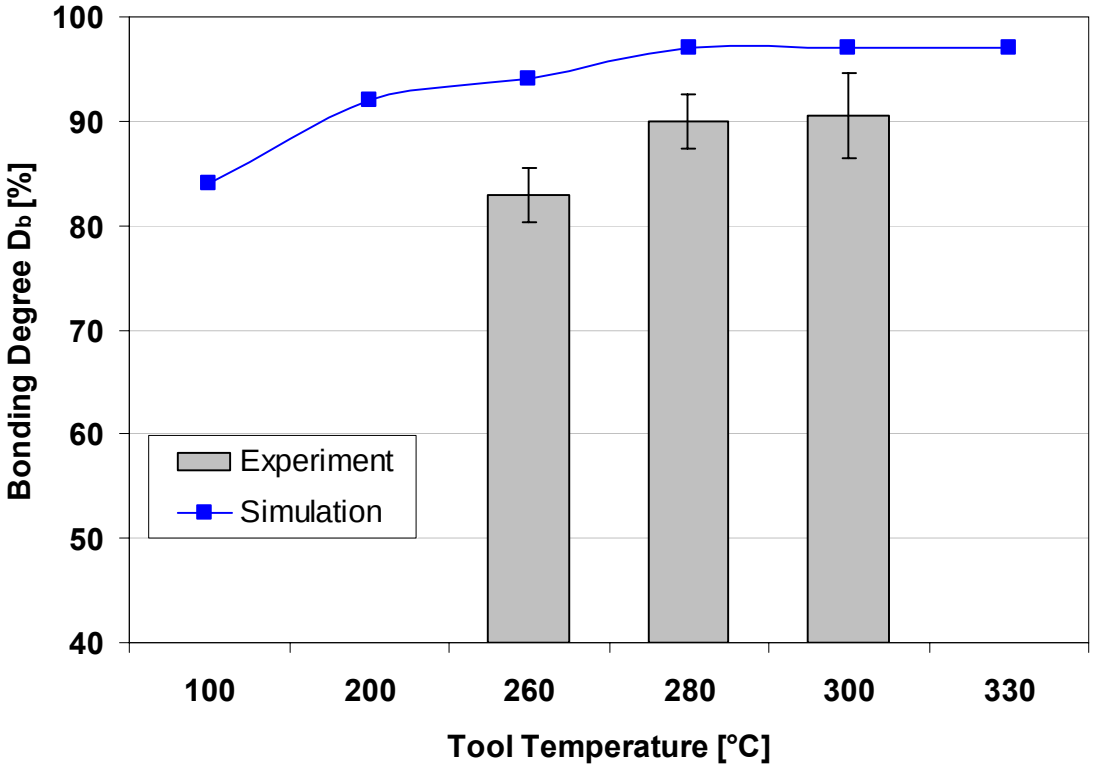

Figure 4.22: ILSS test results for laminates manufactured at different temperature. (Gas volume 8 norm liter/min, velocity 3 m/min).

4.6.4 Overview

All other parameters listed in Table 4.2 were analyzed in the similar fashion [82]. Referring back to Figure 4.16, laminate quality based on the degree of bonding can be classified into three levels.

- High quality laminate with $D_b > 90\%$
- Intermediate quality laminate with $90\% > D_b > 70\%$
- Low quality laminate with $D_b < 60\%$

For every gas volumes, these three quality levels exist as variable band in combination of lay up velocities. Also these levels are wide spreads at higher gas volume compared to the lesser gas volume.

By considering the gas volume of 8 norm liter/min, the bench mark values for the D_b and void contents at these three levels can be obtain at lay up velocities of 3, 5 and 9

m/min. The relative assessment of quality improvement with the variation of all selected process parameters was carried out by comparing the obtained D_b and void content values with these bench mark values. Change in laminate quality is represented by following symbols in Table 4.3

Table 4.3: Parameters influence on laminate's quality at three levels.

	D_b [%]			Void consolidation [%]		
Performance level	**H.E**	**I.E**	**L.E**	**H.E**	**I.E**	**L.E**
Bench mark (Gas volume 8 liter/min)	96.98	89.86	62.32	2.3	1.91	1.44
Parameters	**Influence on D_b**			**Influence on void contents**		
Higher gas volume	0	+	++	--	--	-
Higher process velocity	-	--	--	0	+	++
Roller dia. 25 mm	0	0	-	+	+	++
Roller dia. 100 mm	-	0	-	-	-	--
Heating length 10 mm	--	--	--	++	++	+
Heating length 50 mm	+	+	++	-	--	--
Consolidation force 50- 500 N	0	+	+	+	++	++
Tool temperature 100 °C	-	--	--	++	++	--
Tool temperature 330 °C	0	+	++	-	-	-
Roller temperature 25 °C, Consol. length 1 mm	0	-	-	++	++	++
Roller temperature 25 °C, Consol. length 2.3 mm	-	--	--	++	++	++
Roller temperature 25 °C, Consol. length 4.7 mm	-	-	0	++	++	++
Roller temperature 280 °C, Consol. length 1 mm	0	0	+	--	--	--
Roller temperature 280 °C, Consol. length 2.3 mm	+	+	+	--	--	-
Roller temperature 280 °C, Consol. length 4.7 mm	+	++	++	--	--	-
Reconsolidation passes 1-4	+	+	0	+	+	0
4 Plies in laminate	-	--	--	++	++	++
20 Plies in laminate	0	+	++	-	-	--
Roller number 2, Gas volume 6 norm liter/min	0	+	++	-	--	--
Roller number 3,Gas volume 6 norm liter/min	0	+	++	-	--	--
Second torch Gas volume 4 norm liter/min	+	++	++	0	-	--
Second torch Gas volume 10 norm liter/min	+	++	++	--	--	--
Roller 2 consolidation force 50 N	0	+	++	-	-	--
Roller 2 consolidation force 500 N	0	0	++	-	-	--
Consolidation length 1 mm, Force 500 N	+	++	++	0	--	+
Consolidation length 4.7 mm, Force 500 N	+	+	+	+	+	++
Low viscosity (PEEK)	0	+	++	--	--	--
Initial void content 1%	0	0	0	++	++	--
Initial void content 10%	0	0	0	--	--	--
Commulative force F1>F2	0	+	++	--	--	--
Surface roughness	0	+	++	+	++	++

where

- '**0**' shows no change
- '**+**' or '**-**' shows up to 10% improvement or deterioration
- '**++**' and '**--**' shows over 10% improvement or deterioration

To further summarize the results and to get the global idea about the parameter variations, variation in bonding degree and void content for each parameter change is sum up in Table 4.4. First column shows the parameter variation and subsequent column represents the influence over the D_b and void contents. '+' sign shows the advantage while '-' sign indicates the disadvantage.

Table 4.4: Process parameters and their influence on the laminate quality.

	D_b	Void Content
Process Parameters		
Gas volume ↑	**+**	**-**
Lay up velocity ↑	**-**	**+**
Roller diameter ↑	**-**	**+**
Heating length ↑	**+**	**-**
Consolidation force ↑	**+**	**+**
Tool temperature ↑	**+**	**-**
Roller temperature ↑	**+**	**-**
Reconsolidation pass	**+**	**+**
Laminate thickness ↑	**+**	**-**
Process Setup		
Multiple roller	**+**	**-**
Additional torch gas volume ↑	**+**	**-**
Force on additional roller ↑	**+**	**-**
Line compactor with high forces	**+**	**+**
Material Properties		
Low viscosity	**+**	**-**
Initial tape Void ↑	**0**	**-**
Surface roughness ↓	**+**	**+**

Some interesting observations are as follows:

- All parameter variations, which supplements the additional heat energy (e.g. high gas volume, low lay-up velocity) during the lay-up process contributes to an improvement in the D_b value. At the same time such combination increases the volume void content and reduces the laminate quality.

- Large roller diameter or consolidation length only benefits in combination with higher force, by extending line pressure to improve both D_b and better void consolidation in the laminate.

- For any particular combination, laminate thickness build-up seems to be positive, the underneath layer acts as an insulator by hindering the rapid heat flow from top layer to relatively cold tool. Thus providing more time for polymer diffusion.

- Increase in roller temperature enhanced the bonding process on one side but accelerates the void expansion (deconsolidation) at the roller exit.

- High tool temperature (up to 300 °C) supports polymer diffusion to improve the bonding strength.

- Laminate's top layers always lack the complete consolidation, additional passes over these layers not only helps in improving the D_b values but also in eliminating trapped void from the laminate.

- Noteworthy improvement in D_b value can be obtained through placement head with multiple rollers. Simulation indicates an additional roller is sufficient to get this benefit.

- Higher consolidation force on the first roller results in better laminate strength, as the incoming tape and substrate interface receives high thermal energy by first torch before entering the consolidation roller.

- Laminate quality is highly influenced by the tape's initial void content. Tape with fewer voids is less prone to void deconsolidation.

- Tape with flat surface or with less roughness, results in better intimate contact generation and enhance the bonding between the layers.

5 Results and discussion

For the large industrial application, processing technique should be updated to satisfy the new requirements. Industrial application of tape placement technology not only demands the high production rate but also the laminate quality comparable with some of the fully developed traditional composite manufacturing techniques e.g. autoclave, VARTM [84-85]. Aerospace structures demand structures with high inter-laminar bonding strength (comparable to autoclaved processed laminate see Table 5.1) and less void content (<1%). By controlling the processing conditions, a structure with desired mechanical characteristic can be manufactured. Compilation of information through experimental characterization and the development of a simulation tool provide a way to understand and to explain the incurring technological limitation and challenges to the existing level of tape placement technology. The following section will discuss some phenomena hindering the way to achieve high laminate quality and some possible strategies to deal with.

Table 5.1: Reported achievable ILSS values for CF/PEEK laminates manufactured through autoclaved process.

Processing Condition	IVW [86]	UD-CCM [8]	Accudyne [87]	EirComposites + ESA [88]
Material manufacturer	Suprem		Cytec	Gurit Suprem
Hand lay-up + Autoclaved	92	-	-	85
Tape placed + Autoclaved	94	95	103	-

5.1 Weight loss

Based on TGA experiments for the CF-PEEK material, the maximum degradation rate (4.8 %/min) occurs when the conversion level is less than 10%. Using equation (3.4), with the E_a= 156 KJ/mol and Log A= 5.27 min^{-1} from Table 3.6, weight loss diagram at constant isotherm for the duration of 5 minute can be plotted as shown in Figure 5.1. It is evident that slope changes sharply from thermal degradation temperature range of 550 °C to 900 °C. In the lay-up process, the incoming tape and the substrate surface have the chances for high temperature exposure. Direct contact

with the impinging hot gases from the torch increases the layer temperature but the duration of exposure is relatively short for the existing single roller setup. The low lay-up velocity of 3 m/min and large hot gas flow volume of 18 norm liter/min describes the high energy input combination. Even with these parameters, cumulative exposure time over 550 °C for a single layer is limited to only 4.5 seconds in entire 15 layered lay-up. Using a conservative approach by considering the complete exposure at constant temperature of 700 °C resulted in negligibly small weight loss value of 0.17%. Sonmez [89] uses the thermal degradation model [75] for optimizing the lay-up process and Fink [90] performs the experimental investigation on degradation effects. Both studies concluded that the high quality laminate can be manufactured without any noticeable loss of mass.

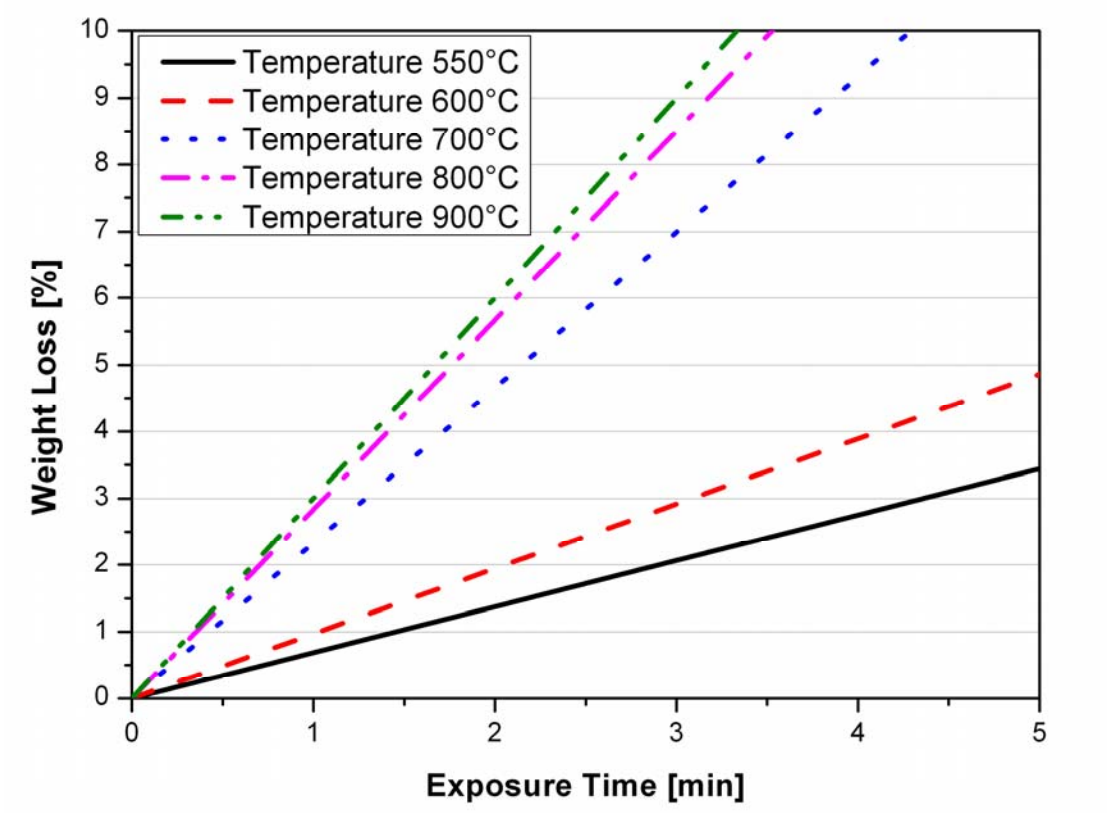

Figure 5.1: Weight loss diagram for CF-PEEK material in air at different exposure time and temperature.

5.2 Thermal degradation

The strength analysis is presented to delineate the relative effect of polymer bonding and thermal degradation. The origin of polymer degradation during lay-up is uncertain. It may be due to (1) removal of polymer matrix rich layer from the tape surface caused by high velocity impinging hot gas flow, unveiling the carbon fibers at bonding interface (2) cross-linking or cyclization of the polymer chains reducing the chain mobility and hence the ability to diffuse and bond [90]. The first postulate demands heat and mass flow studies of turbulent hot gas plume at the interface of incoming tape and substrate material. But the photo micrograph analysis shows the presence of matrix rich layer (4-7 µm) in the samples manufactured even with large gas flow undermined this assumption at least for the existing setup. Nicodeau [18] on the other hand combines the kinetic laws for polymer diffusion and thermal ageing with heat transfer model to explain the drop in the bonding strength. She observed an increase in crosslinking rate over the melt temperature which begins to hinder adhesion between the layers. Hence the difference between the D_b simulated and experimental values is investigated by considering crosslinking phenomena for the process.

Simulations were performed for the 15 layered laminates to determine the cross linking rate over the wide range of the lay-up velocity and hot gas volume combinations. Generated iso-curves for the crosslinking rate follow a similar slope and demonstrate a higher crosslinking trend at low process velocity as shown in Figure 5.2.

As discussed before, polymer healing and crosslinking depends on the localized heating under the hot gas torch. At low lay-up velocity large thermal exposure improves the polymer healing (diffusion) at the laminate interface and results in the higher bond strength. For such cases the effect of the crosslinking has secondary concern. But the strength degradation is more evident for the high velocity lay-up, where the polymer healing is not fully accomplished and crosslinking hinders it additionally. Referring back to Figure 3.36, a major drop in the ILSS starts to appear over the gas volume of 6 norm liter/min. Considering the highest lay-up process velocity 9 m/min, which is ideally subjected to minimum thermal exposure, indicates the major strength drop between 6 and 8 norm liter/min, the iso-crosslinking curve between these two chosen gas volume flows in Figure 5.2 has a value of 10^{-4} mol/g.

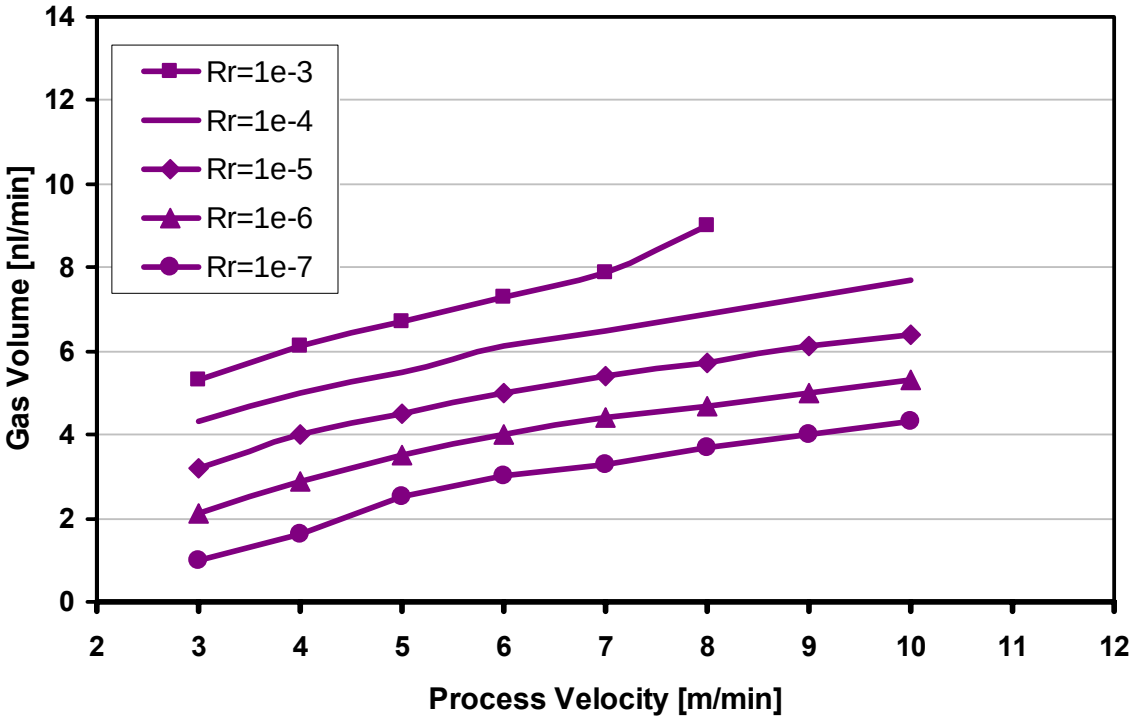

Figure 5.2: Iso-curves for crosslinking rate R_r [mol/g] at different lay-up configuration.

Hence this curve indicates the border below which the crosslinking effect is not dominant and all the combination above will have a sinking effect in strength due to higher crosslinking of polymer chains. To see this behavior the selected iso-curve for the crosslinking rate (10^{-4} mol/g) is overlapped on the D_b iso curves as shown in Figure 5.3.

Experimental D_b values match well with the simulated D_b contour plot under this limiting crosslinking curve. Consider the 4 norm liter/min gas volume, the experimental D_b value of 82% lie exactly in the narrow simulated D_b contour band of 80-90%. Good matches also exist for the other velocities. Disagreement arises at higher gas volumes over this limiting curve where the polymer crosslinking increase actively. For a particular lay-up velocity, the trend of strength improvement is visible up to or near to the limiting crosslinking curve and which is then followed by the fluctuation and drop of D_b values.

So, for a particular D_b, those combinations are permissible which are not affected by the crosslink phenomenon. In such way laminates can have a better chance for further post consolidation improvements, or process should be limited to low lay-up ve-

locity by allowing more time for polymer healing at interface by overcoming hindering effect due to crosslinking.

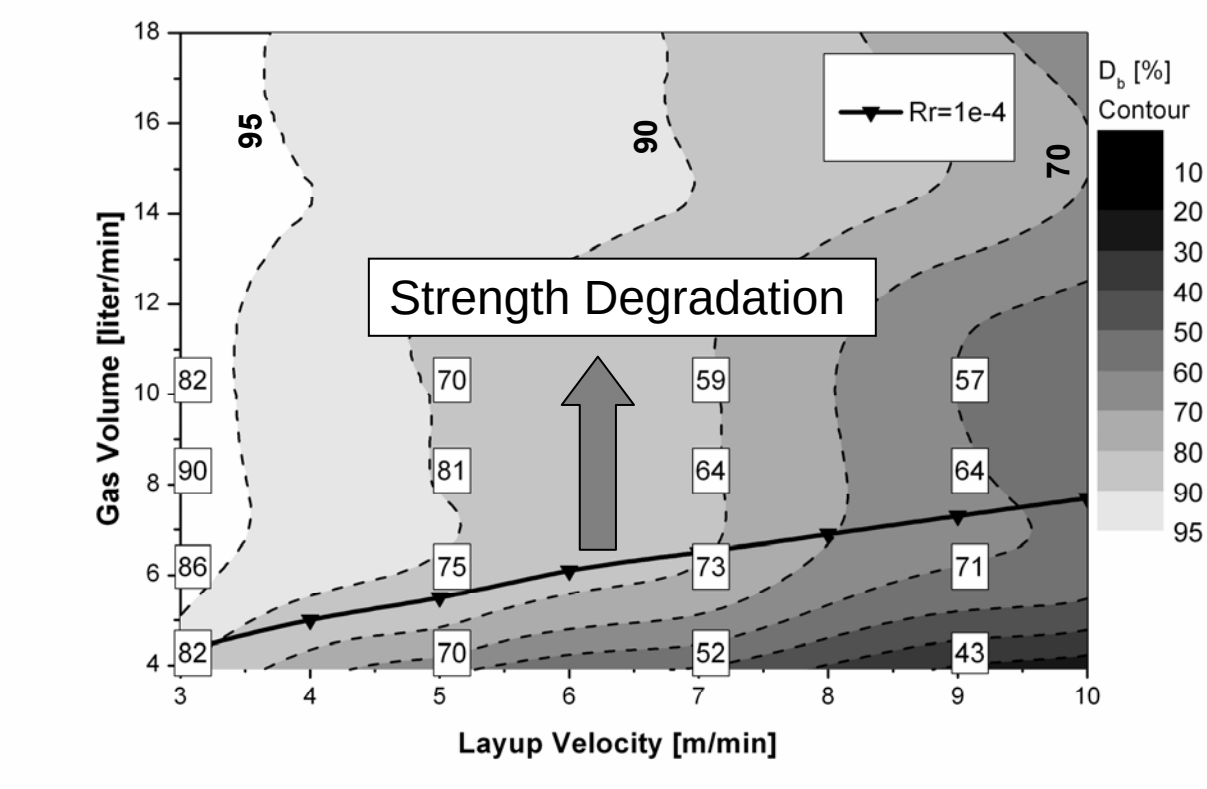

Figure 5.3: Strength degradation above the limiting crosslinking curve.

5.3 Transverse bonding

Based on the width change study carried out for a single tape, investigation in this section is focused on the corresponding influences over the laminate quality. As with the interlaminar bond development, perfect contact between the tapes edges also assist the polymer diffusion in joint region. Proper side by side positioning and edges deformation during the placement process not only alters the laminate microstructure but affects significantly on its mechanical properties [91]. Extensive testing was carried out to investigate the laminate's mechanical and microstructural properties. Laminates were manufactured from the gap between the adjacent tapes configuration to increasing overlaps. With the known simulated tape deformation, laps and gaps were calculated and the placement head was correspondingly positioned for the lay-up through control software.

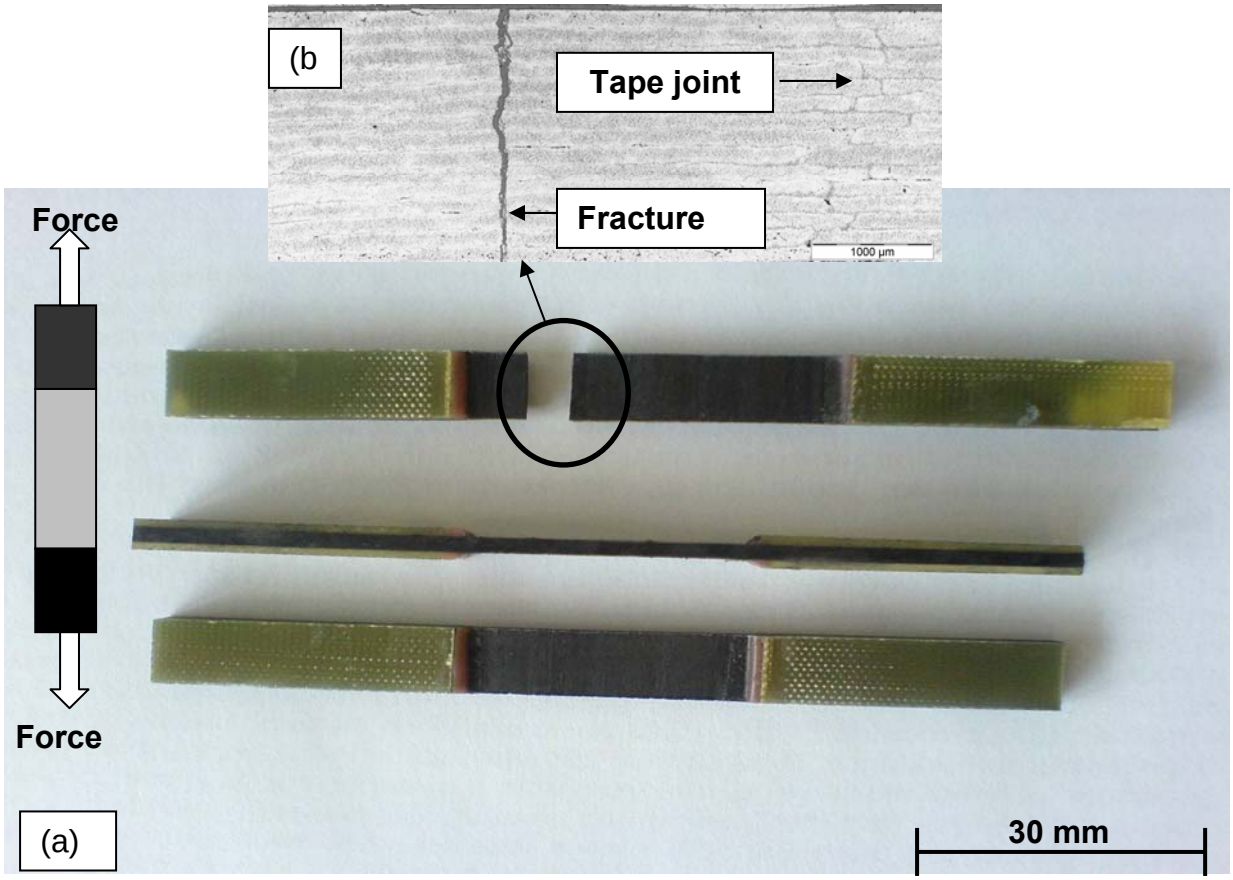

Figure 5.4: (a) Sample specification for the transverse tensile test (b) Transverse fracture away from joint (Gas volume 14 norm liter/min, velocity 3 m/min).

Transverse tensile test has been historically used to measure the 90° tensile properties of unidirectional composite materials. Major draw back of the direct transverse testing method are the premature failure of the test sample as a result of the existence internal flaws and failure at the grips. Therefore this test is not recommended for the joint strength evaluation. For this experimental study more than 60% of the tested samples experienced these failures making it difficult to interpret the actual joint strength. Figure 5.4(a) shows the transverse tensile strength test sample along with transverse fracture, the Figure 5.4(b) clearly shows the fracture propagate away from the transverse joint.

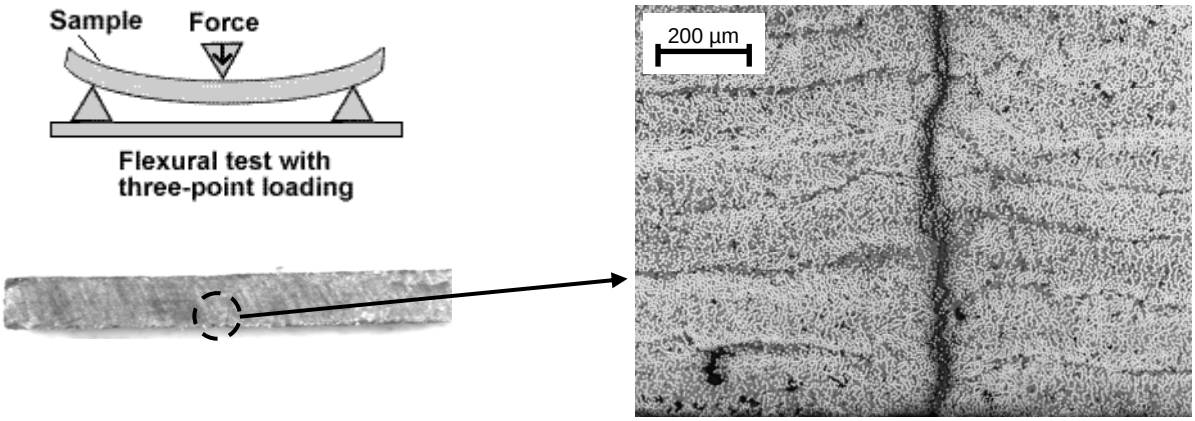

Figure 5.5: Transverse flexural failure at joint section.

Another technique to create transverse failure in tension is by subjecting the laminate to bending loads. For example under a simple three point flexural loading, the maximum tensile stress occurs only along a line across the tensile surface at the specimen mid span. Accordingly, if the test sample's joint section is positioned exactly under the loading nose then this specimen should be significantly less flaw sensitive than a transverse tensile sample. Therefore, the strength results obtained should be more representative of the actual joint transverse tensile strength [92]. Hence the transverse flexural samples 20 mm wide and 10 mm long were fabricated. The loading conditions for the test were selected as per DIN EN ISO 178 standards. Figure 5.5 shows the transverse flexural sample after fracture in transverse direction, the fracture surface passed exactly through the joint section.

The curves in Figure 5.6 shows the two different failure mode experienced in the testing. In both cases forces increased linearly with increasing flexure of the sample, till the sample failed with the crack initiating from the bottom. The load represents the maximum transverse load which thereafter falls to zero. However in some sample the force did not fall immediately, as it recovered midway while the crack continue to grow. The crack diversion was observed in those samples, as it grew sideways until the test sample completely broken.

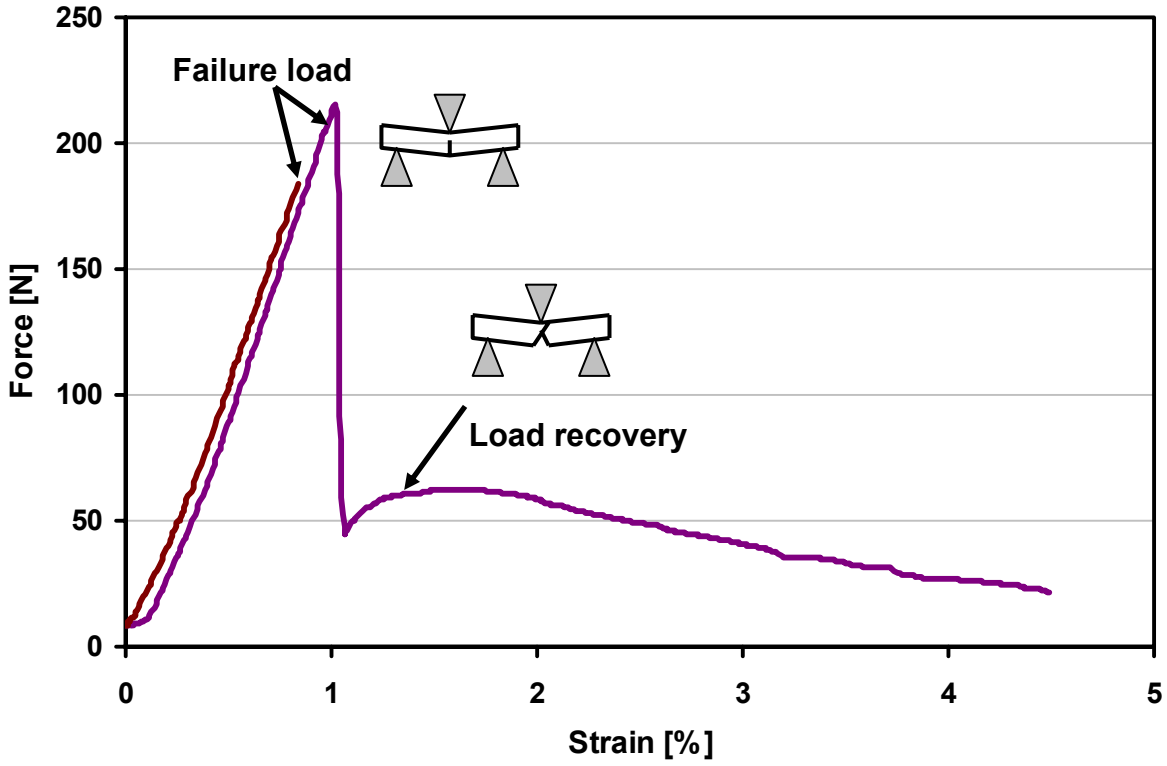

Figure 5.6: Failure load curve for transverse flexural test (Gas volume 8 norm liter/min, velocity 3 m/min).

Based on the energy levels identified for the single tape deformation in Figure 3.18, samples from the laminates manufactured with low energy level (Gas Volume. 6 norm liter/min, Velocity 8 m/min) and intermediate energy level (Gas volume 8 norm liter/min, Velocity 3 m/min) were tested. Photomicrographs from the laminate manufactured with low energy level combinations are shown in Figure 5.7 (a & b). Apparent is the fine resin bonded region between the rectangular edges in the first configuration. Edges follow type II & III deformation and produced perfect bond with each other. The second photomicrograph represents a laminate with 0.15 mm of side overlaps.

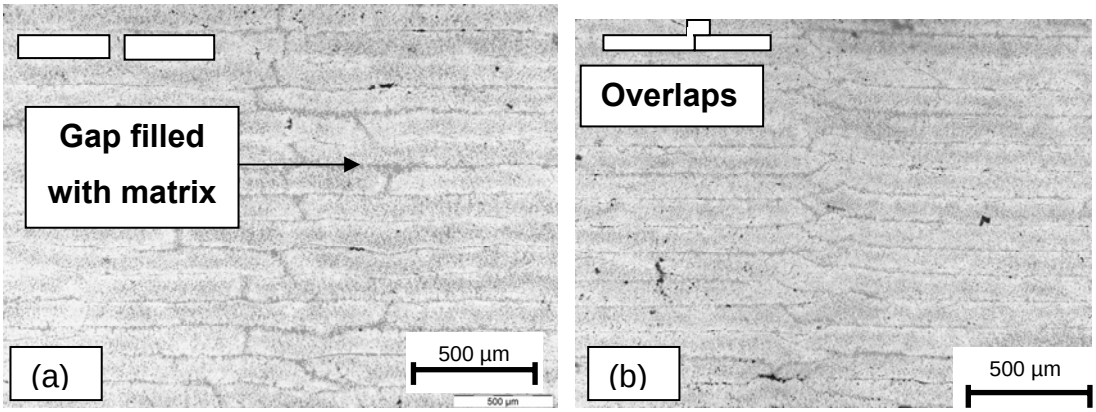

Figure 5.7: (a) Transverse joint with no overlap (b) Transverse joint with 0.15 mm overlap (Gas Volume. 6 norm liter/min, velocity 8 m/min).

Figure 5.8 shows the apparent difference in mean transverse flexure strength for the two cases. As the failure and crack propagation in pure bonded region took place at low loading. But in the second laminate where the bonded region is filled with the carbon fibers with slight overlapping, the transverse flexural strength increased over 10%.

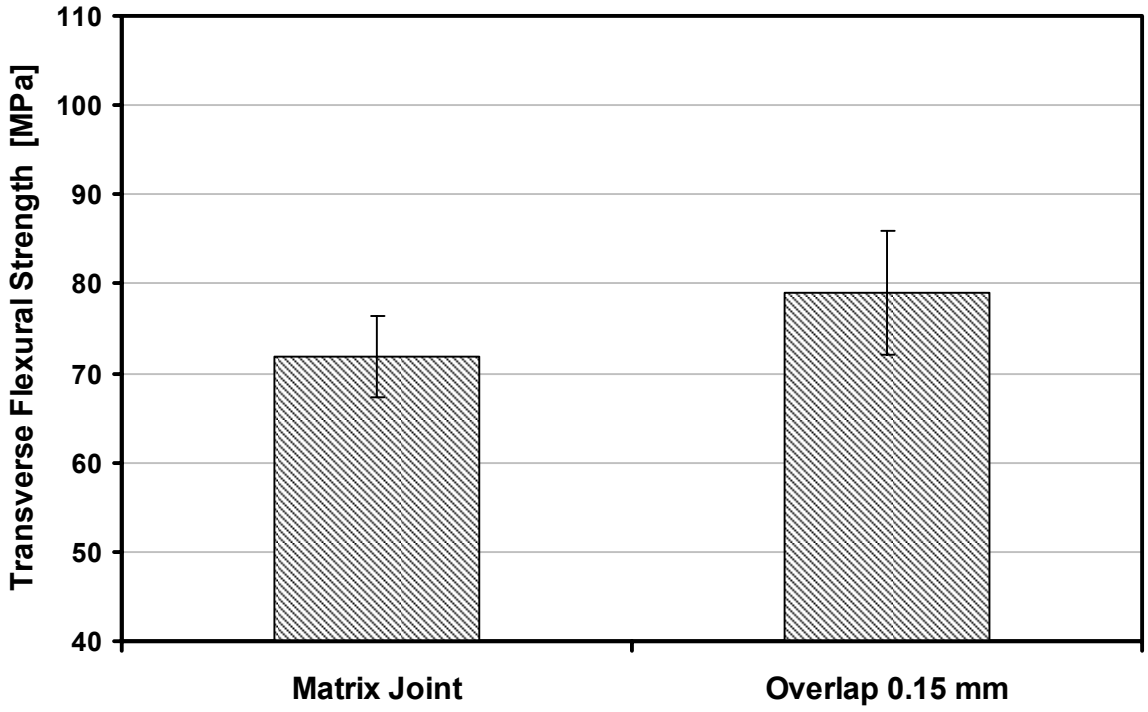

Figure 5.8: Transverse flexural strength comparisons between pure matrix joint and overlap joint for the LE laminate (Gas volume 6 norm liter/min, velocity 8 m/min).

Tests were then performed on the laminate manufactured with intermediate energy level. The objectives were two folds, firstly to find out the maximum achievable value of transverse flexural strength for the laminate manufactured using tape placement process and secondly the effect of increasing tape overlaps. The laminate produced with generated gap of 0.1 mm was very fragile to cut and broke away during the flexural sample preparation. Hence no samples were prepared for the transverse testing.

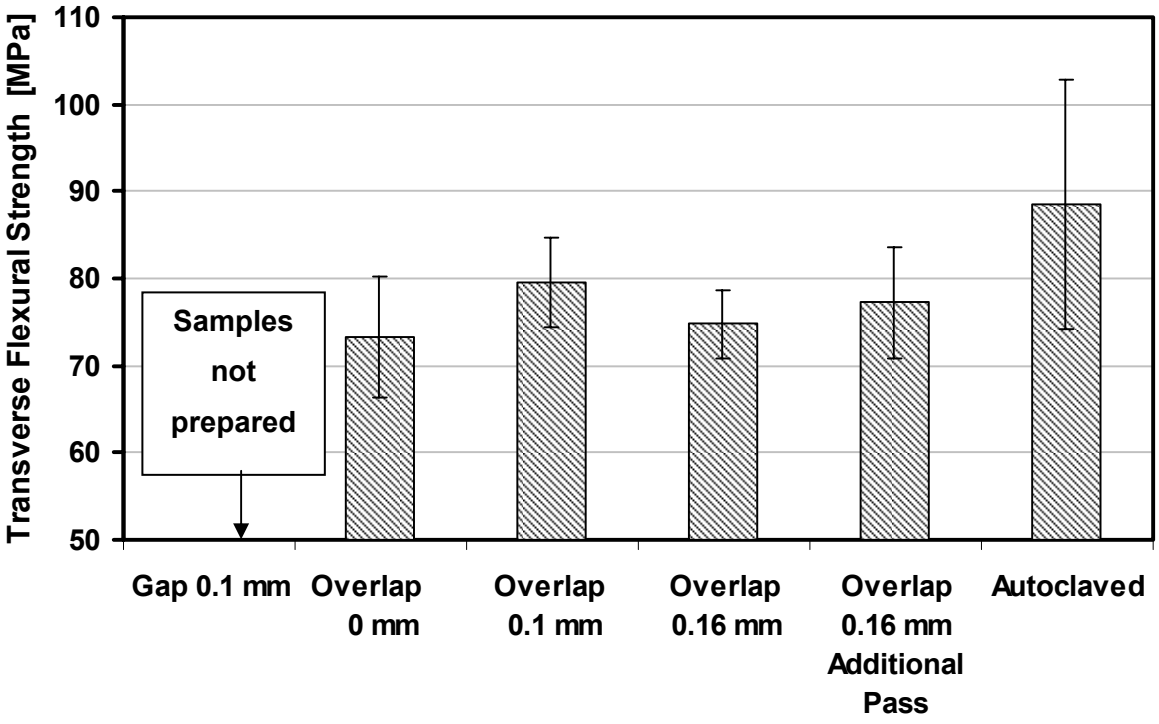

Figure 5.9: Effect of overlap and gaps on the laminate's transverse and interlaminar shear strength (Gas Volume. 8 norm liter/min, velocity 3 m/min).

Laminates manufactured with perfect edge contact (no gap/overlap) and with increasing overlap show the very slight variation in strength (see Figure 5.9). The mean value for transverse flexural strength is around 75-80 MPa. Light microscopic examination revealed that the fibers translated into the matrix region even for the no overlap configuration. Presence of the fiber reinforced the transverse joint and consequently provides higher values. Increase in overlap distance (0.16 mm) in fact reveals a slight decreasing trend. Photomicrograph from these sample showed the presence of the interlaminar void near to the joint region in top layers see Figure

5.10. Presence of interlaminar void thus reduced the transverse strength as the fracture propagation could shift to the nearby weak regions. An improvement was performed by consolidating the top layers with two additional passes with hot gas torch turned off. The elimination of the trapped void in top layer improved the strength. Comparison with autoclave plate shows the relative strength difference of about 10%. But the tape placed laminates showed less strength variation and the mean values from these plates lie within the scatter range of autoclaved plate.

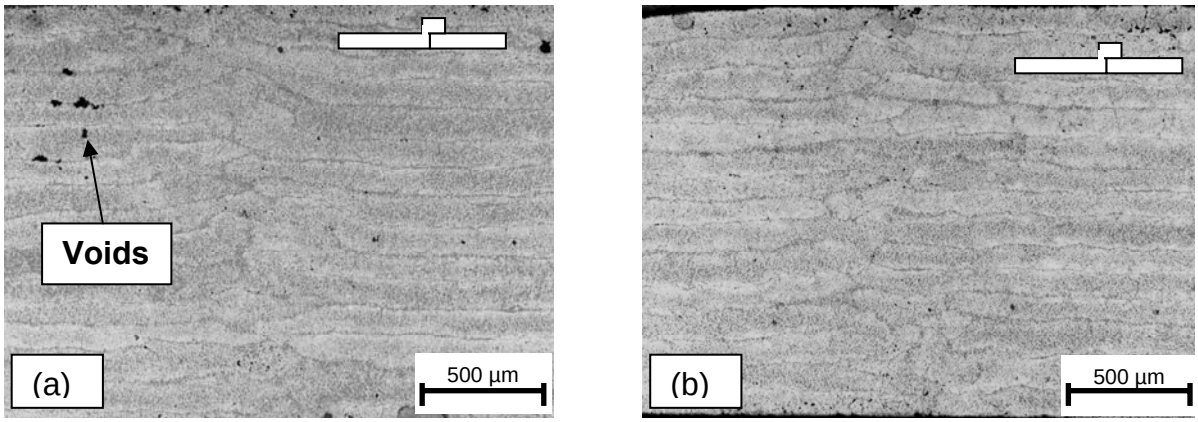

Figure 5.10: (a) Void within the top layers (b) Void elimination with additional consolidation passes. (Gas volume 8 norm liter/min, velocity 3 m/min).

5.4 Lay-up parameters selection for manufacturing

The preparation stage in lay-up process involves selection of several setup parameters as shown in Figure 2.3. Using high interlaminar strength as the criteria, a quick setup scheme for the laminate lay-up is presented here by considering the IVW setup.

- Higher roller temperatures foster the bonding process. But to avoid the material sticking maintain the roller below the glass transition temperature. For the water controlled tempered roller, 90 °C is the fine compromise.

- Parameter study disclosed that the temperature up to 280 °C is fair enough to improve the bonding in the early layers and it also provides the proper first ply sticking mechanism.

- Compaction force less than 50 N generate insufficient consolidating pressure

and the forces over 150 N have negligible influence on laminate's final strength for high energy combinations. In the present study, 165 N force is found suitable for a setup with 220 N as upper limit.

- Select the lay-up velocity and hot gas volume combination from Figure 4.16 for higher D_b.
- Select the adjacent tape placement distance from Figure 4.14.
- Lay-up the material on the tool to obtain the laminate with desired geometrical dimensions. Use the thickness buildup and width change data to identify the number of layers in thickness and width dimension.
- For the intermediate and high energy combinations, perform additional reconsolidation passes on top layer for improvements. Use Figure 3.18 for identifying the combination, which requires additional reconsolidation.
- Cool the tooling and laid down material to room temperature.

As an example Figure 5.11 represent a selection cycle (from a to d) for manufacturing laminate with following chosen conditions.

Plate A: D_b > 95% (equivalent to 89 MPa) with 14 norm liter/min, 3 m/min

Plate B: D_b > 95% (equivalent to 89 MPa) with 8 norm liter/min, 3 m/min

Plate C: D_b > 65% (equivalent to 61 MPa) with 6 norm liter/min, 8 m/min

For 14 and 8 norm liter/min the strength comparison in Figure 5.11(d), indicate that the laminates bears the same ILSS values as that of autoclave plates. But the high speed lay up (8 m/min) at the gas volume of 6 norm liter/min, did not provide sufficient conditions for heating and interlaminar bonding development. Overall, the strength values show the exact trend as selected initially for the D_b. The transverse flexural strength in all the laid up laminates have the same strength and the values are slightly less than that of autoclaved plate. But the keeping the scatter in transverse flexural strength data for autoclaved plates, the values of the laid up plates shows better performance.

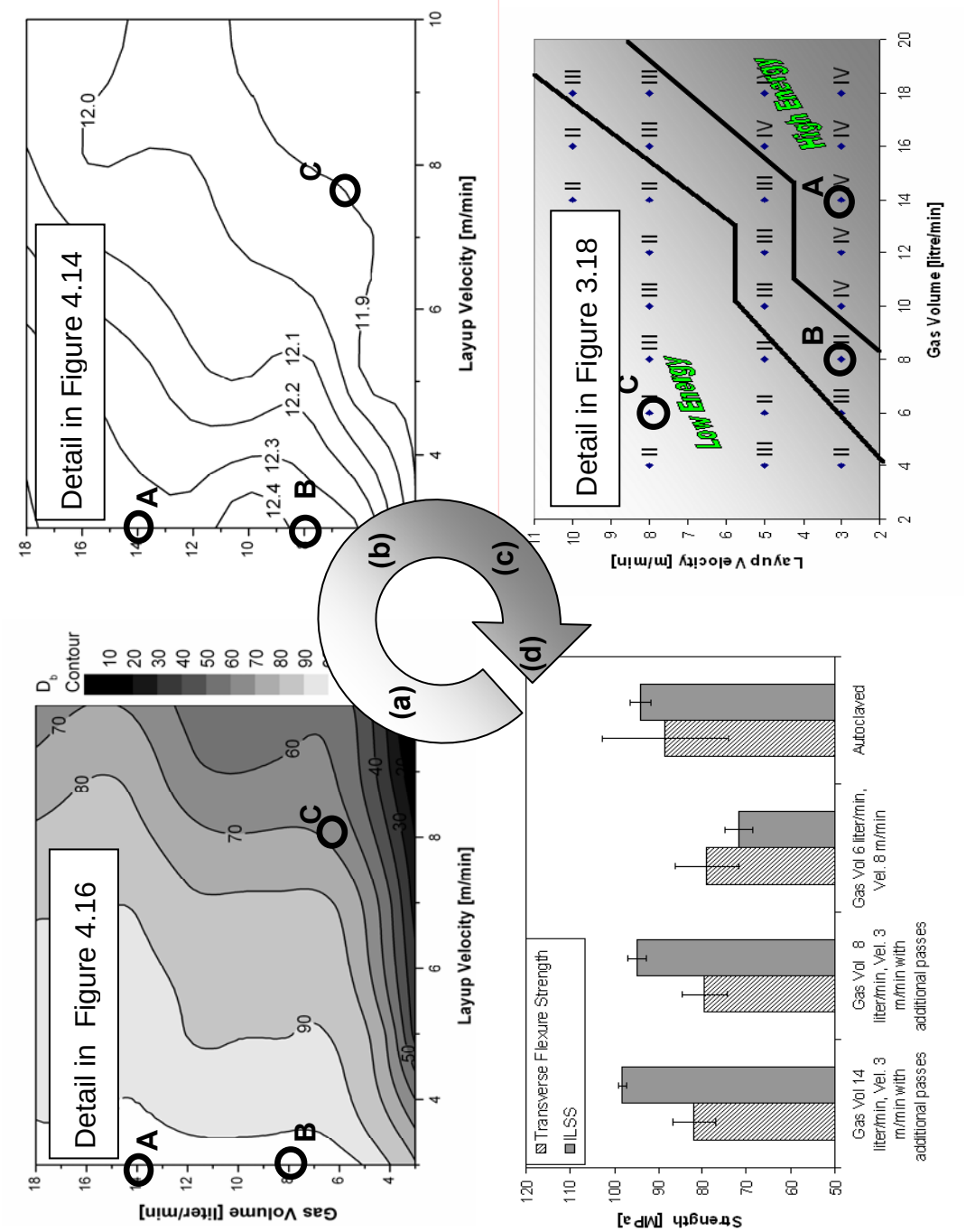

Figure 5.11: Process parameters selection cycle.

5.5 High quality thermoplastic prepreg material

Although the existing setup can produce the laminate with suggested bonding strength but the control over the void content values still need some attention. By far the use of high quality thermoplastic tape seems to be more easy and efficient way to obtain structure with high mechanical performance. Unfortunately no standard criteria have been recognized so far but studies have been performed conformable to the individual placement setup. Some possible criteria for the tape material are discussed below for technological development.

5.5.1 Tape edges

Beresheim [3] developed a criterion to classify the tape edges into seven different classes. Tape with rectangular edges was designated best for the transverse bondings while the tape with distorted edges or with cracks was found not feasible for perfect bonding. Study on tape edges deformation as discussed before fortified these facts by indicating the effect on laminates transverse joint. Tapes with rectangle edge or edge with slight roundness is recommended, as the deformation behaviour for these geometries can be predicted [81] and lay-up head can be positioned to have proper overlaps for transverse joint.

5.5.2 Surface roughness

As discussed before the irregularities on tape surface hinder the contact development between the layers while the flat tape facilitate in attaining high interlaminar bonding strength. Simulation for intimate contact development for a 15 layered laminate by assuming a highly rough tape surface (FD = 1.8), moderately rough surface (FD = 1.4), and relatively smooth surface (FD = 1.2) is shown in Figure 5.12. The higher intimate contact through out the laminate with smooth tape is evident.

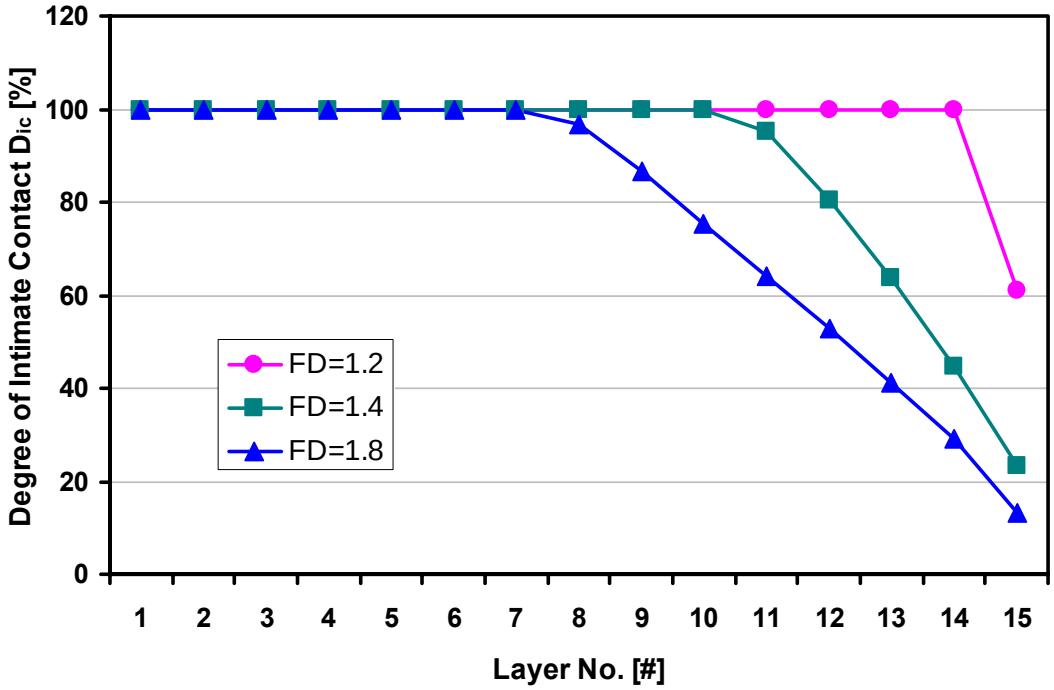

Figure 5.12: Development of intimate contact within the laminate (Gas volume 8 norm liter/min, velocity 3 m/min).

The original tape and surface modified tape (see Figure 3.20), were then used to analyze the drop in the bonding strength using peel resistance test. Double ply peel samples were manufactured with a gas volume of 10 norm liter/min and lay-up velocity of 8 m/min from the original and altered rough tapes. A computer tomography image (Figure 5.13) indicates the incomplete intimate contact for the original tape and a clearly more pronounced effect for the altered rough tape.

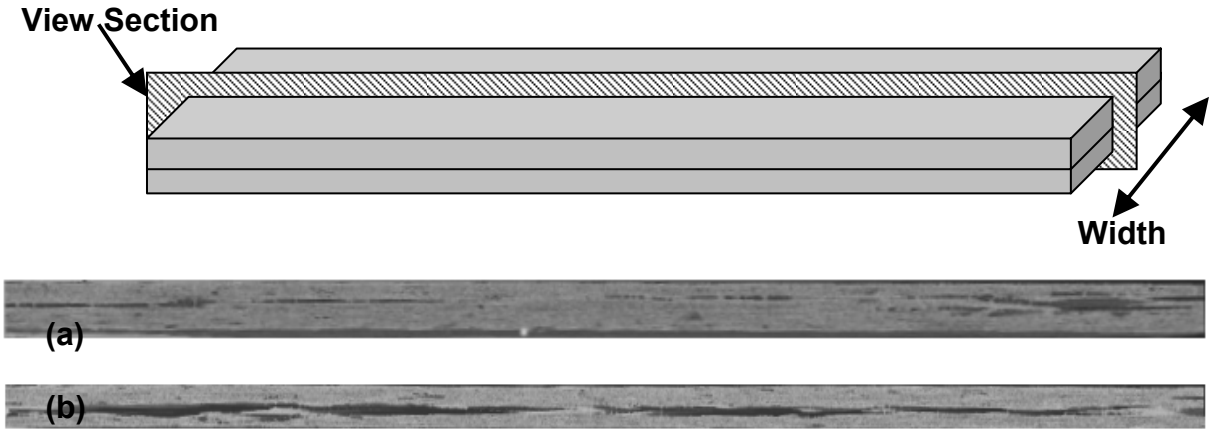

Figure 5.13: µCT images for the intimate contact development in peel test sample (a) Original tape (b) Altered tape with rough surface. (Gas vol. 10 norm liter/min, vel. 8 m/min)

Again, simulations were performed by using experimentally measured surface fractal data. Figure 5.14 compares the simulated D_b with the experimentally determined peel resistance; a tendency of greater strength reduction is visible in both cases. For the original tape, a simulated D_b value of 35% corresponds to the experimental peel resistance of 1206 N/m. The simulation gives comparatively higher D_b value of 23% (this theoretically corresponds to peel resistance of 792 N/m) for the rough tape compared to the experimentally obtained value of 389 N/m. The probable cause of this difference could be the fiber breakage, loss of material, and elimination of the matrix rich layer from the altered tape surface, which were not considered in this simulation. Overall decrease in strength is evident in both cases (simulation and experiment) with additional surface roughness.

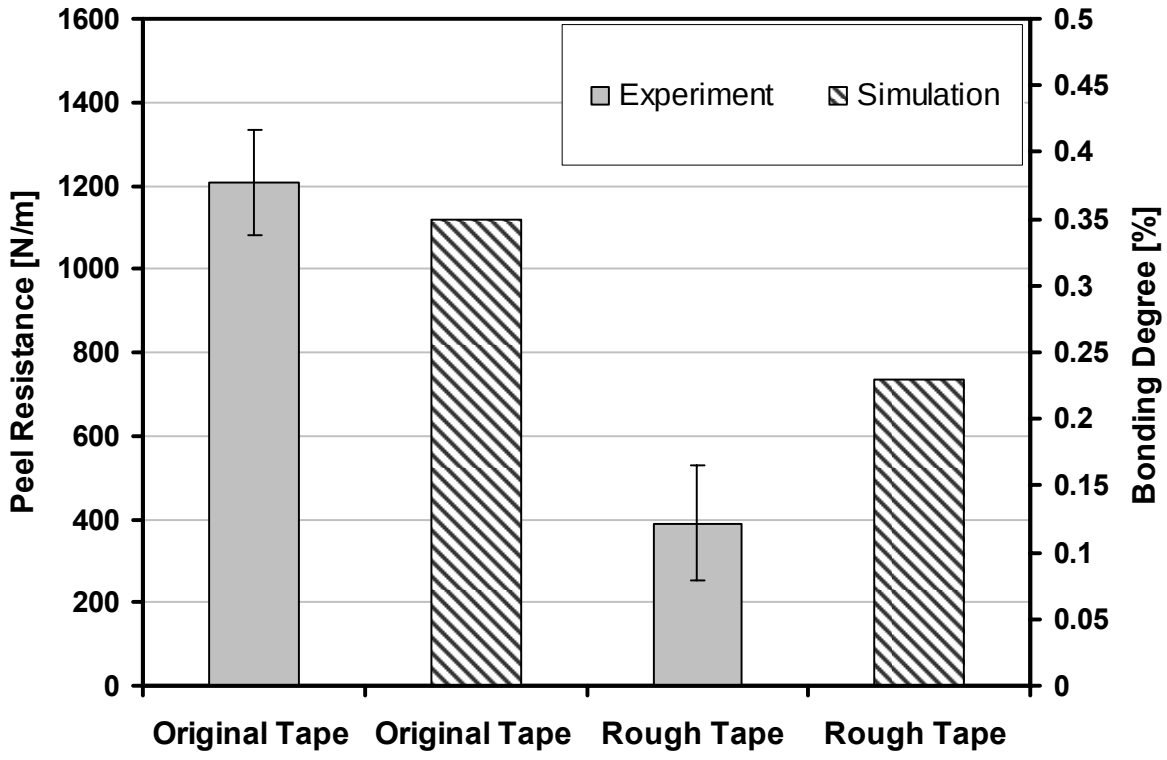

Figure 5.14: Effect of surface roughness on peel resistance (Gas volume 10 norm liter/min, velocity 8 m/min).

5.5.3 Tape with less initial void

Void inside the tape are more viable to deconsolidation at the roller exit. Phenomenon of deconsolidation is a function of the temperature dependent material viscosity, applied force, void surface tension and initial void content of the tape. Tape with initially large voids results in the laminate with higher average value for void content [20, 82]. Thermoplastic tape manufacturers have already identified this industrial requirement. Cytec Engineered Materials is developing a tape to meet the placement grade specification [87] see Figure 5.15

Table 5.2: Recommended specifications for CF-PEEK thermoplastic tape material [87].

Tape Specification	
Fiber areal weight	145 g/m^2
Resin weight fraction Tape placed + Autoclaved	35%
Thickness variation	<6% across width
Width variation	+0.0 to -0.1mm
Void content	<1%

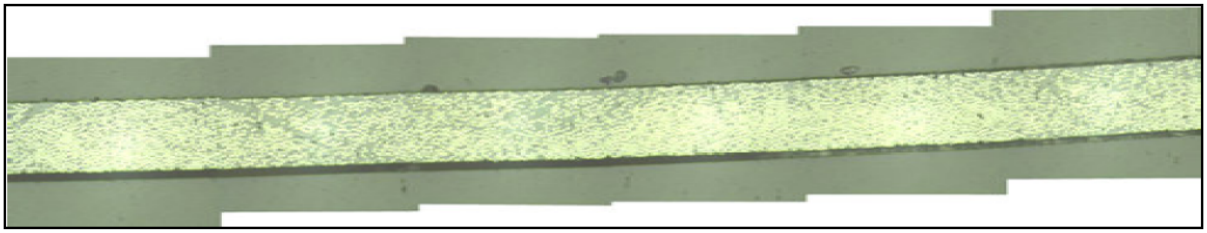

Figure 5.15: Cytec APC-2 AS-4 tape with less void and dimensional variation [87].

The commercial availability of the tape with such specifications will make it possible to lay-up the composite structure even with existing setup, which can be comparable in its mechanical performance to any other composite manufacturing processes. Figure 5.16 represent the expected interlaminar shear strength and void content percentage, for a 15 layered laminate lay up with the tape bearing the characteristics as per Table 5.2. The ILSS values reaches the reported values in the Table 5.1 for the autoclaved process and void content values remain under 1% by fulfilling the need

for high quality laminate.

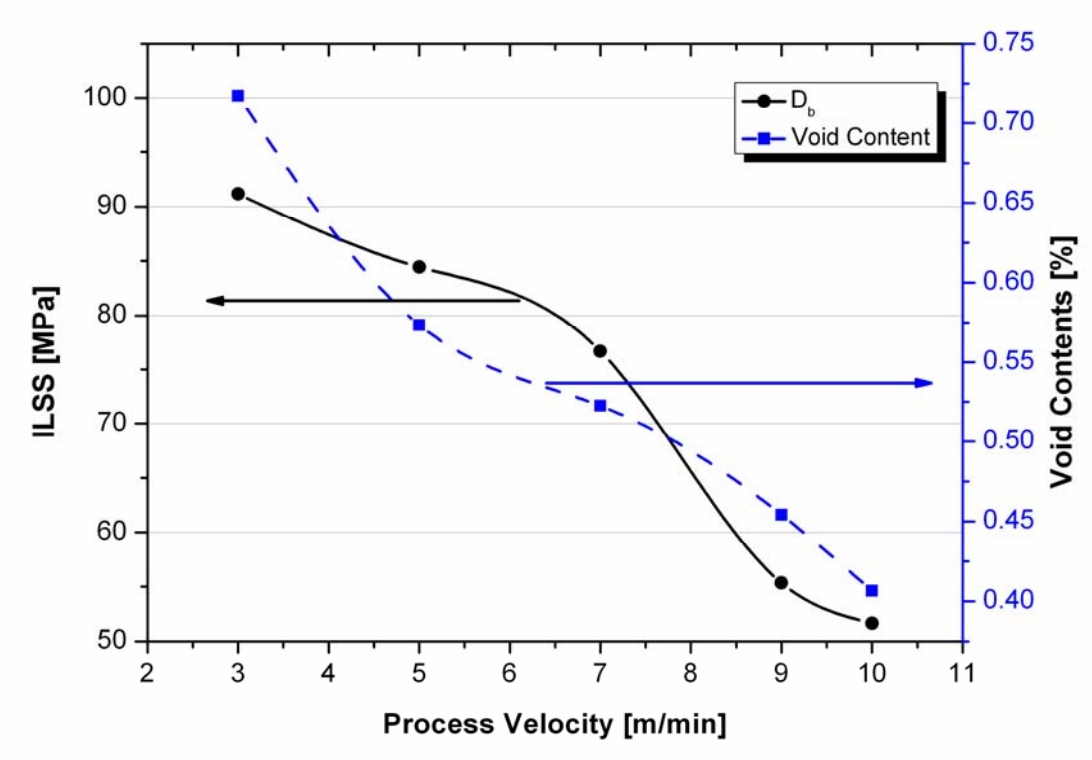

Figure 5.16: Simulated ILSS and void contents values for the laminate laid up with high quality tape. Gas volume 8 norm liter/min.

5.6 Technological advancement

Although the tape placement technique is mature enough for the vast industrial application, but lay-up with exiting grade of thermoplastic materials still demands further advancement. Considering the existing tape with typical void content range between 3-5 %, it's difficult to control the intra lamina void generation. Some possible future solutions to tackle these situations are discussed below. Void removal from the thermoplastic polymer process is limited because of (1) short processing times, and (2) the compactor used for consolidation acts as a boundary. In autoclave processing the laminate is enclosed in a vacuum bag, but a bleeder ply beneath the bag fosters matrix flow through the laminate.

This mechanism for void removal is absent with thermoplastic insitu processing since compactor is solid and occupy space directly above process spot. The main void reduction mechanism for insitu placement is void compression. The state of void con-

tent in first lay-up dictate the final interlaminar void values, as it become more difficult to compress out the buried trap voids inside the laminate.

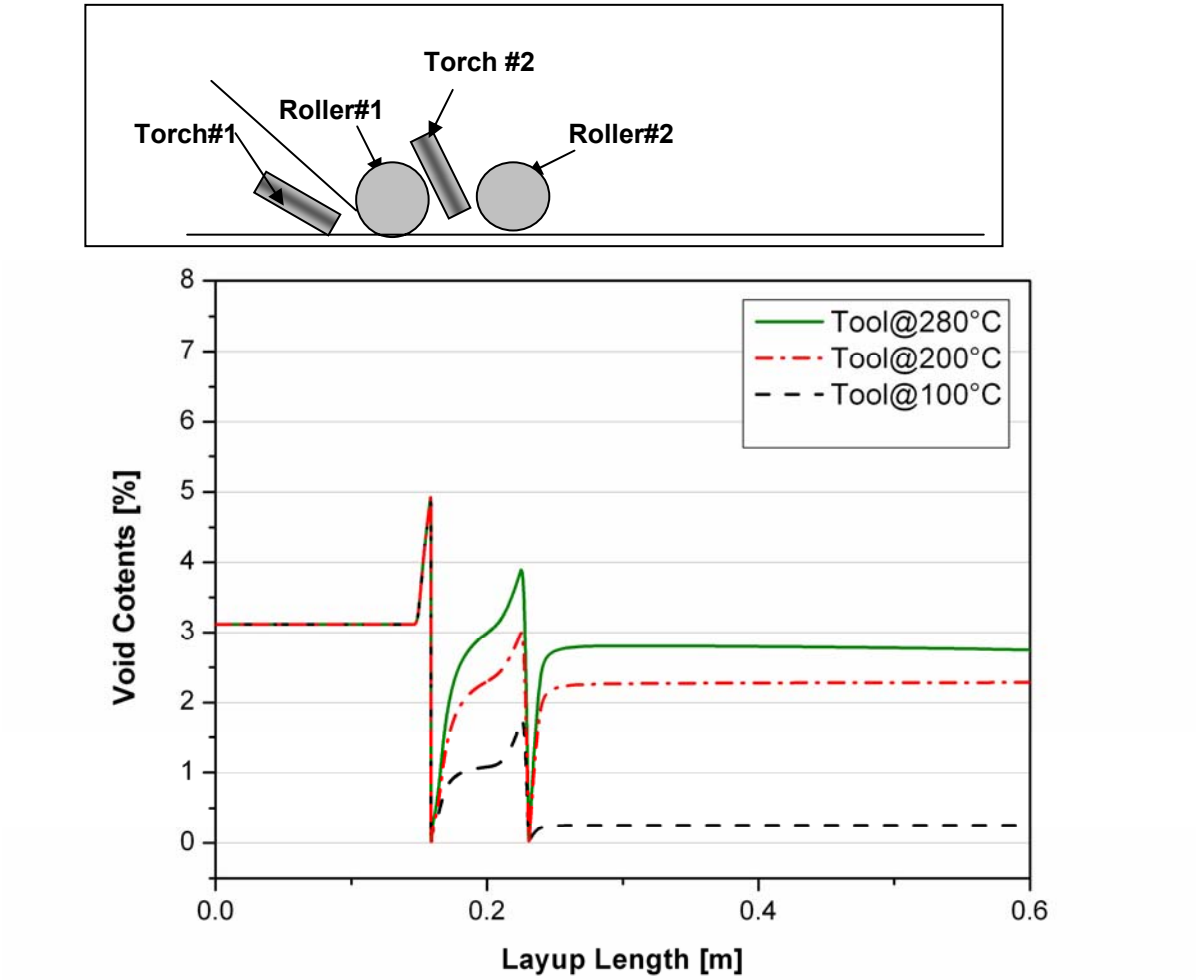

Figure 5.17: Void compaction in a tape at different processing tool temperature. (Gas volume 12 norm liter/min, velocity 3 m/min).

In Figure 5.17 void compressions for the double roller lay-up setup using standard input with different tool temperature is illustrated. If the tool is held at cold crystallization temperature 280 °C, the tape with initial void content of 3.1% raises to 5% under the first torch before being compress down to 0% under roller no. 1, then the decompression occur following the ideal gas law and void stabilize it self accordingly with the surrounding [93]. The void then again rises to 4% under the second torch and again compress down and leave the second roller with almost no consolidation.

Since the tool temperature is well above the T_g, tendency of void deconsolidation is

very high. If the tool is maintained at low temperature, significant amount of heat from the tape sink into the cold tool. Increase in tape viscosity due to sudden temperature drop restricted the void deconsolidation at roller exit. In Figure 5.18 the laminate's average void content for the three cases shows that <1% void can be achievable with the tool maintain at 100 °C.

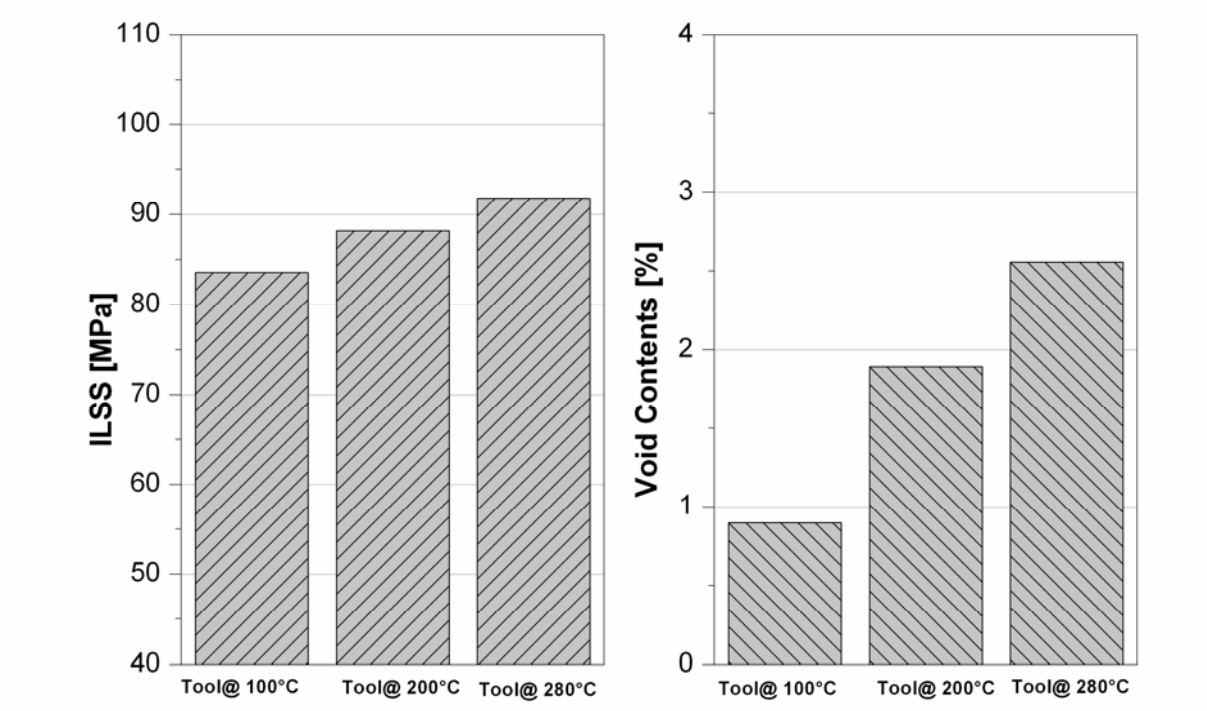

Figure 5.18: Relative comparison between the laminate simulated shear strength and void content. (Gas volume 12 norm liter/min, velocity 3 m/min).

Practically the tool temperature below 260 °C generates major adhesive problem between the first layer and metal tool. The residual stress arises due to thermal expansion / shrinking upon rapid heating / cooling of the material and the plate detached from the tool due to the thermally induced bending stresses. Also due to larger heat sink at tool side, the intimate contact and healing within the laminate cannot reach 100% values. Photomicrograph in Figure 5.19 shows the problem encountered during the laid up of laminate over tool maintained at 200 °C. Detachment of the first layer from tool and its insufficient bonding with second layer represents the large amount of heat flow on tool side. By resolving the first layer and cold tool bonding problem, using focused heat source close to the nip point and by extending consolidation length under the roller, there is a possibility to lay-up high quality laminate (i.e.

Void content less than 1% and ILSS value up to 84 MPa) even with existing tape grade.

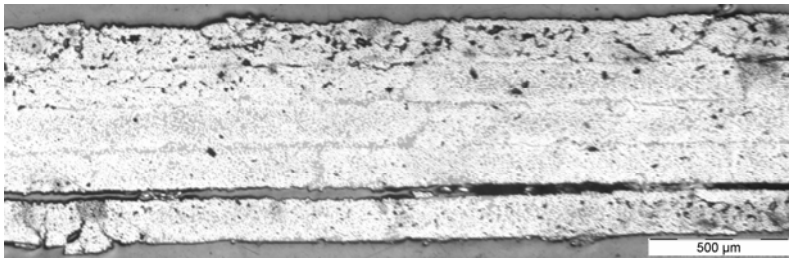

Figure 5.19: Lay-up at over the tool maintained at 200 °C and corresponding effect on laminate quality (Gas volume 8 norm liter/min, velocity 3m/min).

6 Conclusion and outlook

The study describes the consolidation in thermoplastic tape placement process to obtain the high quality structure for industrial application such as aerospace. The major barrier in achieving high interlaminar bonding strength is very short residence time under the roller for consolidation. Hence investigation is performed for the development of material; process and product testing procedure, to find out the influencing process parameters and possible improvement for high strength laminate manufacturing.

Temperature distribution under the hot gas torch is mapped out. The initial supposition of higher heat transfer at higher gas volume is proved to be partially true. The sinusoidal nature of convective heat transfer coefficient cause the drop of heat transfer even at higher gas volume. Consequently the translation effect of this behavior is highly noticeable in interlaminar strength development.

The mechanism of surface roughness flattening is a gradual function and degree of intimate contact D_{ic} at plies interface improves with each successive pass. Similarly, the polymer diffusion initiates only on the completely contacted tape sections. Hence the consecutive lay-up (laminate thickness build-up) improve the consolidation level in the underneath (already placed) layers, but this trend is effective only for the top few layers (3-6 layers) where the temperature rises above the melting point. For the low energy parameter combinations, the energy input to the incoming tape and substrate material is limited and incomplete intimate contact restricts the bonding process. High energy input although could increase the bonding degree D_b even up to the 97%, but activate also the thermal degradation phenomena. The rate of polymer healing (diffusion) and polymer crosslinking follows the Arrhenius laws with the activation energies of 43 KJ/mol and 276 KJ/mol. The polymer crosslinking at high temperature exposure hinder the polymer diffusion process and reduce the strength development. So the intermediate energy combination can provide laminate with good mechanical strength.

A multi parameter study shows that extended consolidation either by mean of additional pass or by increasing consolidation length or by using multiple roller and torch

setup widens the D_b 90% contour. Thus high lay-up velocity up to 7 m/min is viable for high industrial production rate. For the single roller IVW tape placement setup, laminate manufacturing with autoclaved comparable quality (in terms of ILSS and void content) is practically realizable, if provided with the flat preimpregnated tape with less than 1% void content.

Deformation of tape edges is identified as the dictating factor for the laminate's transverse strength. Tape placement with slight overlap reinforced the transverse joint by 14% as compared to pure matrix joint. Lay-up with high energy process parameters produces voids pockets at the joint section and reduces the transverse strength. The post consolidation steps like additional passes with low hot gas volume flow found to be beneficial in removing these trapped voids and improving the overall laminate quality.

Finally the simulation tool developed in this research work is used for identifying the existing limitation to achieve full consolidation. The parametric study identifies the manufacturing conditions to achieve D_b>97% with exiting prepreg thermoplastic material, but with the higher intralaminar void contents. Although the presence of intralaminar void prove to be ineffective for the ILSS values through experimental testing, but some application (like aerospace or medicine) demands overall laminate void content <1%. Tool temperature is identified as one of the highly influencing parameters beside hot gas temperature and lay-up velocity. The tool at high temperature (260-290 °C) on one side foster the bonding within the laminate but on the other hand facilitate the void deconsolidation at roller exit. Simulation indicates that the void can be freeze down to prevent the void deconsolidation inside the laminate, if laid down on cold tool. But the limitation to maintain the adhesion between the first layer and tool hinder such advancement.

The methodology outlined in this work may be extended to carry out the remaining development in the tape placement process. The process improvement should be supported by the parallel advancement in theoretical technological knowledge or vice versa. Address to the following points is suggested for the continual improvement to the tape placement process.

- Material improvement is inevitable in future to foster the large industrial adap-

tation of tape placement process. Thermoplastic pre-peg tapes in future should inherit smoother face (*FD*< 1.2), less void contents (<1%) and at least a fiber diameter thick resin rich layer on top surfaces.

- Compared to the hot gas torch, laser technique has demonstrated [94] the effective heating over a constant area. Efforts are required to focus the heat flux as close to the nip point region.

- Laminate manufacturing with less costly polymer thermoplastic material like PP, PPS, PA12, PEKK and quality testing with other methods like open hole compression testing (OHC), in plane shear strength (IPSS) should be exploited.

- The effect on polymer melt viscosity by crosslinking phenomenon has been discussed. The model may be modified and kinematic constant can be determined with experimentation for fiber reinforced polymer material.

- Simulation tool can be extended with the non isothermal crystalline and residual thermal stress model to analyze different heating/cooling rate and environment.

- To theoretically explain the transverse bonding phenomenon, a 3D heat transfer model [15] is proposed for simulating thermal distribution over tape width and length.

- Finally, for larger computational problem, solving capabilities of Matlab software are limited. Other scientific programming languages like FORTRAN or C++ may be exploited for faster solution.

7 Appendix

7.1 Code for calculating pressure under rotating roller

```
h=data(tmy,3) ;
w=data(tmy-1,6) ;
if (tmy>wdivtemp) & (tmy<=wdivtemp+wdiv)
hdot=data(tmy-1,4);
C=[hdot;h;tmy];
options = [];
solinit = bvpinit(linspace(0,w,wdiv),[0 patm]);
sol = bvp4c(@twoode,@twobc,solinit,options,C,data2);
x = linspace(0,w,wdiv);
y = deval(sol,x);
if (tmy > wdivtemp+1)
if (y(1,1) < 0.9*data2(1,5,tmy-1))
y(1,:) = data2(:,5,tmy-1)'.*0.8;
y(2,1)=0;
y(2,2:end)= (diff(y(1,:)')./diff(x'))';
end
end
data2(:,5,tmy)=y(1,:)';
data2(:,7,tmy)=y(2,:)';
else
data2(:,5,tmy)=patm;
data2(:,7,tmy)=0;
end
data2(:,6,tmy)=[linspace(0,h,wdiv)]';
data(tmy,8)=(data2(1,5,tmy))        ;
data(tmy,12)=mean(data2(:,5,tmy));
```

7.2 Code to calculate heat transfer inside the laminate

```
function[utemp,u,t]=tempcal(Lt,Tt,ht,wdivLl,wdivhl,thk,tdiv,N,qin,qsub )
global alpha1 rho cp Ve k utool
time=Lt(2)/Ve;
time1=Lt(1)/Ve;
time2=time1+(Lt(2)-Lt(1))/Ve;
time1div=linspace(0,time1-.0001,wdivLl);
time2div=linspace(time1,time2,wdivhl);
alpha1=k/(rho*cp);
m = 0;
x = linspace(0,thk,tdiv);
t=[time1div time2div];
options = odeset('MaxStep',0.1*time1);
if N==0
```

```
u(:,:,1)= pdepe(m,@pdex1pde,@pdex1ic,@(xl,ul,xr,ur,t)
pdex2bc(xl,ul,xr,ur,t,Lt,Tt,ht,qin,qsub),x,t);
elseif N==1
u(:,:,1)= pdepe(m,@pdex1pde,@pdex1ic2,@(xl,ul,xr,ur,t)
pdex1bc(xl,ul,xr,ur,t,Lt,Tt,ht,qin,qsub,N),x,t,options);
elseif N==2
u(:,:,1)= pdepe(m,@pdex1pde,@(x) pdex1ic3(x,thk),@(xl,ul,xr,ur,t)
pdex1bc(xl,ul,xr,ur,t,Lt,Tt,ht,qin,qsub,N),x,t,options);
end
utemp=rot90(u) ;
x1=linspace(0,1,tdiv)   ;
utemp=[x1' utemp] ;
```

7.3 Code for void calculation

```
So=(Ro^3/Vvo)^(1/3);
Sos=So/Ro ;
Ros=Ro/Ro;
Plyr=2;
while Plyr<=NNlyr
h2=[INPSTR '\layup' num2str(Plyr)];
load(h2)  ;       layup2=0;
layup2=dat1;
dat1=0;
h1=[INPSTR '\layup' num2str(Plyr-1)] ;
load(h1,'dat1')
layup1=0;
layup1=dat1;
dat1=0;
h3=[INPSTR '\tempdata' num2str(Plyr)];
load(h3,'tempdata')
tempdata2=0;
tempdata2=tempdata;
tempdata=[];
for Tylr=1:Plyr-1
curlyup=layup2(:,:,Tylr);
prvlyup=layup1(:,:,Tylr) ;
tempdata(1,:)=tempdata2(Tylr+1,:);
[prvlyup,curlyup]=voidmodel
(Ro,Sos,Pgo,To,Vvo,prvlyup,curlyup,tempdata,Tg,Plyr,Tylr,wdiv,wdivtr,Tsigma);
layup2(:,:,Tylr) =curlyup;
end
dat1=layup2;
flname=[INPSTR '\layup' num2str(Plyr)];
save(flname,'dat1','wdiv','wdivtr','hsin','NNlyr','hsin','Llin','Lc','Lhin','Ltrin')
Plyr=Plyr+1;
end
```

8 References

1. Gutowski, T.G.P.: Advanced composites manufacturing. 1997, New York, NY: Wiley.

2. Carpenter, C.E.; Colton, J.S.: On-line consolidation mechanisms in thermoplastic filament winding. Polymer Composites, 1994. 15(1): p. 55-63.

3. Beresheim, G.: Thermoplast-Tapelegen –ganzheitliche Prozessanalyse und -entwicklung, in Institut für Verbundwerkstoffe GmbH. 2002: Kaiserslautern, Germany.

4. Latrille, M.: Prozessanalyse und -simulation von Verarbeitungsverfahren für faserverstärkte thermoplastische Bändchenhalbzeuge. 2003, Institut für Verbundwerkstoffe GmbH: Kaiserslautern.

5. Gallet, C.: Innovative and economic fibre placement machines and software. in 3rd Innovative and economic fibre placement machines and software. 2006. NLR Marknesse, The Netherlands.

6. Lamontia, M.A., et al.: Stringer-, honeycomb core-, and tigr -stiffened skins, and ring-stiffened cylinders fabricated from automated thermoplastic fiber placement and filament winding. in SAMPE Europe conference 23. 2002. Paris: p. 213-224.

7. Miscellaneous gallery | Automated Dynamics. Available from: http://www.automateddynamics.com/gallery/affordable_automation/miscellaneous_gallery.

8. Tierney, J.; Gillespie, J.W.: Modeling of In Situ Strength Development for the Thermoplastic Composite Tow Placement Process. Journal of Composite Materials, 2006. 40(16): p. 1487-1506.

9. Steeg, M.; Schledjewski, R.; Schlarb, A.K.: Automation implementation and process development of thermoplastic tape placement for 3-dimensional parts. SAMPE Journal, 2006. 42(5): p. 18-24.

10. Lamontia, M.A., et al.: Developing A Contoured Deposition Head for In-Situ Tape Laying and Fiber Placement, in Sampe International Symposium and Exhibition. 2003: Long Beach, CA.

11. Lamontia, M.A.; Gruber, M.B.: Remaining developments required for commercializing in situ thermoplastic ATP. in SAMPE 2007. Baltimore, MD.

12. Kim, H.J.; Kim, S.K.; Lee, W.I.: A study on heat transfer during thermoplastic composite tape lay-up process: Peter Bradshaw 60th Birthday Issue: Part II. Experimental Thermal and Fluid Science, 1996. 13(4): p. 408-418.

13. Shih, P.J.; Loos, A.C.: Heat Transfer Analysis of the Thermoplastic Filament Winding Process. Journal of Reinforced Plastics and Composites, 1999.

18(12): p. 1103-1112.

14. Hassan, N., et al.: A Heat Transfer Analysis of the Fiber Placement Composite Manufacturing Process. Journal of Reinforced Plastics and Composites, 2005. 24(8): p. 869-888.

15. Toso, Y.M.P.; Ermanni, P.; Poulikakos, D.: Thermal Phenomena in Fiber-reinforced Thermoplastic Tape Winding Process: Computational Simulations and Experimental Validations. Journal of Composite Materials, 2004. 38(2): p. 107-135.

16. Mantell, S.C.; Springer, G.S.: Manufacturing Process Models for Thermoplastic Composites. Journal of Composite Materials, 1992. 26(16): p. 2348-2377.

17. Latrille, M.; Schledjewski, R.: Processing of unidirectional fiber reinforced tapes--fundamentals on the way to a process simulation tool (ProSimFRT). Composites Science and Technology, 2003. 63(14): p. 2111-2118.

18. Nicodeau, C.: Modelisation du soudage en continu des composites a matrice thermoplastique. 2005, Ecole Nationale Superieure d'Arts et Metiers de Paris: Paris.

19. Agarwal, V., et al.: Thermal Characterization of the Laser-Assisted Consolidation Process. Journal of Thermoplastic Composite Materials, 1992. 5(2): p. 115-135.

20. Pitchumani, R., et al.: Analysis of transport phenomena governing interfacial bonding and void dynamics during thermoplastic tow-placement. International Journal of Heat and Mass Transfer, 1996. 39(9): p. 1883-1897.

21. Sonmez, F.O.; Hahn, H.T.: Modeling of Heat Transfer and Crystallization in Thermoplastic Composite Tape Placement Process. Journal of Thermoplastic Composite Materials, 1997. 10(3): p. 198-240.

22. Colton, J.; Leach, D.: Processing parameters for filament winding thick-section PEEK/carbon fiber composites. Polymer Composites, 1992. 13(6): p. 427-434.

23. Dai, S.-C.; Ye, L.: GF/PP Tape Winding with On-Line Consolidation. Journal of Reinforced Plastics and Composites, 2002. 21(1): p. 71-90.

24. Tierney, J.; Gillespie, J.W.: Modeling of Heat Transfer and Void Dynamics for the Thermoplastic Composite Tow-Placement Process. Journal of Composite Materials, 2003. 37(19): p. 1745-1768.

25. Khan, M.A.; Mitschang, P.; Schledjewski, R.: Tracing the Void Content Development and Identification of its Effecting Parameters During in situ Consolidation of Thermoplastic Tape Material. Polymers and polymer composites, 2010. 18(1): p. 1-15.

26. Hinkley, J.A.; Marchello, J.M.; Messier, B.C.: Thermoplastic Ribbon-Ply Bonding Model. NASA Technical Memorandum 110203, 1997.

27. Gutowski, T.G.; Morigaki, T.; Zhong Cai: The Consolidation of Laminate Composites. Journal of Composite Materials, 1987. 21(2): p. 172-188.

28. Ranganathan, S.; Advani, S.G.; Lamontia, M.A.: A Non-Isothermal Process Model for Consolidation and Void Reduction during In-Situ Tow Placement of Thermoplastic Composites. Journal of Composite Materials, 1995. 29(8): p. 1040-1062.

29. Rogers, T.G.: Squeezing flow of fibre-reinforced viscous fluids. Journal of Engineering Mathematics, 1989. 23(1): p. 81-89.

30. Khan, M.A.; Schledjewski, R.: Infuencing factors for an online consolidating thermoplastic tape placement process, in 17th International conference on composite materials, ICCM-17. 2009: Edinburgh, UK.

31. Sonmez, F.O.; Hahn, H.T.: Thermoviscoelastic Analysis of the Thermoplastic Composite Tape Placement Process. Journal of Thermoplastic Composite Materials, 1997. 10(4): p. 381-414.

32. Loos, A.C.; Li, M.-C.: Processing of composites: Consolidation during thermoplastic composite processing. 2000, Munich: Hanser.

33. Lee, W.I.; Springer, G.S.: A Model of the Manufacturing Process of Thermoplastic Matrix Composites. Journal of Composite Materials, 1987. 21(11): p. 1017-1055.

34. Yang, F.; Pitchumani, R.: Fractal Description of Interlaminar Contact Development during Thermoplastic Composites Processing. Journal of Reinforced Plastics and Composites, 2001. 20(7): p. 536-546.

35. Yang, F.; Pitchumani, R.: Interlaminar contact development during thermoplastic fusion bonding. Polymer Engineering & Science, 2002. 42(2): p. 424-438.

36. Yang, F.; Pitchumani, R.: A fractal Cantor set based description of interlaminar contact evolution during thermoplastic composites processing. Journal of Materials Science, 2001. 36(19): p. 4661-4671.

37. Yang, F.; Pitchumani, R.: Healing of Thermoplastic Polymers at an Interface under Nonisothermal Conditions. Macromolecules, 2002. 35(8): p. 3213-3224.

38. Ageorges, C., et al.: Characteristics of resistance welding of lap shear coupons. Part I: Heat transfer. Composites Part A: Applied Science and Manufacturing, 1998. 29(8): p. 899-909.

39. Phillips, R.; Glauser, T.; Månson, J.-A.E.: Thermal stability of PEEK/carbon fiber in air and its influence on consolidation. Polymer Composites, 1997. 18(4): p. 500-508.

40. Cole, K.C.; Casella, I.G.: Fourier transform infrared spectroscopic study of thermal degradation in films of poly(etheretherketone). Thermochimica Acta, 1992. 211: p. 209-228.

41. Gupta, Y.N., et al.: Thermal and thermooxidative degradation of engineering thermoplastics and life estimation. Journal of Applied Polymer Science, 2004. 92(3): p. 1737-1748.

42. Park, J., et al.: Kinetic analysis of thermal decomposition of polymer using a dynamic model. Korean Journal of Chemical Engineering, 2000. 17(5): p. 489-496.

43. Ageorges, C., et al.: Characteristics of resistance welding of lap-shear coupons. Part III. Crystallinity. Composites Part A: Applied Science and Manufacturing, 1998. 29(8): p. 921-932.

44. Ozawa, T.: Kinetics of non-isothermal crystallization. Polymer, 1971. 12(3): p. 150-158.

45. Velisaris, C.N.; Seferis, J.C.: Crystallization kinetics of polyetheretherketone (peek) matrices. Polymer Engineering & Science, 1986. 26(22): p. 1574-1581.

46. Tierney, J.J.; Gillespie Jr, J.W.: Crystallization kinetics behavior of PEEK based composites exposed to high heating and cooling rates. Composites Part A: Applied Science and Manufacturing, 2004. 35(5): p. 547-558.

47. Choe, C.R.; Lee, K.H.: Nonisothermal crystallization kinetics of poly(etheretherketone) (PEEK). Polymer Engineering & Science, 1989. 29(12): p. 801-805.

48. Tobin, M.C.: Theory of phase transition kinetics with growth site impingement. I. Homogeneous nucleation. Journal of Polymer Science: Polymer Physics Edition, 1974. 12(2): p. 399-406.

49. Maffezzoli, A.M.; Kenny, J.M.; Nicolais, L.: Welding of PEEK/Carbon fiber composite laminates. SAMPE Journal, 1989. 25: p. 35-39.

50. Chapman, T.J., et al.: Prediction of Process-Induced Residual Stresses in Thermoplastic Composites. Journal of Composite Materials, 1990. 24(6): p. 616-643.

51. Lawrence, W.: Prediction of residual stresses in continuous fiber semicrystalline thermoplastic composites. in Proceedings of American scociety for composites 5th technical conference. 1990: p. 401-408.

52. Tierney, J.J.; Eduljee, R.F.; Gillespie Jr, J.W.: Material response during robotic tow placement of thermoplastic composites. in Proc. of 11th annual advance composites conf. 1995: p. 315-329.

53. Jeronimidis, G.; Parkyn, A.T.: Residual Stresses in Carbon Fibre-Thermoplastic Matrix Laminates. Journal of Composite Materials, 1988. 22(5):

p. 401-415.

54. Hexcel: Carbon fiber data sheets. 2010; Available from: http://www.hexcel.com/Products/Downloads/Carbon+Fiber+Data+Sheets.htm?ds=Continuous.

55. Lindemann, A.; Schopper, A.: Thermophysical properties of CF filled PEEK samples.Netzsch Report no. 821.004/09, 2009.

56. Cremers, M.F.G., et al.: Heat transfer mechanisms of laminar flames of hydrogen + oxygen. Combustion and Flame, 2004. 139(1-2): p. 39-51.

57. Baukal, C.E.; Gebhart, B.: Heat transfer from oxygen-enhanced/natural gas flames impinging normal to a plane surface. Experimental thermal and fluid science, 1998. 16(3).

58. Baukal, C.E.; Gebhart, B.: Surface condition effects on flame impingement heat transfer. Experimental thermal and fluid science, 1997. 15(4).

59. Martin, H.: Advances in Heat Transfer. Heat and mass transfer between impinging gs jets and solid surfaces. Vol. 13. 1977: Academic Press.

60. Kim, H.J.; Kim, S.K.; Lee, W.I.: Flow and Heat Transfer Analysis during Tape Layup Process of APC-2 Prepregs. Journal of Thermoplastic Composite Materials, 2004. 17(1): p. 5-12.

61. Lawal, A.; Kalyon, D.M.: Squeezing flow of viscoplastic fluids subject to wall slip. Polymer Engineering & Science, 1998. 38(11): p. 1793-1804.

62. Majumdar, A.; Bhushan, B.: Fractal Model of Elastic-Plastic Contact Between Rough Surfaces. J. Tribol., 1991. 113(1): p. 1-11.

63. Khan, M.A.; Mitschang, P.; Schledjewski, R.: Identification of some optimal parameters to achieve higher laminate quality through tape placement process. Advances in polymer technology, 2010. 29(2): p. 98-111.

64. Barnes, J.A.; Cogswell, F.N.: Transverse flow processes in continuous fibre-reinforced thermoplastic composites: Flow Processes in Composite Materials. Composites, 1989. 20(1): p. 38-42.

65. Cogswell, F.N.: Thermoplastic aromatic polymer composites: A study of the structure, processing and properties of carbon fibre reinforced polyetheretherketone and related materials. 1992, Oxford: Butterworth-Heinemann.

66. Balasubramanyam, R.; Jones, R.S.; Wheeler, A.B.: Modelling transverse flows of reinforced thermoplastic materials: Flow Processes in Composite Materials. Composites, 1989. 20(1): p. 33-37.

67. Deng, Y., et al.: The rheological characterization of fluorinated thermoplastics using squeezing flow viscometry. Polymer Engineering & Science, 1994.

34(3): p. 213-220.

68. Lin, H.-R.; Advani, S.G.: Processing models and characterization of thermoplastic composite wound parts. Polymer Composites, 1997. 18(3): p. 405-411.

69. Scobbo, J.J.; Nakajima, N.: Dynamic mehcanical analysis of molten thermoplastic / continous graphite fiber composites in simple shear deformation. in 21st Internatinal SAMPE technical conference. 1989. CA.

70. Stanley, W.F.; Mallon, P.J.: Intraply shear characterisation of a fibre reinforced thermoplastic composite. Composites Part A: Applied Science and Manufacturing, 2006. 37(6): p. 939-948.

71. Shuler, S.F.; Advani, S.G.: Transverse squeeze flow of concentrated aligned fibers in viscous fluids. Journal of Non-Newtonian Fluid Mechanics, 1996. 65(1): p. 47-74.

72. Nicodeau, C., et al.: In-situ consolidation process optimization for thermoplastic matrix composites, in SAMPE 2006 Technical Conference Proceedings. 2006, Society for the Advancement of Material and Process Engineering: Long Beach, CA.

73. Agarwal, V.: The role of molecular mobility in the consolidation and bonding of thermplastic composite materials. CCM Report 91-93, 1991.

74. Advani, S.G.; Sozer, E.M.: Process modeling in composites manufacturing. Vol. 59. 2002, New York, NY: Marcel Dekker.

75. Nam, J.-D.; Seferis, J.C.: Generalized composite degradation kinetics for polymeric systems under isothermal and nonisothermal conditions. Journal of Polymer Science Part B: Polymer Physics, 1992. 30(5): p. 455-463.

76. Hulcher, A.B.; Marchello, J.M.; Hinkley, J.A.: Wedge peel testing for Automated fiber placement. Journal of advanced materials, 1999. 31(3).

77. Hulcher, B.; Marchello, J.M.; Hinkley, J.A.: Correlation Between Double Cantilever Beam and Wedge Peel tests for automated tow placement. SAMPE Engineering Series, 1998. 43: p. 1955-1965.

78. Schledjewski, R.: Investigation of testing mechanisms by doping of bonding surfaces with nano particles, in ECCM-13. 2008: Stockholm.

79. Yee, R.Y.; Stephens, T.S.: A TGA technique for determining graphite fiber content in epoxy composites: Advances in International Thermal Sciences: Environment, Polymers, Energy and Techniques. Thermochimica Acta, 1996. 272: p. 191-199.

80. Kim, J.; Moon, T.J.; Howell, J.R.: Cure Kinetic Model, Heat of Reaction, and Glass Transition Temperature of AS4/3501-6 Graphite-Epoxy Prepregs. Journal of Composite Materials, 2002. 36(21): p. 2479-2498.

81. Khan, M.A.; Lichtner, J.; Schledjewski, R.: An investiagtion on the development of the transverse bonding in automated tape placement process, in ECCM-14. 2010: Budapest, Hungary.

82. Khan, M.A.; Schledjewski, R.: Process simulation and parametric study of an online consolidated composite manufacturing setup. in Solids, Structures and Coupled Problems in Engineering. IV European Congress on Computational Mechanics (ECCM IV) 2010. Paris.

83. Guan, X.; Pitchumani, R.: Modeling of spherulitic crystallization in thermoplastic tow-placement process: spherulitic microstructure evolution. Composites Science and Technology, 2004. 64(9): p. 1363.

84. Ghose, S., et al.: High Temperature VARTM of Phenylethynyl Terminated Imides. High Performance Polymers, 2009. 21(5): p.653-672.

85. Goren, A.; Atas, C.: Manufacturing of polymer matrix composites using vacuum assisted resin infusion molding. Archives of Materials Science and Engineering, 2008. 34(2): p. 117-120.

86. Schledjewski, R.: Thermoplastic Tape Placement-Challenging the Autoclave Process, in 1st European Conference on Materials and Structures in Aerospace (EUCOMAS). 2008: Berlin, Germany. p. 245-251.

87. Lamontia, M.A., et al.: Insitu thermoplastic ATP needs flat tapes and tows with few voids., in SAMPE conference. 2008: Paris.

88. Kilroy, J.P.; Ó Brádaigh, C.M.; Semprimoschnig, C.O.A.: Mechanical and Physical Evaluation of New Carbon Fibre/Peek Composites for Space Applications. SAMPE Journal, 2008. 44(3): p. 22-34.

89. Sonmez, F.O.; Hahn, H.T.: Analysis of the On-Line Consolidation Process in Thermoplastic Composite Tape Placement. Journal of Thermoplastic Composite Materials, 1997. 10(6): p. 543-572.

90. Fink, B.K.; Gillespie, J.W.; Ersoy, N.B.: Thermal Degradation Effects on Consolidation and Bonding in the Thermoplastic Fiber-Placement Process, Army Research Lab Report 1998.

91. Wang, E.L.; Gutowski, T.G.: Laps and gaps in thermoplastic composites processing. Composites Manufacturing, 1991. 2(2): p. 69-78.

92. O'Brien, T.K., et al.: Influence of Specimen Preparation and Specimen Size on Composite Transverse Tensile Strength and Scatter, in NASA/TM-2001-211030. 2001.

93. Ye, L.; Lu, M.; Mai, Y.-W.: Thermal de-consolidation of thermoplastic matrix composites--I. Growth of voids. Composites Science and Technology, 2002. 62(16): p. 2121-2130.

94. Schledjewski, R.; Miaris, A.: Thermoplastic tape placement by means of diode

laser heating, in SAMPE 2009 Technical Conference Proceedings. 2009: Baltimore, MD.

List of the students supervised for practical training

Following students did theoretical and experimental work during this research work.

1. Ricardo Medina Rueda: ‘Quality investigation of tape placed laminate through experimental testing’, 2008.

2. Carmen Cobo Sánchez: ‘Experimental process parameter study for tape placement process’, 2009.

3. Vicente Rouco Sanromán: ‘Influence of hot gas temperature and initial tape width, on the final mechanical strength of fabricated thermoplastic composite structure’, 2009.

4. Jorge Carracedo: ‘Evaluation of thermal degradation phenomenon in carbon reinforced thermoplastic material’, 2010.